Shared control authority between human and autonomous driving system for intelligent vehicles

Shriram Jugade

Par **Shriram JUGADE**

Shared control authority between human and autonomous driving system for intelligent vehicles

Thèse présentée pour l'obtention du grade de Docteur de l'UTC

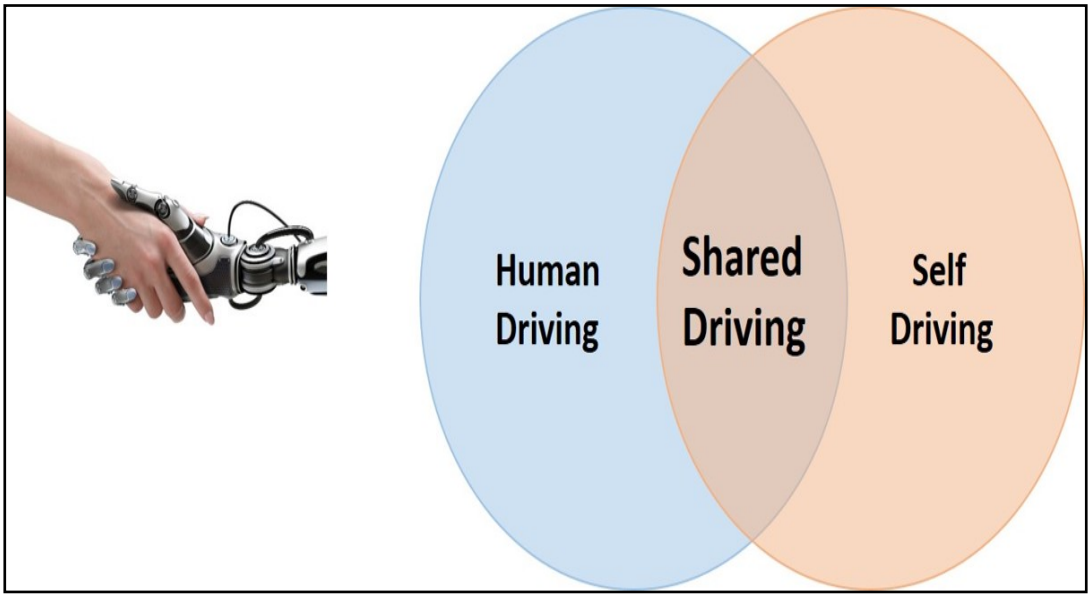

Soutenue le 20 septembre 2019
Spécialité : Automatique et Robotique : Unité de recherche Heudyasic (UMR-7253)

D2507

Shared Control Authority between Human and Autonomous Driving System for Intelligent Vehicles

Shriram JUGADE

Spécialité : Automatique et Robotique

Thesis defended on 20/09/2019, before the jury composed of:

Jury president:
Prof. Barys SHYROKAU,
Section of Intelligent Vehicles
Department of Cognitive Robotics,
Delft University of Technology

Jury members:
Prof. Jean-Christophe POPIEUL
Université Polytechnique Hauts-de-France

Prof. Aldo SORNIOTTI
Centre for Automotive Engineering
University of Surrey

TALJ, Reine, CR1 CNRS - HDR
Heudiasyc UMR CNRS 7253
Université de Technologie de Compiègne

Directeurs de thèse:
CORREA VICTORINO, Alessandro, Maître de Conférences - HDR
CHERFAOUI, Véronique, Professeur des Universités

Université de Technologie de Compiègne
Heudiasyc UMR CNRS 7253
Labex MS2T

To my family. Loving mother, supportive father, driven sister and loving wife

Acknowledgements

Firstly, I would like to express my sincere gratitude to my supervisors Prof. Alessandro Victorino and Prof. Veronique Cherfaoui for the continuous support of my Ph.D study and related research, for their patience, motivation, and immense knowledge. Their guidance helped me in all the time of research and writing of this thesis.

Besides my supervisors, I would like to thank the rest of my project network ITEAM: Prof. Valentin Ivanov and my colleagues, for their insightful comments and encouragement, but also for the hard question which incented me to widen my research from various perspectives.

My sincere thanks also goes to Dr. Phil Barber, who provided me an opportunity to join their team for my placement at Jaguar Land Rover, and who gave access to the facilities. The final validation of the research was carried out smoothly with his support.

Last but not the least, I would like to thank my wife and my family. Without their support it would not have been possible to pursue doctorate in France.

I would also like to thank European Commission and for LABEX MS2T, ROBOTEX financially supporting this project under the H2020 Grant agreement ITEAM No. 675999.

Abstract

Road traffic accidents have always been a concern to the driving community which has led to various research developments for improving the way we drive the vehicles. Since human error causes most of the road accidents, introducing automation in the vehicle is an efficient way to address this issue thus making the vehicles intelligent. This approach has led to the development of ADAS (Advanced Driver Assistance Systems) functionalities. The process of introducing automation in the vehicle is continuously evolving. Currently the research in this field has targeted full autonomy of the vehicle with the aim to tackle the road safety to its fullest potential. The gap between ADAS and full autonomy is not narrow. One of the approach to bridge this gap is to introduce collaboration between human driver and autonomous system. There have been different methodologies such as haptic feedback, cooperative driving where the autonomous system adapts according to the human driving inputs/intention for the corrective action each having their own limitations.

This work addresses the problem of shared control authority between human driver and autonomous driving system without haptic feedback using the fusion of driving inputs. The development of shared control authority is broadly divided into different stages i.e. shared control framework, driving input assessment, driving behavior prediction, fusion process etc. Conflict resolution is the high level strategy introduced in the framework for achieving the fusion. The driving inputs are assessed with respect to different factors such as collision risk, speed limitation, lane/road departure prevention etc in the form of degree of belief in the driving input admissibility using sensor data. The conflict resolution is targeted for a particular time horizon in the future using a sensor based driving input prediction using neural networks. A two player non-cooperative game (incorporating admissibility and driving intention) is defined to represent the conflict resolution as a bargaining problem. The final driving input is computed using the Nash equilibrium. The shared control strategy is validated using a test rig integrated with the software Simulink and IPG CarMaker. Various aspects of shared control strategy such as human-centered, collision avoidance, absence of any driving input, manual driving refinement etc were included in the validation process.

Contents

List of figures

List of tables

Acronyms

ADAS: Advanced Driver Assistance Systems

BFT: Belief Functions Theory

AutoSys: Autonomous Driving System

IntelSys: Intelligent System

Introduction

Contents

1.1 Intelligent Vehicles

Automobiles have changed the way of living and has become a necessity for the people. It is a key factor influencing the urban structure and transportation policies. Along with enormous advantages, there have been ill effects especially in the aspect of safety. According to the World Health Organization an estimated 1.2 million people worldwide are killed each year, and about forty times this number injured, due to traffic accidents [Broggi et al., 2008]. Machines have always been envisioned as a human partner assisting in the complex tasks. This led to an evolution with the research field of robotics with the aim of incorporate intelligence in the machines. Automotive field was not far away from this influence of robotics and vehicle started becoming intelligent with the help of automation.

A human driver need to perform multiple complex tasks ensuring safety and optimal performance. An intelligent vehicle is defined as a vehicle enhanced with perception, reasoning, and actuating devices that enable the automation of driving tasks such as safe lane following, obstacle avoidance, overtaking slower traffic, following the vehicle ahead, assessing and avoiding dangerous situations, and determining the route [Broggi et al., 2008]. These functions were being automated in the vehicle with the aim of assisting human drivers. It was then collective named as Advanced Driver Assistance Systems (ADAS). ADAS improved the vehicle safety and performance along with reducing the workload of human drivers.

The evolution of ADAS led to the research and development of full autonomous vehicles. To promote this research the Defense Research Projects Agency (DARPA) launched a Grand Challenge in 2003 which was a race between autonomous vehicles in an unstructured environment. In 2005, DARPA conducted this competition in a rough desert terrain scenario with no traffic, few known obstacles and few road markers. Some of the cars which completed this 211 km course are shown in Fig. ?? [Broggi et al., 2008].

The general driving is very different than these competition where the intelligent vehicle encounter a lot of traffic, the road maps are not always available, environment dynamics is highly unpredictable, legal issues and human factors. The current research in the autonomous vehicles have an all round focus. The issues for the intelligent vehicles increase in proportion to the task complexity. These issues can broadly be categorized as technical and non-technical. Another perspective of incorporating automation in the vehicles is to have a human-machine collaboration using shared control authority. This approach can not only compensate for the current autonomous driving system limitations but also can complement its further development.

One of the factors affecting the environment pollution is the traffic density. For making the traffic flow efficient, it is important for the vehicles to communicate with each other. This communication can also greatly help in the increase of road safety. Connected vehicles can be separately perceived from the point of view of research. To summarize, intelligent vehicle technology can broadly classified into 4 categories as shown in Fig. 1.1.

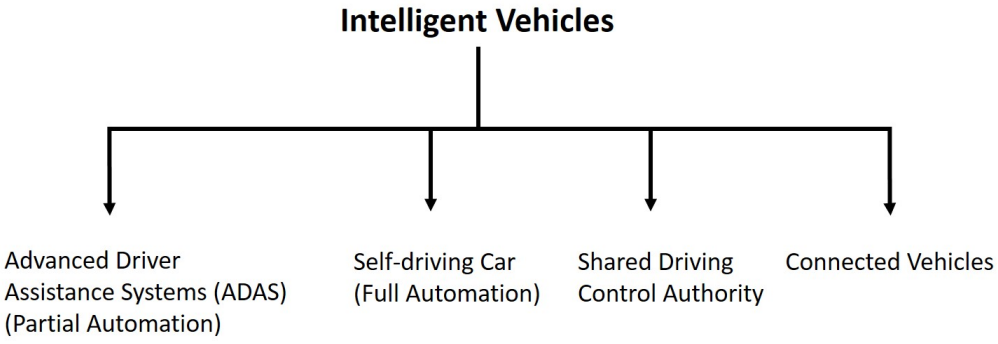

Figure 1.1 – Classifications of Intelligent Vehicles

1.2 Related Works

1.2.1 Autonomous Driving

This section provides an overview of different aspects of autonomous driving which will help to derive the functional limitations. These limitations can then be used to define the objectives of the shared control strategy.

ADAS has led to partial automation of the vehicle but these systems work for specific functionalities i.e. the systems are implemented differently for different automated functionalities like adaptive cruise control, lane keeping, lane changing, emergency braking, driver distraction warning etc. The evolution of ADAS led to the blending of these functionalities into a single system leading to fully autonomous driving. This single system will then handle all the functionalities necessary for safe and efficient driving including collision avoidance, handling vehicle dynamics to keep the vehicle stable, lane keeping/changing, adjusting the driving behavior according to the surrounding vehicles/pedestrians etc. The autonomous driving function can be divided into three functional categories namely environment perception, navigation/motion planning and vehicle control.

The final objective of fully autonomous driving is planned through achieved through series of levels defined by American SAE J3016 standard. These levels of autonomy (L0-L5) are designed with the aim to gradually increase the incorporation of automation in the vehicle. Currently most of the research is focused on the development of L3/L4 automation. Developing a fully autonomous driving system in an urban environment is the most challenging task for the researchers because of the unpredictable environment dynamics, traffic density, complex road infrastructure and less error tolerance with respect to decision making and collision avoidance.

The vehicle platform development for autonomous driving includes various subsystems of hardware and software targeted at different functionalities [Levinson et al., 2011]. It includes different functionalities such as environment perception, mapping, localization, traffic light detection, motion planning, vehicle dynamic modeling and control etc are presented. Other factors like hardware, software and the sensor calibration are also significant along with the algorithms for the overall development. Multiple sensors like LIDAR, cameras, RADAR and GPS are used to acquire the vehicle and environment states. Similarly, the current trends in the autonomous driving research are defined with respect to different methodologies and approaches used for the development of functionalities like environment perception [Yu et al., 2015], trajectory planning, mapping, localization, navigation [Alves de Lima and Corrêa Victorino, 2016] etc [Luettel et al., 2012].

The driving environment is very complex and there can be thousands of different driving scenarios and situations encountered. The expectation of the autonomous driving system to work smoothly in all kinds of situations add to the complexity of the algorithms of various functionalities. Hence, the researchers focus on developing a particular functionality for e.g. environment perception to the full extent. Environment perception includes sub functionalities like lane detection, object detection, object segmentation and tracking etc. Various methodologies have been developed in the past research [Zhu et al., 2017] using various frameworks and multiple sensors like LIDAR, Camera, RADAR etc. A sample comparison of the lane detection methodologies is shown in Fig. 1.2.

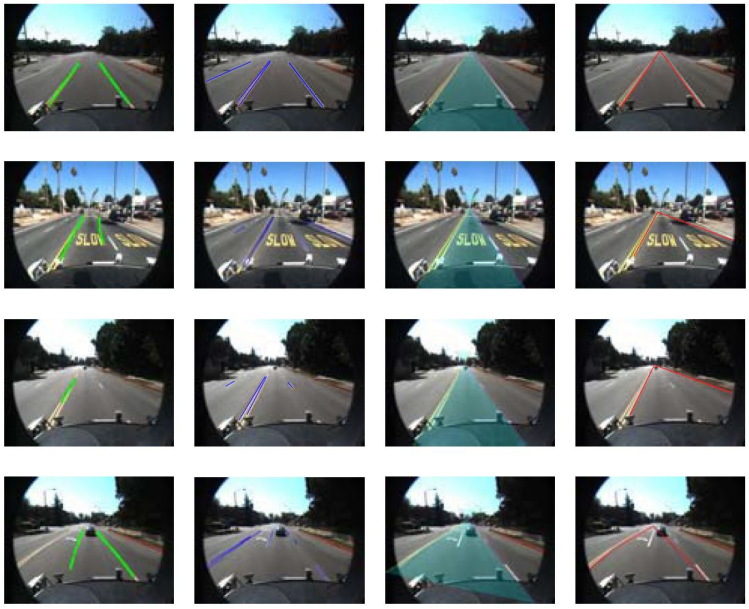

Figure 1.2 – Lane detection samples by these four algorithms. The first column is the RANSAC line fitting-based method results, the second column is the feature pattern-based method results, the third column is the Hough transform based method results, and the fourth column is the B-Snake-based method results. The first row is the frame=65, the second row is the frame=67, the third row is the frame=201, and the fourth row is the frame=222 [Zhu et al., 2017]

Simultaneous localization and mapping is an important part of the research in the development of autonomous driving system. Localization of the ego vehicle is important to perceive and assess the environment and further decision making. It is perceived as a state estimation problem. GNSS (Global Navigation Satellite System) is not sufficient to solve the localization problem because of the accuracy limits, signal degradation and unavailability of signals in different conditions. Different methodologies have been developed in the past research to solve the SLAM problem using various sensors and their data fusion [Bresson et al., 2017]. Trajectory or motion planning is another major functionality of autonomous driving system. The

environment around the ego vehicle is dynamic is nature and hence all the major functionalities are performed in closed loop. The planned trajectory is used by the vehicle control system for the implementation and tracking. Hence, it is important to plan the future vehicle trajectory in real time. One such motion planning strategy is presented in [Li et al., 2016a] which uses a hierarchical framework. A high level behavioral planner and a digital map is used to derive the future trajectory which is used as a reference for the low level control. The global architecture is shown in Fig. 1.3.

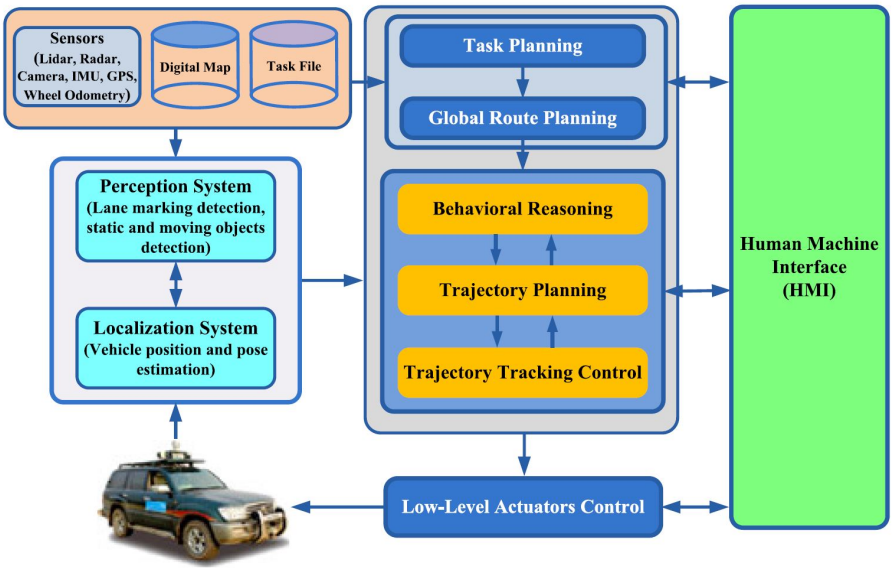

Figure 1.3 – Software system architecture [Li et al., 2016a]

Decision making can be viewed as the derivation of the trajectory and driving commands from the environment perception. Humans tend to perform this function very naturally. Due to a wide range of complex driving scenarios and situations, it is very challenging to build a single non-linear model or algorithm to perform decision making. It is very effective and efficient to learn this function for the human way of driving. Hence, machine or deep learning algorithms such as convolutional neural networks, reinforcement learning are widely and most commonly used for this learning as shown in [Li et al., 2018a], [Zhu et al., 2018a] and [Zhu et al., 2018b] respectively. The environment perception data acquired from different sensors is used as input for the convolutional neural network. In most of the cases, this data need not be transformed before forwarding it. In the case of reinforcement learning, the driving data is acquired and stored to be used later to recreate the driving scenarios in a closed loop environment.

The driving decisions are made mainly with respect to the environment, vehicle localization, location map and traffic laws. The motion planner have to use all

these entities to derive the future vehicle trajectory which is not only safe but also efficient with respect to time or fuel usage. In most of the methodologies, prebuilt HD maps are used but for the unknown environments, the maps need to be built separately. All the above mentioned entities can be combined in a single map which can then be used for the motion planning [Shim et al., 2015]. This unification makes the planned trajectory more efficient with respect to collision avoidance.

Driving is performed in the lane which need not be mentioned specifically and is by default embedded in autonomous driving with the help of lane detection algorithms. This adds to the vehicle localization. There are some exceptional use cases such as wet road surface or snow conditions etc where the conventional algorithms for road/lane detection and vehicle localization do not work (Fig. 1.4). Hence, separate algorithms are developed to build the localization system as presented in [Aldibaja et al., 2017] where the LIDAR data is enhanced and reconstructed using principal component analysis. The road edges from the LIDAR and map images are matched to improve the localization accuracy.

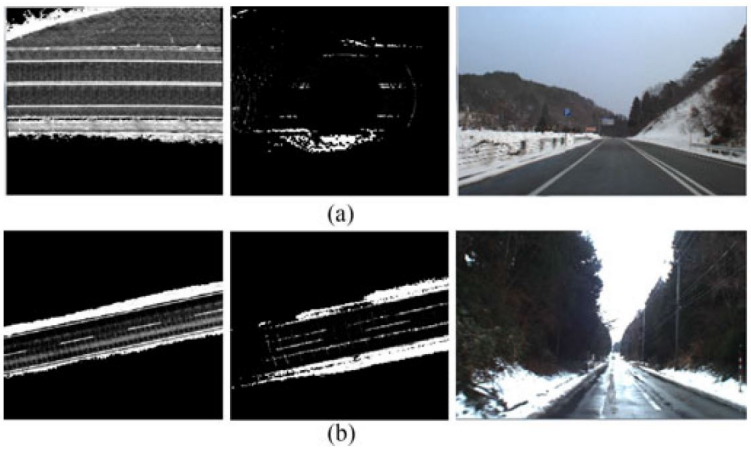

Figure 1.4 – Localization problems illustrated by map image, corresponding enlarged LIDAR image, and camera image. (a) Low LIDAR image quality because of wet ground. (b) Deformed road structure due to snow lines inside the lane [Aldibaja et al., 2017].

With the overall development of autonomous driving, the number of autonomous vehicles on the road will increase gradually. Hence, the autonomous vehicles will have to interact and cooperate with the surrounding vehicles with human driver as well as the pedestrians. It is necessary to understand the human drivers for the accurate interpretation of their driving actions which will then help in the decision making. These aspects of the autonomous driving are important because of the subjective human driving behaviors [Brown, 2017]. The development of the systems and algorithms are mainly approached from the robotics field perspective. There are certain areas where is development of autonomous vehicles deviate from

that of autonomous robots. One of the areas to be affected by autonomous vehicles is urban planning and related policies [Fraedrich et al., 2019]. The compatibility of the autonomous vehicles with respect to the urban transport objectives is explored. For e.g. the autonomous vehicle can disturb the plan to promote the use of public transportation but on the other hand shared autonomous vehicles might help and support the urban development strategies targeting pollution and traffic congestions. Human driving actions are not only defined by the intentions, perception and planning but also by the ethics. Human driver has a mutual understanding with other drivers or pedestrians for e.g. even if the pedestrian behaves incorrectly against the traffic laws, the human driver will adapt and adjust to the situation. This aspect is explored in [Goodall, 2016] for the autonomous vehicles.

Experimentation on a vehicle platform is essential for the autonomous driving system development. Embedded architecture is critical with respect to the implementation of algorithms [Belbachir, 2017]. These also include the installation of various sensors which are essential for the functionality but negatively influences the aesthetics of the vehicle. The common method is to use a conventional vehicle which is then modified for the purpose of implementation and experimentation. Hence, the modifications to a conventional vehicle should not only make the vehicle of driving autonomously but also make it aesthetically good. One such example of a vehicle platform for the research is presented in [Wei et al., 2013]. The research vehicle includes drive-by-wire systems such as brake, steering and gear selection actuation, control system, power system, sensor installation, perception system, user interface and the computing platforms necessary for the autonomous driving functionality.

1.2.2 Issues, Challenges and Human Factors

Considering the rapid progress in the autonomous driving system development, there are still many issues, challenges and unsolved problems associated with it. These need to be analyzed and resolved before getting the autonomous vehicles on road in the hands of public.

Considering the autonomous cars to be the high end objective in the evolution of ADAS, their performance need to be assessed in different aspects. The challenges faced in the development of autonomous driving can be divided into various categories like technical, non-technical, social and policy etc as shown in Fig. 1.5 [Hussain and Zeadally, 2019].

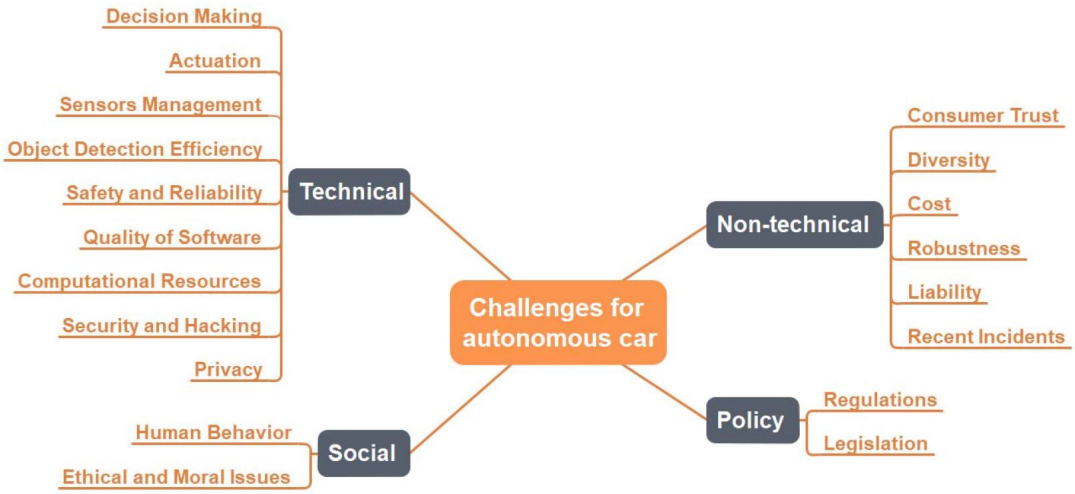

Figure 1.5 – Current and future challenges for autonomous cars [Hussain and Zeadally, 2019].

Aspect	Challenge	Implications	Possible solutions
Cost	• Hardware cost • Software cost • Management cost	• Reduction in car ownership • Adverse effect on business and auto industry	• Mass production will relax this issue
Maps	• Real-time map generation takes enormous computing resources • Storage overhead • Extreme weather conditions • Changing environment and road structures	• Poor mapping may jeopardize the functionality and maneuvers of autonomous cars • Need for more resources	• Big data solutions • Cooperative mapping through neighbors
Software Complexity	• Testing and validation • Requirements are not complete • Environmental complexity causes software instability • Software cost • Software security • Right-of-way provisions through software are difficult	• Delay in commercialization • Consumer trust is an issue • Investment risk to investors	• Driving profiles and fail-safeness • Focus more on AI and deep learning-based solutions
Simulation	• No universal simulator • Different simulators for different modules • Proprietary tools • Difficult to test all the requirements	• Incomplete testing and validation • Economic alternative for autonomous car testing • Validation of simulation results is hard	• Focus on open source tools • Make the data available for testing • A holistic approach is essential

Figure 1.6 – Summarized design and implementation challenges for autonomous cars [Hussain and Zeadally, 2019]

The future development of the autonomous driving technology is dependent on various factors such as robustness, safety, fail-safe functions, hardware, software and consumer. Hence, the design and implementation need to provide precision, reliability and especially safety. The main factor differentiating autonomous cars from autonomous robots is the inclusion of the human factors. From the point of view of implementation, the some of the aspects presenting challenges are cost, maps, software complexity and simulation. The cost of a single LIDAR sensor is 75,000 US dollars which is higher than the overall cost of a car. Sensor technologies are progressing in this area to optimize the sensor cost especially to make it viable for mass production. The challenges provided by these aspects along with their

respective implications and sample solutions are shown in Fig. 1.6 [Hussain and Zeadally, 2019].

Machine learning/Deep learning is the most common approaches used to develop the algorithms for environment perception, decision making and vehicle control. For the development of any automotive functionality for a given ECU (Electronic Control Unit), the functional requirements need to be provided precisely and in detail. Automakers follow the V-cycle for the development and validation of any automotive functionality. In the case of autonomous driving, the V-cycle can not be applied in a similar manner. This leads to the management challenges especially for the validation.

The application of deep neural networks to the development of autonomous driving has led to major advances with the use of data from sensors like camera, LIDAR, RADAR, GPS etc. Due to the new legislations, many researchers and companies have started to test their autonomous cars on public roads to fasten the process. The testing demonstrate unexpected or incorrect behaviors in driving scenarios/situations which may lead to collisions. Unfortunately, there have been some cases where the use of autonomous driving on public roads have led to fatality. These incorrect behaviors have been detected in a testing tool named DeepTest [Tian et al., 2018]. The tool generated driving situations with multiple driving conditions like rain, fog or lurring etc. A sample of the erroneous behavior is shown in Fig. 1.7.

1.1 original 1.2 with added rain

Figure 1.7 – A sample dangerous erroneous behavior found by DeepTest in the Chauffeur DNN [Tian et al., 2018].

The development of automotive functionality for the ECU is based on the safety standards such as ISO 26262 which assumes the human driver to be responsible for the overall safety of the driving [Koopman and Wagner, 2017]. In the case of autonomous cars, human driver is not always responsible for the safety. The reliance on the autonomous cars instead of human driver is a major change in the standard as compared to the ADAS functionalities in which the responsibility still

lies with the human driver. Thus the safety requirements in the case of autonomous cars will increase in a drastic manner. Hence, whether the standard ISO 26262 can be used for autonomous cars without any modifications is an open question. Reliability and safety go hand in hand. The validation/testing of the autonomous cars is being done in detail with thousands of driving situations encountered. The researchers target maximum mile coverage to cover maximum testing spectrum. The next logical questions relevant that need to be assessed and answered by the researchers [Kalra and Paddock, 2016] are:

• How many miles would autonomous vehicles have to be driven without failure to demonstrate that their failure rate is below some benchmark? This provides a lower bound on the miles that are needed.

• How many miles would autonomous vehicles have to be driven to demonstrate their failure rate to a particular degree of precision?

• How many miles would autonomous vehicles have to be driven to demonstrate that their failure rate is statistically significantly lower than the human driver failure rate?

As autonomous cars are being tested on the public roads in some countries like US, regulatory actions come into picture for safety factor. One such important regulatory action is to have a backup human driver in the case of disengagement from the autonomous driving mode. Separate data is collected to analyze these disengagements to observe the related trends like frequency, average mileage driven before failure etc [Favarò et al., 2018]. These factors play an important role especially in the development of level 3/4 autonomy where human driver need to be attentive and ready to take over the vehicle control whenever necessary. The collected data is analyzed over different factors such as different vehicles/companies, cause of disengagements, human factors, driving scenarios/conditions. A sample disengagement data is shown in Fig. 1.8 [Favarò et al., 2018].

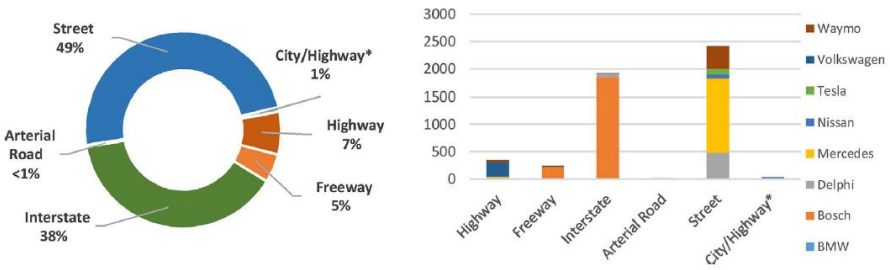

Figure 1.8 – Reported disengagement location breakdown and distribution by manufacturer. *Nissan reported location as both City and Highway 36 times. Total number of disengagements included n = 4977 (location not reported in 9% of the cases) [Favarò et al., 2018].

Autonomous cars are expected to increase safety and driving performance and simultaneously decrease the workload on the human drivers i.e. its development is centered around humans. Hence, human factors play an important role and the impact and influence on the humans need to be considered in the development. Human driving behavior is subjective in nature and the impact of the autonomy is also going to be subjective. Once the vehicle goes into autonomous driving mode, it is necessary to analyze the state of the human driver. One such study compared the impact of adaptive cruise control and automated driving [de Winter et al., 2014] which found that in the case of automated driving, the drivers are more likely to engage in different tasks (not related to driving). It was also found that the driver is not always active in monitoring the autonomous driving and signs of over-trust are observed in their behavior [Banks et al., 2018] i.e. drivers are happy to completely become hands and feet free and place hands on the wheels only in the case of warnings. These results are also affected by the familiarity of the human driver to the ADAS and autonomous driving functions [Naujoks et al., 2016].

Human factors research has also looked into the area of transitions in automated driving. Autonomous driving system currently may not be able to handle all kinds of driving situations in which human driver need to takeover vehicle control. The transition from autonomous to manual driving mode is critical from the point of view of vehicle safety and stability due to the conflict between human driver and autonomous system at the time of transition. This transition is not only associated with the driving states but also with the monitoring and control states. [Lu et al., 2016] studies these transitions using a framework by dividing the control transitions into different types for e.g. optional driver-initiated driver-in-control, mandatory driver-initiated driver-in-control etc. Another similar study focused on the driver behavior during and after transition based on the visual attention and alertness of the human driver [Merat et al., 2014]. The responsibility of the safe and smooth transition of the control to human driver thus fall on the autonomous driving system. More human factors related to the trust, acceptance, preferences and cost of automation, cognitive behavior etc have been explored in [Hulse et al., 2018], [Daziano et al., 2017], [Haboucha et al., 2017], [Kalra and Paddock, 2016], [Wen et al., 2011], [Ohn-Bar and Trivedi, 2016]. The influence of the autonomous driving system on the transportation policies also remain an open question [Bagloee et al., 2016], [Khan et al., 2012].

Thus, the path to have fully autonomous vehicles on public roads is still long. Hence, a different point of view need to be taken in this development to include human in the loop to compensate for the challenges and issues faced.

1.2.3 Human Robot Collaboration

One of the solutions to compensate for the limitations and errors of automated systems is to keep human in the loop. Human robot collaboration is critical for effective functioning because they have different control behaviors. Humans are adaptive and have better perception while robots are more precise and consistent in their performance. The main idea behind human-robot collaboration is to combine these individual skills to improve the performance and efficiency of the overall system. Robots assist the humans to reduce the workload and improve performance are termed as collaborative robots. Human-robot collaboration is not just limited to the field of robotics but has been applied in different fields of research in the past [Chandrasekaran and Conrad, 2015], [Ajoudani et al., 2018]. In this section, various aspects related to the human-robot collaboration in the field of robotics are explored.

Human-robot interaction plays an important role for the effective collaboration. Humans can naturally communicate the messages/actions through different gestures. Hence, gesture recognition techniques are very critical for creating an efficient shared working environment [Liu and Wang, 2018]. Data from multiple sensors act as an input for the gesture recognition techniques. The overall function consists of various sub-functions such as sensor data collection, gesture identification, gesture tracking, gesture classification and gesture mapping etc. Different techniques are used according to the sub-functionality for e.g. for gesture classification there have been advances in the use of machine learning techniques which provides high level of accuracy. The interaction between human and robot has to be both ways. As humans can communicate through different gestures, robots on the other hand can use haptic feedback to communicate effectively. The robots can also take corrective actions to assist humans. Humans are very good in perception. Hence, it is easy for the human to interpret the haptic feedback and the corrective actions associated with it. There can be various mediums to deliver the haptic feedback. The hardware interface used by the humans to express and implement their action is most commonly used for the feedback. In other cases, separate interfaces can be designed as demonstrated in [Scheggi et al., 2014] and [Scheggi et al., 2017].

The collaboration may lead to various issues especially related to human factors. Since the robots function in an assistance mode, these human factors issues are critical and need to be taken into consideration during the development of collaboration strategy. For e.g. guidelines can be developed for the incorporation of these issues in the human-machine interface design. These issues are dependent on the collaboration framework [Chen and Barnes, 2014]. For e.g. in the teaming

framework, the human-robot team performance is more sensitive to the complexity of tasks as compared to the human-human team. Similarly, in the mixed-initiative framework where the decision making is collaborative, it is challenging to communicate the individual intents and take them into consideration for final decision making.

The advances in the field of artificial intelligence especially machine learning have found applications in various research fields. Reinforcement learning is a type of machine learning where an optimal policy for the reward allocation depending on the learning action. Hence, the actions are selected to maximize the total reward. Reinforcement learning can be applied to the collaboration control strategy for learning optimal parameters of the model responsible for the decision making in a closed loop environment [Modares et al., 2016]. Machine learning has evolved to deep learning which can learn more complex tasks and requires not data transformations or preprocessing. Deep learning is adopted in the collaboration strategies mainly for functions like classification and recognition. The robots working with humans in the manufacturing sector need to recognize the intent and state of the human operator to assist effectively. The intent recognition through a detail human communication is an intensive task. Hence, deep learning can be used for body, hands, voice recognition etc to understand the human state and intent [Liu et al., 2018], [Dröder et al., 2018] thus leading to a smarter collaboration. A sample application of deep learning for the collaboration strategy is shown in Fig. 1.9 [Liu et al., 2018]. The human state can be defined by different parameters depending on the task for e.g. visual focus of attention [Das et al., 2015].

Using the human state and intent, the robot adapts to the human to provide necessary assistance or corrective actions. On the other side, the human operator is also observing the robot estimating the state and intent i.e. the human may also adapt or change the actions according to the robot behavior. This adaptation from both the sides may make the overall system unstable. A series of experiments conducted to test this phenomenon [Amirshirzad et al., 2019] showed that after an initial phase of difficult learning, the task execution performance improved when both are in charge and humans can easily adapt through learning the robot behavior to use it for maximum assistance.

1.2.4 Shared Control Authority

Shared control is a system that uses both user control and an automation component. Unlike semi-automated systems, the human and robot or AI act as peers

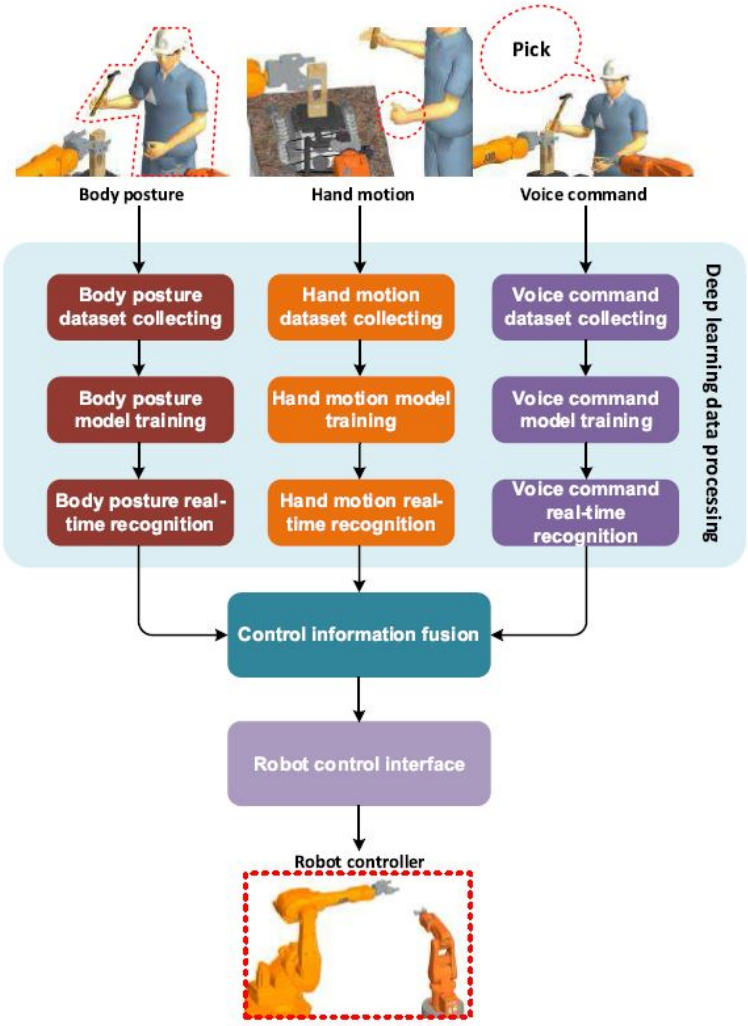

Figure 1.9 – Deep learning-based multi-modal control for human-robot collaboration [Liu et al., 2018].

and can act independently from each other. In this section, different approaches and applications of shared control are explored. Further detailed review of the shared control methodologies is presented in the later chapters.

The main objective of shared driving control is to keep the human driver in the loop. Shared control research and application emerged mainly in the field of robotics and can be perceived as an extension to human-robot collaboration. One of the focus of shared control is to assist the human to carry out particular tasks efficiently. Reduced mobility is one such application [Andreetto et al., 2017]. Older adults or humans with some disability face the challenge of mobility even with the use of walkers. The walkers are mechanical in nature and are not capable of providing any cognitive support. The presented solution added control through the electromechanical brakes on the rear wheels of the walker. The control authority is shared between the human and the hysteresis controller designed through the

modeling of the walker. The controller provides appropriate correction to the path with respect to the deviation from the reference path. The schematic representation of the shared control system is shown in Fig. 1.10.

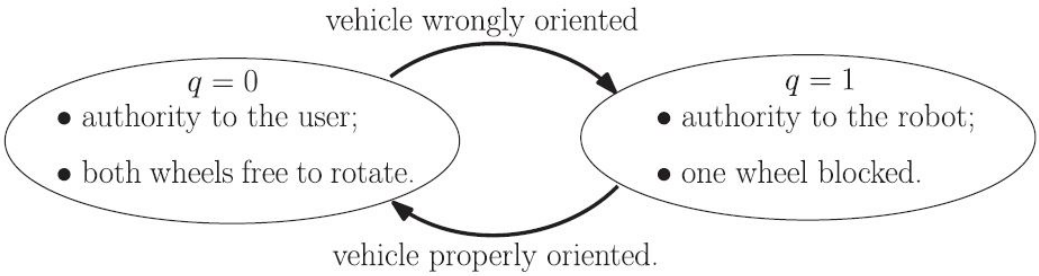

Figure 1.10 – Schematic representation of the shared control system. ([Andreetto et al., 2017])

Shared control system can be a human centered design i.e. the actions of the controller are dependent on the human intentions and necessity of assistance. One of the important aspects in shared control is the trust of human operator in the automation. This trust can be quantified as trust metric using a reward function or deviation from the reference output trajectory (defined by the human user). The shared control authority i.e. the human input is modified according to the trust parameter [Broad et al., 2017](Crane Automation). The shared control approach is represented by the control framework or architecture which defines the role of the human and automation. In some applications, these roles are defined in a hierarchical manner for e.g. in [Thomsen et al., 2019] (aerial vehicle navigation), human has the supervisory role while the automation is the low level controller for the implementation of the high level decisions.

Shared control has also medical applications for surgical function assistance [Nudehi et al., 2005] used mainly for training and mentoring the surgeons. A haptic feedback through an interface is essential considering the nature of assistance required. The feedback is proportional to the deviations from the proper actions during a surgical operation i.e the control authority is dependent on the level of surgical skills to minimize invasive surgical task. The shared control architecture is designed from the point of view of distribution of functionalities, parameters used (trust, self-confidence), final control input generation method, feedback interface for the human operator etc. Some of the shared control architectures used in robotics are shown in Fig. 1.11 and 1.12 [Musić and Hirche, 2017].

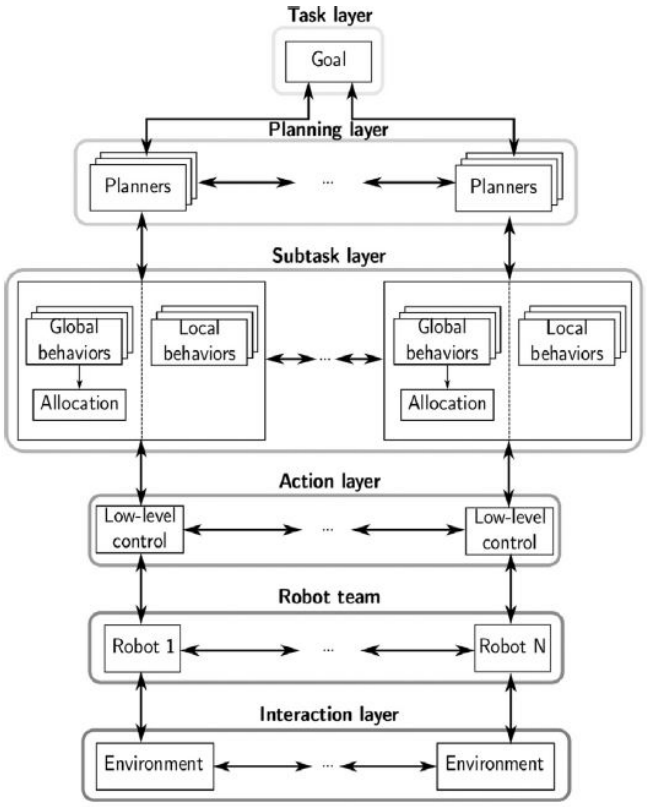

Figure 1.11 – Hierarchical control architecture for robot teams. Goal of the robot team is determined and monitored in the task layer . Based on the goal, a set of global and local behaviors are activated in the subtask layer through the planning layer. The outputs of this layer are control inputs for the low-level controllers of robots in the action layer [Musić and Hirche, 2017]

Similar to the robotics, shared control can contribute to the automotive field to reduce the workload of the human driver, improve driving safety and performance etc. There are multiple ways to achieve shared control between human driver and autonomous driving system. With the advent of autonomous driving functionality, the transition from autonomous to manual driving mode is critical from the point of view of vehicle safety and stability. The possibility of different driving intentions and lack of direct interaction between human and autonomous system adds complexity to these transitions. Haptic shared control can be used for the smooth transfer of control authority [Saito et al., 2018],[Kim and Yang, 2017] through the addition of shared control authority mode in the transition as shown in Fig. 1.13. [Wada et al., 2016] proposes a method for the smooth transfer of the steering control authority specifically in the situations where quick steering actions are required i.e. the transfer need to be achieved in minimum time.

The shared control strategy is highly dependent on the human driving intention which is very challenging to predict. Maintaining vehicle safety along with minimum deviation from the human driving intention is a challenging task. One way to

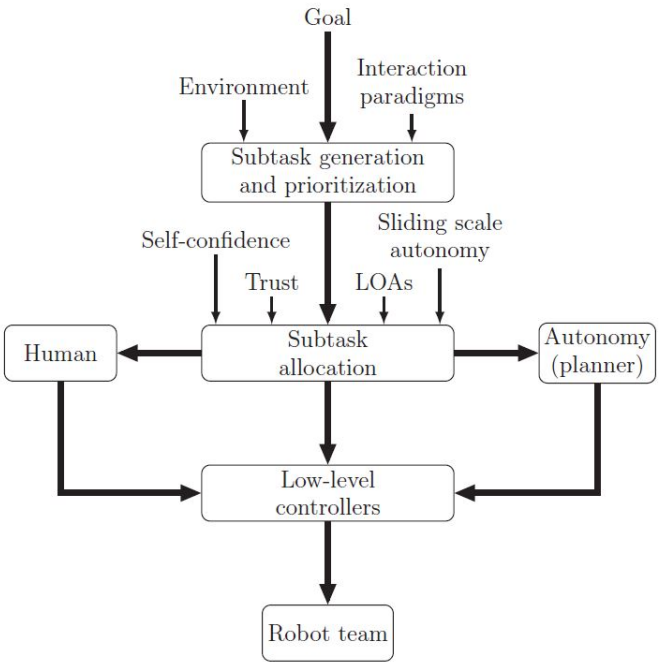

Figure 1.12 – Block structure of the general hierarchical shared control architecture for human-robot team interaction. Based on a desired goal of the interaction and the environment state subtasks are generated and prioritized. Allocation of subtasks to the human and the robot team is dynamical and determined depending on the available levels of autonomy , current self-confidence of the human and its trust in automation. Low-level controllers receive desired control inputs either from human or from the built-in robot team planners [Musić and Hirche, 2017]

achieve this is by assigning constraints on the human driving actions for safe driving. The human is free to operate within these constraints [Anderson et al., 2013]. These constraints can be applied to the position field or velocity search space of the vehicle. A sample of the shared control application using constraints is shown in Fig. 1.14 [Anderson et al., 2013].

Shared control can specifically be applied to steering or lateral control. The shared controller take corrective steering actions using the haptic feedback. The steering control authority is thus shared between human and automation. During manual driving the gaze behavior is highly correlated to the steering actions. During the shared control, the human driver can feel the change in the workload and control authority through the haptic feedback. This affect the correlation between the gaze behavior and steering actions. A respective study [Wang et al., 2019] shows reduction in this correlation with the increase in control authority of automation along with the reduction in lead time of gaze. This relationship can be useful for the effective shared controller design.

One of the solution to decrease the human workload and increase the trust in automation is driver initiated automation i.e. human driver will decide the to

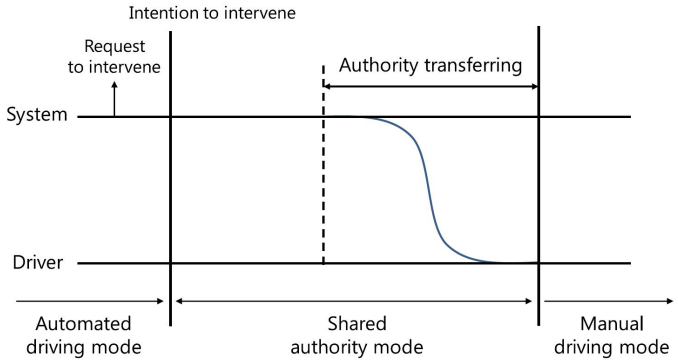

Figure 1.13 – Conceptual diagram of the authority transfer method via the shared authority mode [Saito et al., 2018].

accept or ignore the support from automation. The issues related to the driver initiated automation are studied in [Banks and Stanton, 2016] which observed that such approach does not improve the trust in the automation significantly. In fact, it may have negative effects such as increase in the response time to unexpected critical situations by 1-1.5 secs, reduced responsibility due to prolonged exposure to automation etc. With the long term use of shared control, human driver may get accustomed to it and hence the driving skills may be negatively affected over a period of time. Shared control authority can be designed not only to support human driver but also improve the driving skills as shown in [Wada et al., 2016].

The driving behavior of humans and autonomous system are very different leading to difference in the driving intentions. This leads to conflict between the two. The performance of the shared control is correlated to the handling of this conflict. The conflicts are not always desirable in every driving situations and need to be resolved over the period of time. Along with the quantification, the conflicts need to be categorized to handle them efficiently. Depending on the source and driving situation, sometimes it is challenging to resolve the conflict. In other words, it is not always desirable to give the control authority to a single operator in the case of high conflict [Itoh et al., 2016]. Conflict can be used as a parameter to define and optimize the performance of the shared control [Li et al., 2019].

The shared control can be designed with a targeted functionality such has obstacle avoidance [Li et al., 2018c], lane departure assistance [Chen et al., 2019] etc. For the obstacle avoidance assistance, the shared controller need to assess the situation to compute the final driving action. The final driving action determines the final intention. The difference between the human and final driving intention may lead to confusion for the human driver. Hence, the driving intention need to be incorporated in the computation of the final driving command. The shared controller design is usually dependent on the vehicle and driving behavior models.

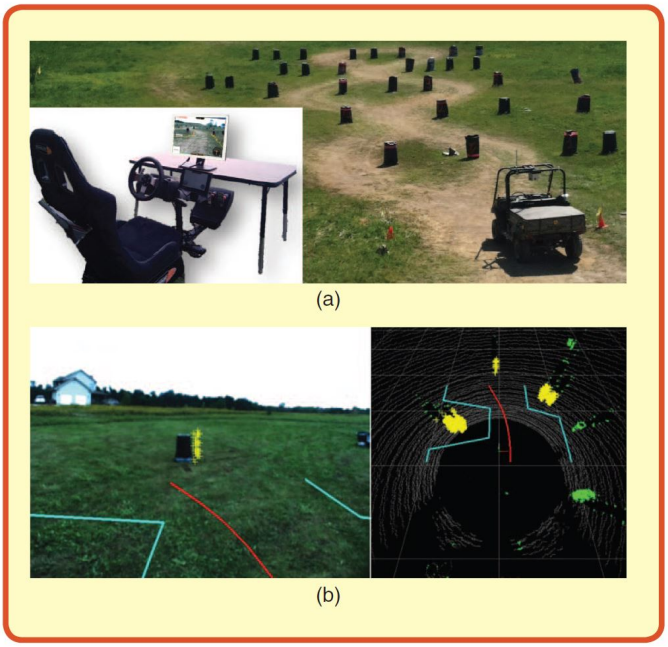

Figure 1.14 – Experimental setup (a), constraints (cyan) and MPC prediction (red) on video and LIDAR feed (b) [Anderson et al., 2013].

Hence, robustness of the shared control to the model output deviation is an add-on [Sadigh et al., 2019]. As mentioned previously, the autonomous driving system is prone to some malfunctions due to design, faulty sensors, weather and light conditions etc. The approach to assist human driver can be also be used to identify compensate for the malfunctions of the autonomous driving system. For e.g. if the autonomous driving system is not able to detect the obstacles, the human driver should be able to takeover the control [Soualmi et al., 2014a].

1.3 Objectives

The present work addresses the sensor-based shared control authority problem between the human driver and autonomous driving system (AutoSys). Considering the overall system development, following aspects are considered:

• **Fusion/Blending the driving inputs:** The fusion gives a much larger set/spectrum of possible final driving inputs as compared to the switching control between the two drivers. The division of the control authority would be equivalent to the fusion of the driving inputs. The shared control authority is viewed as division between manual and autonomous driving modes i.e. to fuse them to form a shared driving mode as shown in Fig. 1.15.

Figure 1.15 – An example of the division of control authority between human and autonomous driving system using fusion system

• **Handling Conflict:** The human driver and AutoSys are bound to have different driving intentions giving rise to the conflict between them. This conflict need to be resolved in the fusion process.

• **Collision avoidance:** This is one of the high priority tasks which is achieved through the assessment of driving inputs of both the drivers with respect to the vehicle and environment state. The assistance to the human driver is represented by the correction in the driving inputs.

• **AutoSys Error Compensation:** The AutoSys is considered to be in developmental stages i.e. it is bound to have some errors in the navigation system i.e. it is not free of collisions. For a given scenario, the probability of both human driver and AutoSys being wrong is very low. Hence, in the situations where the driving input of AutoSys is incorrect with respect to collision avoidance i.e. inadmissible, the shared control system should be able to compensate with a corrective input using the human driving input.

• **Manual driving refinement:** When the driving intentions of human and AutoSys are similar, the final driving command obtained from the fusion process should be a refinement of the human driving command, thus improving the driving experience of the human.

• **Human Centered Design:** The functioning of the shared control system should be surrounded around the human. In the situations, where the human driving intention is very different than that of AutoSys, the shared control system should become human-centric. With this functionality, the intelligent vehicle may also be termed as 'Human Centered Autonomous Vehicle'.

1.4 Context

This project is a part of a project network (15 projects) named 'ITEAM' (INTER-DISCIPLINARY TRAINING NETWORK IN MULTI-ACTUATED GROUND VEHICLES) funded by European Commission under the H2020 Grant agreement ITEAM No. 675999. Various universities and automotive OEMs are partners of this project

network (16 partners (8 Universities, 5 Companies, 3 Technological institutes) (Fig. 1.16).

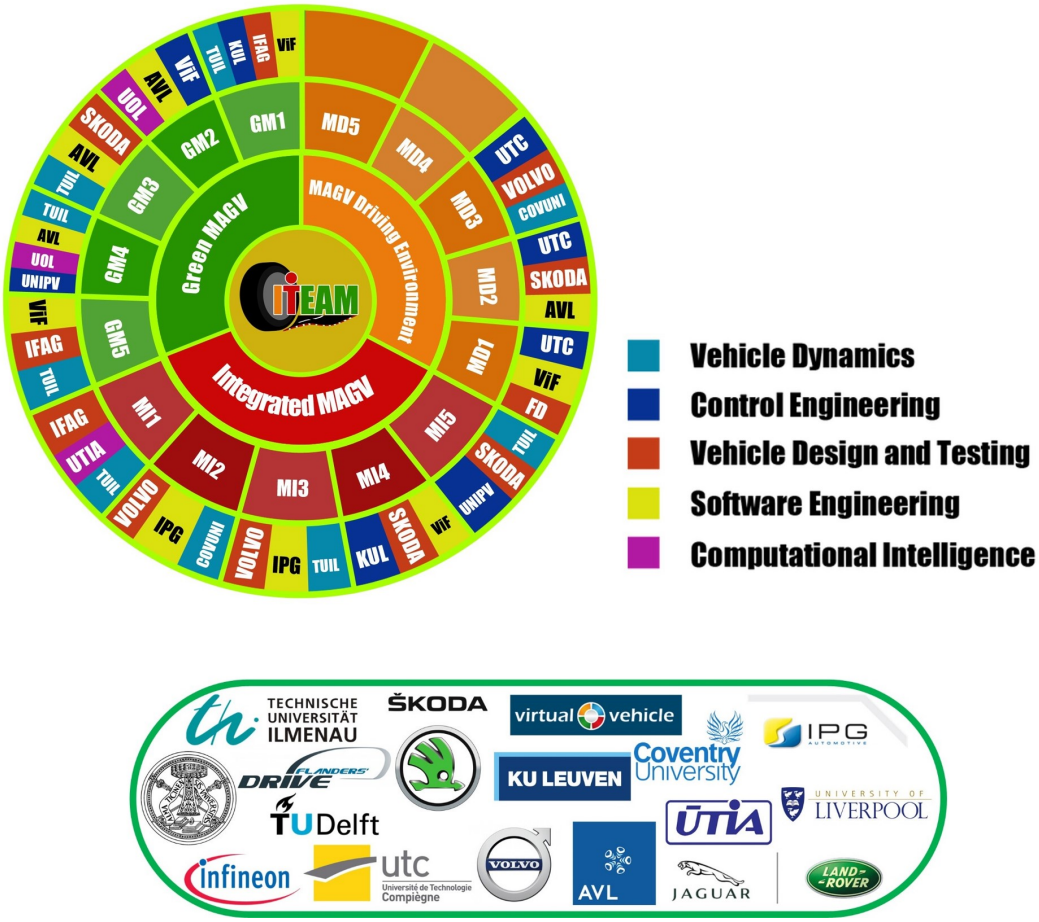

Figure 1.16 – Iteam Project Network and Partners.

1.5 Contributions

This work presents a sensor based shared driving control strategy for intelligent vehicles. With respect to the objectives mentioned earlier, the development of the shared driving control strategy is divided into various stages. We have proposed a fusion system approach i.e. a separate system for blending the driving inputs represented by intended vehicle speed and steering wheel angle: (v, θ). Human driver and AutoSys provide their driving inputs to the fusion system for the computation of the final driving input. The global architecture for achieving the shared control authority using fusion system is shown in Fig. 1.17. We have proposed a shared control framework with the aim of computing and minimizing the conflict between human driver and AutoSys. The flow diagram of the shared driving control is shown in Fig. 1.18.

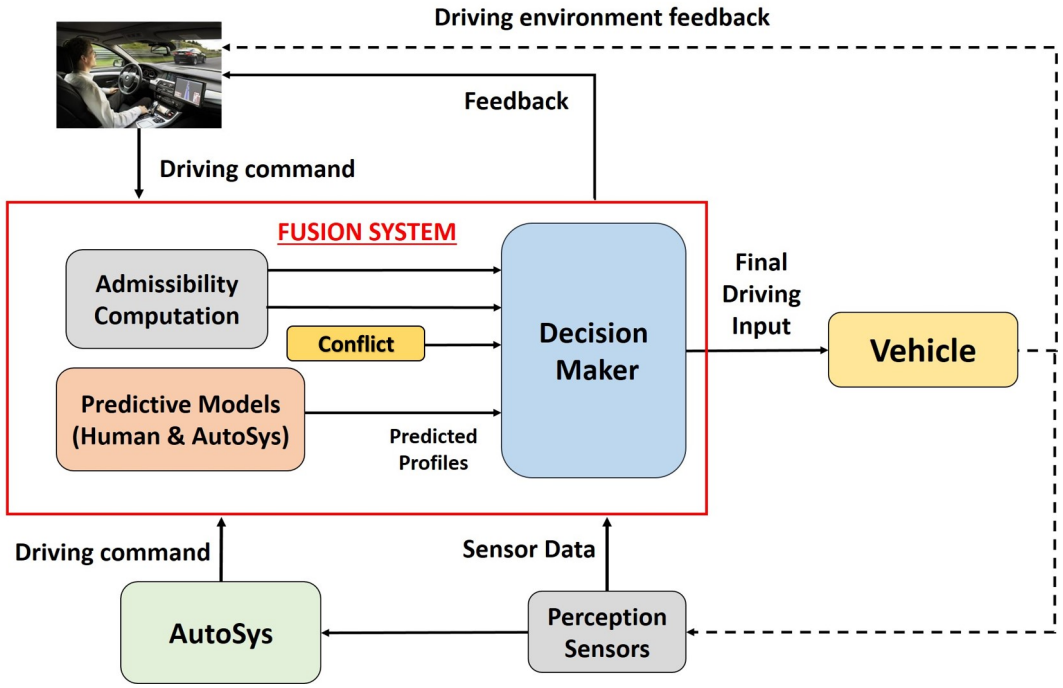

Figure 1.17 – Global Architecture for Shared Driving Control Authority.

The fusion system is divided into various sub-systems each carrying out a particular task/functionality. The conflict between human driver and AutoSys is computed using their individual driving inputs. The fusion is dependent on the driving input assessment with respect to the collision risk, speed limitation, lane/road departure prevention etc. We have proposed an algorithm to compute the admissibility of both the driving inputs. One of the major inputs to this algorithm is the environment data (probabilistic grid map) derived using the LIDAR sensor data. The admissibility of the driving input is calculated using Belief functions theory in terms of degrees of belief to add uncertainty to the output (admissibility).

Similar to the concept of predictive control, the final driving input is computed by looking into the future behavior of both human driver and AutoSys. A neural network based predictive model is developed to predict the driving inputs trajectory over a certain time horizon. A generic model structure is developed which can be applied for the prediction of both human and AutoSys driving behavior. In the case of availability of future intended behavior of AutoSys, this model is applied only for the human driver.

The final driving input is computed at the last stage of decision making using game theory. The conflict handling is perceived as a bargaining problem. A two-player non-cooperative game is proposed with the aim of conflict resolution, incorporating driving input admissibility, driving intention similarity etc. The bargaining solution represents the final driving input. The fusion system is considered

as a high level controller and a separate low level controller can be used for the tracking purpose. Necessary information is fed back to the human driver to avoid any confusion. The validation of individual sub-systems was carried out at Heudiasyc Lab, UTC using the test rig and simulation software MATLAB/Simulink, IPG CarMaker, SCANer Studio. The final closed loop integrated validation of the shared control strategy was carried out on the test rig using the simulation software MATLAB/Simulink, IPG CarMaker at Jaguar Land Rover at Coventry, UK.

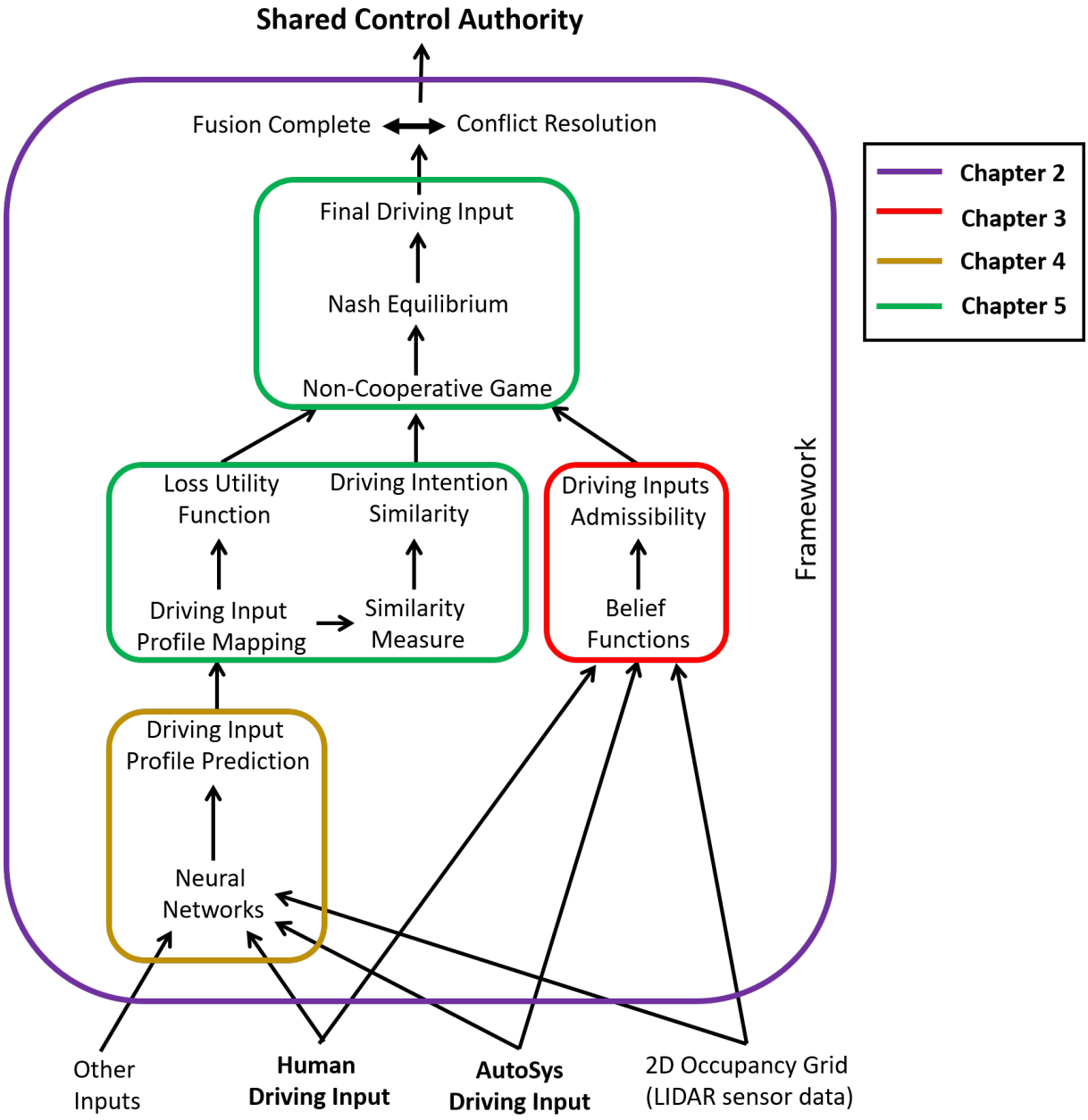

Figure 1.18 – Flow Diagram for Shared Driving Control Strategy Development.

1.6 Organization

Chapter 1 introduced to the topic, presented motivation, related works in the past research and proposed contributions. Chapter 2 presents the development of shared control architecture or framework. It also presents an analysis of the framework from a point of view of control based approach along with a case study application of shared control on simulated pendulum. Chapter 3 presents the methodology to compute driving input admissibility with uncertainty using belief functions theory and the validation results in a simulated environment. Chapter 4 presents the sensor based model development using neural networks for the driving input prediction. The chapter mainly comprises of model architecture, neural network design, training and validation in a simulated environment. Chapter 5 presents the decision making strategy using non-cooperative game theory along with the final closed loop integrated validation results of shared control strategy. The work is concluded in Chapter 6 along with some future work perspectives. The organization of the presented works with respect to a flow diagram is shown in Fig. 1.18.

1.7 Publications

The presented work has been published as follows:

- S. C. Jugade, A. C. Victorino and V. B. Cherfaoui, "Shared Driving Control between Human and Autonomous Driving System via Conflict resolution using Non-Cooperative Game Theory," 2019 21st International Conference on Intelligent Transportation Systems (ITSC), Auckland, New Zealand. (Accepted).

- S. C. Jugade, A. C. Victorino, V. B. Cherfaoui and S. Kanarachos, "Sensor based Prediction of Human Driving Decisions using Feed forward Neural Networks for Intelligent Vehicles," 2018 21st International Conference on Intelligent Transportation Systems (ITSC), Maui, HI, 2018, pp. 691-696. doi: 10.1109/ITSC.2018.8569441

- S. C. Jugade, A. C. Victorino and V. B. Cherfaoui, "Human-Intelligent System Shared Control Strategy with Conflict Resolution," 2018 IEEE 14th International Conference on Control and Automation (ICCA), Anchorage, AK, 2018, pp. 686-691. doi: 10.1109/ICCA.2018.8444218

- S. C. Jugade, A. C. Victorino, "Grid based Estimation of Decision Uncertainty of Autonomous Driving Systems using Belief Function theory," 15th IFAC Symposium on Control in Transportation Systems (CTS 2018), IFAC-PapersOnLine, Volume 51, Issue 9, 2018, Pages 261-266, ISSN 2405-8963. https://doi.org/10.1016/j.ifacol.2018.07.043.

- S. C. Jugade, A. Victorino and V. Cherfaoui, "Driving Decision Admissibility and its applications to ADAS" (Journal Paper, In preparation).

Shared Driving Control Architecture

Contents

2.1 Fusion System Approach

Human-Machine cooperation via shared control can be achieved in different ways. The main objective of such cooperation is to define a methodology to make the best use of both. One of the approach for the shared control is to incorporate the cooperation methodology in the autonomous driving system (AutoSys) i.e. the driving input or behavior of the human driver is taken into consideration by AutoSys to decide its individual driving input. Hence, the AutoSys adapts to the human driving behavior and takes necessary corrective action with respect to its reference (trajectory or driving profile). In such an approach, the final control of the vehicle can be given either to the human driver or AutoSys. When the final vehicle control is given to the human driver, the corrective actions of AutoSys are implemented through haptic feedback either to the pedals or steering or both. In the case where the final vehicle control is given to AutoSys, the methodology is referred to as indirect shared control.

The main drawback of this approach is that it limits the independent driving behavior of AutoSys. Also, there is a need for the interaction between the human driver and AutoSys to understand the individual driving intentions of each other. For example, consider the case of haptic steering control, the human driver senses the corrective action on the steering wheel but without proper and direct interaction, it is not possible to understand the driving intention of AutoSys. In such a case, the human driver tries to predict the driving intention or the necessity of the corrective action. The haptic feedback can also bring some discomfort to the human driver because of the intervention of AutoSys. In other words, the haptic feedback sometimes hinders the expression of human driving commands. In the case of indirect shared control, the human driver has the human driver has to rely on the AutoSys to take the final driving action. One of the objectives of shared control is to compensate for the driving inadmissibilities or errors especially in the high collision risk situations. Consider a driving situation where the human driving input is admissible while that of AutoSys is inadmissible. The assignment of vehicle control authority to AutoSys decreases the reliability on the system. Hence, the indirect shared control approach is reliable only if the driving inputs of AutoSys are admissible i.e. the autonomous driving is free of errors. Also the interaction between the two should be direct and free of any ambiguity.

Another approach to Human-AutoSys shared control is to define a cooperation strategy for example differential games [Flad et al., 2017]. The human driver and AutoSys work with respect to a objective function i.e. their individual driving behaviors are influenced directly through this function and the final driving

command is derived from the optimal solution. This approach is not realistic since the human driver do not operate nor can be trained to behave cooperatively with AutoSys in such a manner. Interaction between human driver and AutoSys is a challenging problem. There is a wide range of research related to the human factors and human-machine interaction relevant to this problem but still this remains an important issue (for e.g. [Abbink et al., 2012]).

In this project, the choice of shared control approach was considered with respect to following factors/functionalities:

• Retaining the independence of the individual driving behavior i.e. both the human driver and AutoSys can express their driving inputs independently without any intervention.

• Implementation of the corrective driving action without intervention.

• Removal of necessity of direct or indirect interaction between human driver and AutoSys.

• Should have the scope to compensate for driving errors of both human driver and AutoSys i.e. neither of them shall have direct control authority of the vehicle.

In this project, the shared control is achieved through the approach of fusion/blending of the individual driving inputs. With respect to the expected functionalities mentioned above, a separate fusion system is considered. The driving inputs of human driver and AutoSys are given to the fusion system along with other inputs. Fusion system computes the final driving command for the vehicle and has direct vehicle control. The driving input or command in the shared driving methodology is considered to be a vector of intended vehicle speed and steering wheel angle. The generalized block diagram of the fusion system approach is shown in Fig. 2.1. The fusion system along with the human driver and AutoSys can be perceived as a multi-agent system with a difference of human centered property (dependence on driving intention, admissibility). The human centric nature is a special case and explained in detail in the Chapter 5.

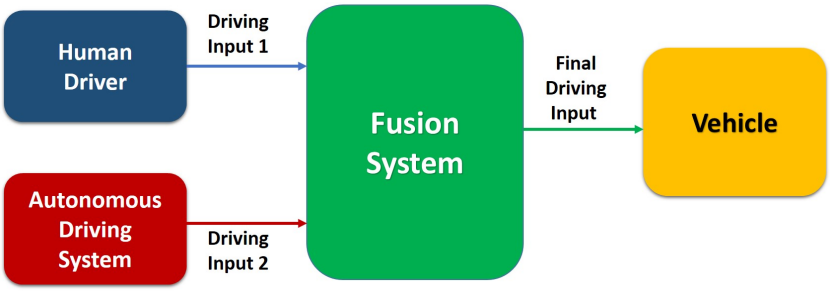

Figure 2.1 – Block diagram of Fusion system approach

The fusion process is dependent on different factors such as individual driving

inputs, sensor/perception data, road data etc. The final driving input computed by the fusion system might be different than the human driving input. Hence, to avoid any confusion, a feedback is provided to the human driver with necessary information related to the driving situation and fusion system decision. The I/O diagram of the fusion system is shown in Fig. 2.2. The LIDAR sensor data is used for computing the driving input admissibility and prediction of the driving behavior.The details of the use of this input are given in the later chapters 3 and 4 respectively. The turn indicator signal input is used for the driving behavior prediction (explained in Chapter 4).

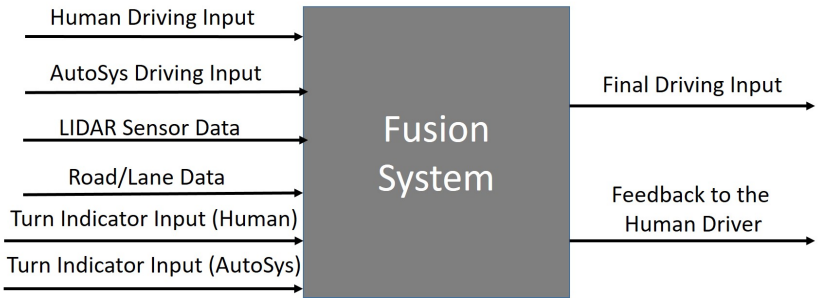

Figure 2.2 – I/O diagram of Fusion System

The main objective of the fusion of driving inputs is to compute the best final driving input and to compensate for individual driving inadmissibilities/errors. Human driver and AutoSys perceive the environment differently and have different driving behaviors. Human drivers are more adaptive while autonomous driving systems are more accurate and consistent. Given a driving scenario, the situation assessment and the decision making of human driver may differ from that of AutoSys. For example, consider a driving scenario with static obstacle. The high level driving intention of both human driver and AutoSys is to decelerate the vehicle and bring it to a halt but the nature of the intended deceleration profile might differ leading to a non-zero conflict. This conflict defines the objective for the fusion process. The increasing conflict in a given driving situation may lead to confusion and discomfort for the human driver. Hence, it is important for to regulate the conflict between the two. In our methodology, the conflict is defined as the difference in the driving inputs as shown in Eq. 2.1 where u_1 and u_2 are the driving inputs of human driver and AutoSys respectively.

$$Conflict(t) = u_1(t) - u_2(t) \tag{2.1}$$

2.2 Shared Controller

Fusion system has to regulate the conflict between the human driver and AutoSys to achieve the shared control. The final driving input is computed with respect to this regulation. Consider the conflict as a state of a system. A control problem can be defined for this state regulation. The control system designed for this purpose is referred to as shared controller. The diagram shown in Fig. 2.1 can be expanded as shown in Fig. 2.3. The conflict at any given time is computed according to the Eq. 2.1. Shared controller receives conflict as the input along with other inputs like individual driving inputs, perception data etc. The final driving input is the output of the shared controller given to a low level controller used for tracking purpose. The development of this low level controller is out of scope in this project.

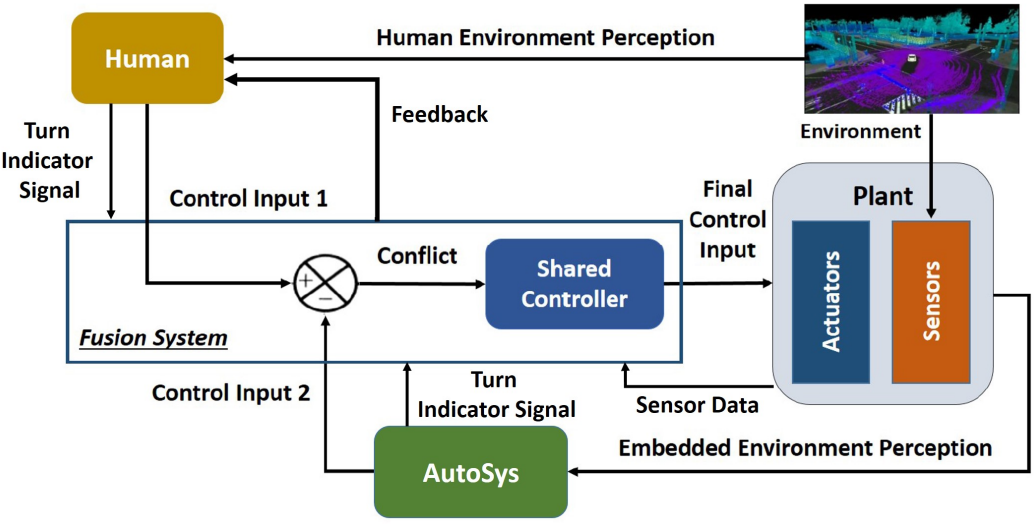

Figure 2.3 – Global Methodology for Shared Control

The global system (Fig. 2.3) is a closed loop system i.e. the final driving input at time t secs affects the conflict state at time $(t + 1)$ secs. Since the conflict is considered to be the state of the global system, the input to the shared controller is the state feedback. From the frame of reference of shared controller, the global system shown in Fig. 2.3 can be represented as shown in Fig. 2.4. The systems (plant and controller) shown in Fig. 2.4 is autonomous from the control theory perspective. The plant is the integrated system of subsystems like human controller, AutoSys controller, vehicle dynamics, environment dynamics etc. The mathematical modeling of this plant is given in the later sections of this chapter.

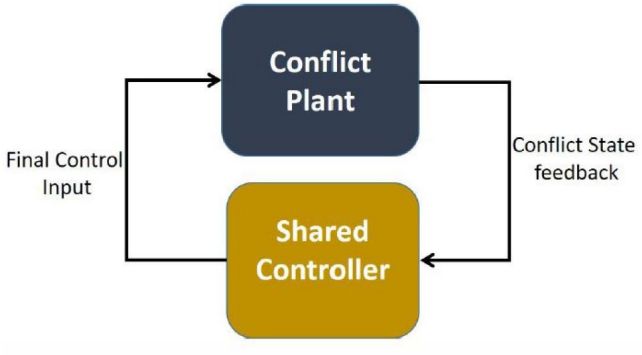

Figure 2.4 – Global System from the reference frame of Shared Controller

The conflict resolution is represented as the state regulation problem and the shared control is a state feedback control. Let I_{sc} and x_d be the output of the shared controller and conflict state respectively, then the control law for the state regulation is assumed to be of the form as shown in Eq. 2.2. Fig. 2.4 can be transformed to Fig. 2.5. The gain K can be computed through different control and decision making methods.

$$I_{sc}(t) = -K * x_d(t) \tag{2.2}$$

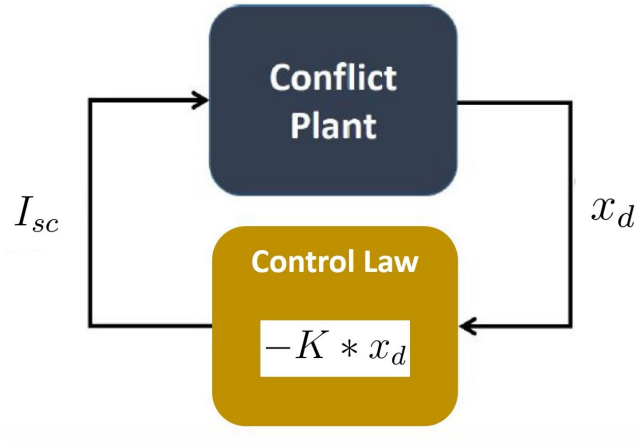

Figure 2.5 – Control Law for the conflict resolution

2.3 Conflict Plant Modeling

To derive a control law for the shared controller, the plant has to be mathematically modeled. The final driving input computed by the shared controller is implemented on the vehicle. The state of the ego vehicle changes in the next time instant according to this driving input and dynamics. The states of other vehicles in the environment change according to their respective driving commands

and intentions. The dynamics of the other vehicles is collectively referred to as environment dynamics. Similarly, the states of other vehicles is referred to as environment state. The states of the ego vehicle and the environment are correlated to each other. Hence, the plant system need a combined model representing ego vehicle and environment dynamics. This model is referred to as multi-actuated plant without loss of generalization. The change in the states of the ego vehicle and environment are perceived by the human driver and AutoSys based on which they provide their respective individual driving inputs. The conflict state for the next time instant $(t+1)$ is thus dependent on the final driving input at time t.

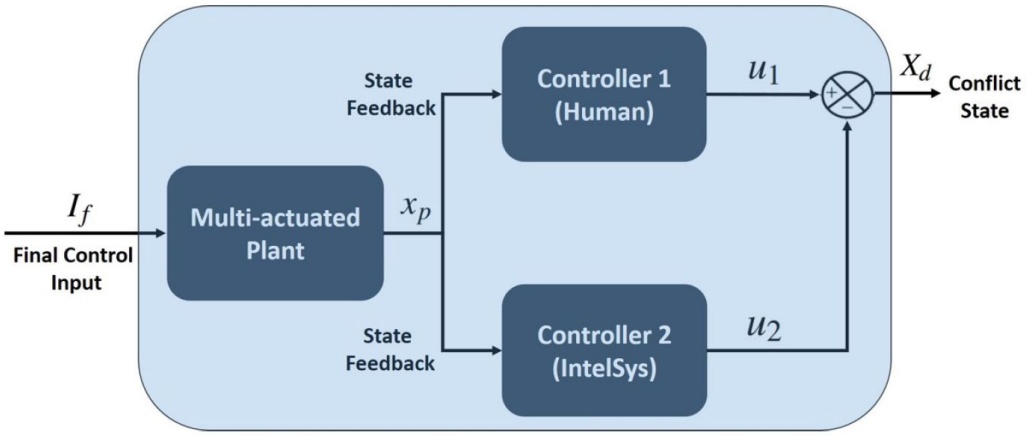

Figure 2.6 – Conflict plant system consisting of subsystems like multi-actuated plant representing vehicle+environment model, human driver and AutoSys control models.

The global plant for the shared controller is referred to as conflict plant. The input of this conflict plant is the final driving input and the output is the conflict. The conflict plant system consists of the integrated model of vehicle and environment referred to as multi-actuated plant and behavioral models of human driver and AutoSys referred to as controllers. The integration of these subsystems are shown in Fig. 2.6. The individual driving inputs u_1 and u_2 consists of intended vehicle speed and steering wheel angle. Hence, the global plant system with conflict as state is a second order system. The generic state space model for the conflict plant is derived for the analysis of the control law as follows:

Discrete State Space Conflict Model:

$$x_d(k+1) = A_d x_d(k) + B_d I_f(k) \tag{2.3}$$

Multi-actuated Plant Model:

$$x_p(k+1) = A_p x_p(k) + B_p I_f(k) \tag{2.4}$$

$$y_p(k+1) = x_p(k+1) \tag{2.5}$$

Controller 1 nonlinear and linearized Model (Control Input at time $k+1$):

$$u_1(k+1) = f_1(x_p(k+1)) \tag{2.6}$$

After linearization:

$$u_1(k+1) = M_1(x_p(k+1)) \tag{2.7}$$

Controller 2 nonlinear and linear Model (Control Input at time $k+1$):

$$u_2(k+1) = f_2(x_p(k+1)) \tag{2.8}$$

After linearization:

$$u_2(k+1) = M_2(x_p(k+1)) \tag{2.9}$$

Conflict State (at time $k+1$):

$$x_d(k+1) = u_1(k+1) - u_2(k+1) \tag{2.10}$$

For the conflict model, we have to relate $x_d(k+1)$ to $I_f(k)$.

Combining linear controller model and plant model i.e Equations 2.7 and 2.4:

$$u_1(k+1) = M_1(A_p x_p(k) + B_p I_f(k)) \tag{2.11}$$

$$u_1(k+1) = M_1 A_p x_p(k) + M_1 B_p I_f(k) \tag{2.12}$$

Similarly,

$$u_2(k+1) = M_2 A_p x_p(k) + M_2 B_p I_f(k) \tag{2.13}$$

Similarly, combining Equations 10 and 1:

$$\hat{x}_{p2}(k+2) = (A_p^2 + B_p M_2 A_p) x_p(k) + (A_p B_p + B_p M_2 B_p) I_f(k) \tag{2.14}$$

Combining the above equations with Local Difference Model (Equation 6 repeated below) (Difference at time $k+1$):

$$x_d(k+1) = u_1(k+1) - u_2(k+1) \tag{2.15}$$

$$x_d(k+1) = (M_1 - M_2)A_p x_p(k) + (M_1 - M_2)B_p I_f(k) \tag{2.16}$$

Hence,

$$x_d(k+1) = (M_1 - M_2)A_p x_p(k) + (M_1 - M_2)B_p I_f(k) \tag{2.17}$$

Similarly,

$$x_d(k+2) = (M_1 - M_2)A_p x_p(k+1) + (M_1 - M_2)B_p I_f(k+1) \tag{2.18}$$

Now plant model equation i.e. Equation 2.4 is:

$$x_p(k+1) = A_p x_p(k) + B_p I_f(k) \tag{2.19}$$

Combining Equations 2.19 and 2.18:

$$x_d(k+1) = (M_1 - M_2)x_p(k+1) \tag{2.20}$$

$$(M_1 - M_2)^T x_d(k+1) = (M_1 - M_2)^T (M_1 - M_2)x_p(k+1) \tag{2.21}$$

$$x_p(k+1) = ((M_1 - M_2)^T (M_1 - M_2))^{-1}(M_1 - M_2)^T X_d(k+1) \tag{2.22}$$

Combining Equations 2.18 and 2.22:

$$\begin{aligned} x_d(k+2) =& (M_1 - M_2)A_p((M_1 - M_2)^T (M_1 - M_2))^{-1}(M_1 - M_2)^T x_d(k+1) \\ &+ (M_1 - M_2)B_p I_f(k+1) \end{aligned} \tag{2.23}$$

Comparing to the following state space equation:

$$x_d(k+2) = A_d x_d(k+1) + B_d I_f(k+1) \tag{2.24}$$

$$A_d = (M_1 - M_2)A_p((M_1 - M_2)^T(M_1 - M_2))^{-1}(M_1 - M_2)^T \tag{2.25}$$

$$B_d = (M_1 - M_2)B_p \tag{2.26}$$

Discrete State Space Conflict model is given as:

$$x_d(k+1) = A_d x_d(k) + B_d I_f(k) \tag{2.27}$$

where

$$A_d = (M_1 - M_2)A_p((M_1 - M_2)^T(M_1 - M_2))^{-1}(M_1 - M_2)^T \tag{2.28}$$

$$B_d = (M_1 - M_2)B_p \tag{2.29}$$

2.3.1 Correlation between Vehicle, Environment and Conflict

Consider the Equation 2.20 as shown below. Let $x_p \in \mathbb{R}^n$, $x_d \in \mathbb{R}^2$, $M_1 \in \mathbb{R}^{2\times n}$ and $M_2 \in \mathbb{R}^{2\times n}$.

$$x_d(k) = (M_1 - M_2)x_p(k) \tag{2.30}$$

Let $M = (M_1 - M_2)$, then the above Equation can be given as:

$$x_d(k) = Mx_p(k) \tag{2.31}$$

The equation can be transformed as follows:

$$x_p(k) = M^T M x_d(k) \tag{2.32}$$

Hence,

$$x_d(k) = (M^T M)^{-1} x_p(k) \tag{2.33}$$

The matrix $M^T M$ is invertible if M has linearly independent columns. The matrices M_1 and M_2 represent the driving behavior of the human driver and AutoSys respectively. Hence, the matrix $M = (M_1 - M_2)$ represent the difference in the driving behavior or intention of the human driver and AutoSys. The linear independence of columns of matrix M is directly correlated to the difference in the driving behavior or intention. In most of the driving situations, the human driver

and AutoSys have different driving behaviors. Hence, for the purpose of analysis, we assume that the matrix $M^T M$ is invertible without loss of generalization.

2.3.2 Controllability and Stability

The global plant system is a second order system. The controllability matrix for the conflict plant can be given as follows:

$$C_{Conflict} = [B_d \quad A_d B_d] \tag{2.34}$$

Equations 2.28 and 2.29 can be rewritten as:

$$A_d = M A_p (M^T M)^{-1} M^T \tag{2.35}$$

$$B_d = M B_p \tag{2.36}$$

Substituting for A_d and B_d from Equations 2.35 and 2.36, we get

$$C_{Conflict} = [MB_p \quad (MA_p(M^T M)^{-1} M^T)(MB_p)] \tag{2.37}$$

After reduction,

$$C_{Conflict} = [MB_p \quad MA_p B_p] \tag{2.38}$$

$$C_{Conflict} = M[B_p \quad A_p B_p] \tag{2.39}$$

Let C_P be the controllability matrix of the Vehicle + Environment system, then the above Equation can be written as:

$$C_{Conflict} = M[B_p \quad A_p B_p] \tag{2.40}$$

The global system is said to be controllable if the matrix $C_{Conflict}$ is of full rank.

In the control theory, the stability of the system is defined with respect to the regulation of the states. In the global plant system, the conflict is considered to be the state. The interpretation of the stability of the global plant system is different from the conventional interpretation of the general plant. The global plant system is stable if and only if the conflict can be resolved. With respect to the state feedback control, the stability of the global system is defined using the eigenvalues of the matrix $(A_d - B_d K)$ i.e. the system is asymptotically stable if the controllable eigenvalues are negative. The matrix $(A_d - B_d K)$ is given as follows:

$$(A_d - B_d K) = M(A_p(M^T M)^{-1} M^T - B_p K) \tag{2.41}$$

2.4 Conflict Resolution: An Optimal Control Problem

The conflict resolution problem is dependent on the individual driving intentions of the human driver and AutoSys. Given the driving inputs to be admissible, the fusion of the driving inputs through conflict resolution is possible only if the individual driving intentions are similar. For example, consider a driving situation where the human driver intend to accelerate while AutoSys intend to continue with constant vehicle speed. The individual driving intentions in this situation are dissimilar. Hence, the fusion of the driving inputs is not compatible. Consider another scenario where both human driver and AutoSys intend to decelerate but the rate of deceleration differ by a large margin. Hence, the driving inputs are considered to be compatible for fusion only if they are similar. The phenomenon of compatibility is explained in detail in the later chapter using quantification of the similarity between the individual driving intentions through a similarity measure.

Consider the driving inputs to be compatible for fusion with respect to the similarity of driving intentions. The control law is considered to be of the form $-K * x_d$ where is the control gain K for the system. This gain can be computed through various methods. We have described here a sample computation of the gain using an optimal control method. The conflict resolution is formulated as an LQR problem. The driving input is considered to be of the form (v, θ), where v and θ are the intended vehicle speed and steering wheel angle respectively. Let the control input is $I_f \in \mathbb{R}^2$, then the cost function for the conflict resolution i.e. LQR problem for the time horizon N secs can be given in Equation 2.42. The time horizon considered for the optimization is equivalent to the horizon over which the linearization of the nonlinear subsystem models of the conflict plant system are valid. The minimization of this cost function leads to the conflict resolution. The final objective is to minimize the conflict state x_d value to zero. The conflict state x_d may also take negative values. Hence, a lower threshold need to apply to the cost function solution in the form of a constraint as shown in Equation

$$Cost = x_d(N)^T S x_d(N) + \sum_{i=1}^{N} (x_d(i)^T Q x_d(i) + I_f(i)^T R I_f(i)) \tag{2.42}$$

$$x_d \geq 0 \tag{2.43}$$

2.5 Driving Behavior Model Uncertainty

The conflict plant system consists of different subsystems which need to be mathematically modeled. The generic models of the subsystem used in the modeling of the conflict plant system are considered nonlinear in nature which are then linearized. Hence, these linearized models of various subsystems are time variant. The modeling of the driving behaviors of human driver and AutoSys is one of the major challenges due to their subjective nature. Hence, the driving behavior model can be expected to deviate from the actual driving behavior i.e. certain uncertainties and modeling errors need to be considered. The effect of this deviation on the development and the global system (conflict plant + controller) is analyzed.

Consider the actual and estimated driving behavioral model (linearized) of the human driver as given in Equations 2.44 and 2.45. The driving behavioral model (linearized) for the AutoSys is given in Equation 2.46. With respect to these equations, the actual and estimated conflict state is given in Equations 2.47 and 2.48.

$$u_1(k) = M_1 x_p(k) \tag{2.44}$$

$$\hat{u_1}(k) = \hat{M}_1 x_p(k) \tag{2.45}$$

$$u_2(k) = M_2 x_p(k) \tag{2.46}$$

$$x_d(k) = u_1(k) - u_2(k) = (M_1 - M_2)x_p(k) = M x_p(k) \tag{2.47}$$

$$\hat{x_d}(k) = \hat{u_1}(k) - u_2(k) = (\hat{M}_1 - M_2)x_p(k) = \hat{M} x_p(k) \tag{2.48}$$

Combination of Equations 2.47 and 2.48 result in Equation compare.

$$(\hat{M}^T \hat{M})^{-1} \hat{x_d}(k) = (M^T M)^{-1} x_d(k) \tag{2.49}$$

Let the estimated model of the conflict plant be given as:

$$\hat{x_d}(k+1) = \hat{A}_d \hat{x_d}(k) + \hat{B}_d I_f(k) \tag{2.50}$$

The control gain K designed for the estimated conflict plant model ensures that the eigenvalues of $(\hat{A}_d - \hat{B}_d K)$ are negative i.e. the conflict state (estimated) $\hat{x_d}$ is reduced to zero from a non-zero initial state.

2.6 Case Study Example

The shared control framework had to be validated on a plant/system with a well-known behavior which will help the validation process. Hence, inverted pendulum system is considered for this purpose as shown in Fig. 2.7.

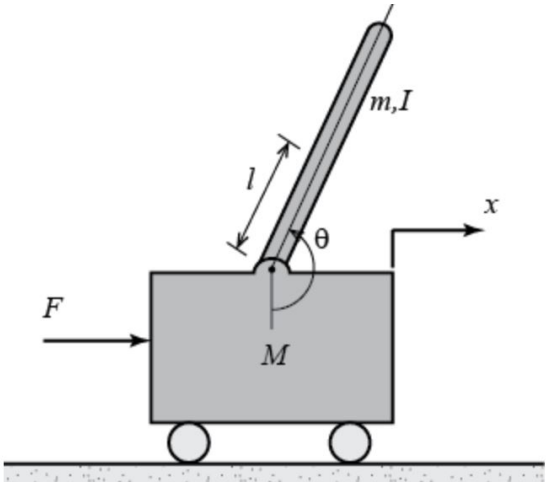

Figure 2.7 – Inverted Pendulum Configuration

The input to the inverted pendulum is Force F. x is the displacement and ϕ is the angular deviation from the vertical position of the pendulum. Pendulum angle from vertical (down) is given by θ and $\theta = \pi - \phi$. Applying the Newton's law, and considering numerical constant values for the parameters M, m, l and g, the model is given as follows:

$$\begin{bmatrix} \dot{x} \\ \dot{\phi} \\ \ddot{x} \\ \ddot{\phi} \end{bmatrix} = \begin{bmatrix} 0 & 1 & 0 & 0 \\ 0 & -0.1818 & 2.673 & 0 \\ 0 & 0 & 0 & 1 \\ 0 & -0.4545 & 31.18 & 0 \end{bmatrix} \begin{bmatrix} x \\ \phi \\ \dot{x} \\ \dot{\phi} \end{bmatrix} + \begin{bmatrix} 0 \\ 1.1818 \\ 0 \\ 0.4545 \end{bmatrix} u_f \tag{2.51}$$

The main goal is to bring the state to zero by considering control inputs of the human and IntelSys (Intelligent Control System). The final control input is calculated by the fusion between Human and IntelSys using the fusion methodology described earlier. All the components in the global methodology are simulated in MATLAB/Simulink. The fusion system is expected to provide final control input which is not only optimal but also admissible since there is a direct relation between the conflict resolution and admissibility of final control input. Hence, the selection of inverted pendulum (unstable system) is very beneficial. Any inadmissibility in the final control input will make the system unstable. The performance of the fusion

system is validated by comparing it with the individual performances of human and IntelSys controllers as shown in the simulation setup in Fig. 2.8. Q and R matrices for the shared controller can be selected depending on the requirement of the conflict resolution.

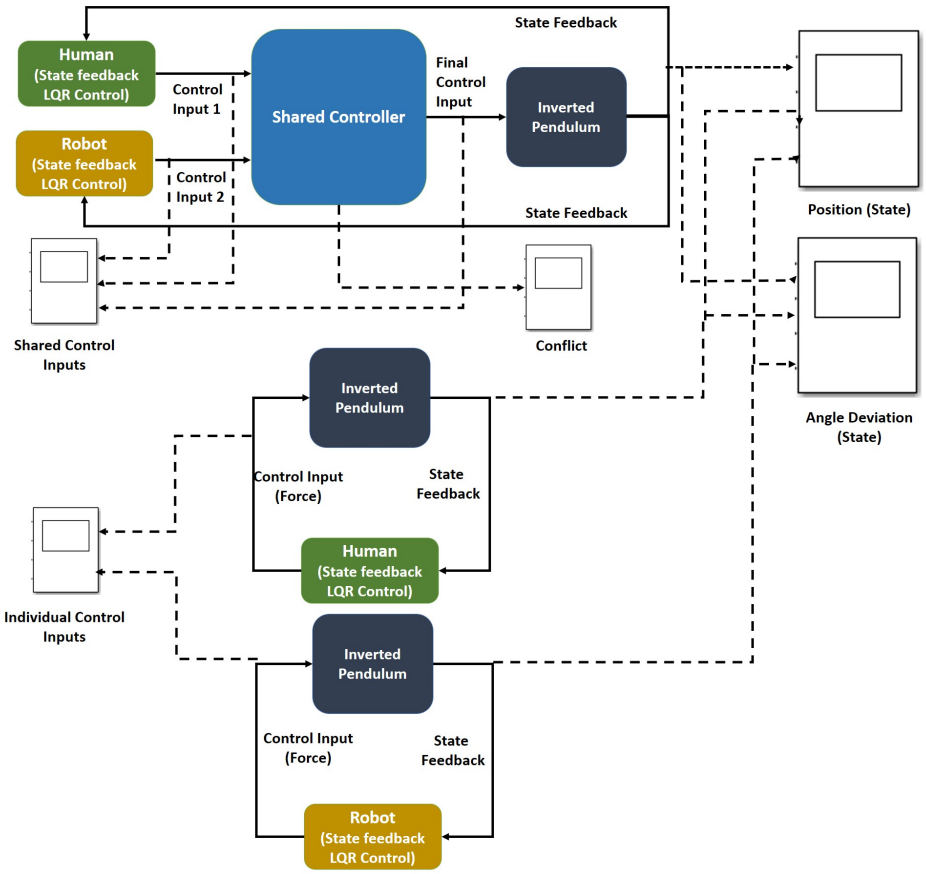

Figure 2.8 – Validation Setup in MATLAB/Simulink

High level use cases for the validation are shown in Table 2.1. Inadmissibility is introduced in the human and IntelSys control inputs by modifying the control model parameters. Since the human and IntelSys are simulated as optimal controllers (LQR), inadmissibility is introduced by modifying the optimal gain. Parameters used in the cost function for conflict resolution are: $Q_d = 10$ and $R_d = 7$ which are fixed using manual tuning.

Case	*Human Input*	*IntelSys Input*	*Conflict Model*
1	Admissible	Admissible	Match
2	Admissible	Admissible	MisMatch
3	Inadmissible	Admissible	MisMatch
4	Inadmissible	Inadmissible	MisMatch

Table 2.1 – Use Cases for the Shared Control Validation

Use case 1:

Human control model parameters: $Q_h = 50I_{4\times4}$, $R_h = 2$. IntelSys control model parameters: $Q_r = 2I_{4\times4}$, $R_r = 10$.

In this use case, the shared controller uses the actual conflict state value for the calculation of final control input. Fig. 2.9 shows the conflict profile. The conflict value is reduced to zero and remains steady at the zero level. The time required for the conflict state to come to zero is dependent on the Q and R matrices used by the Shared controller. Fig. 2.10 show the inverted pendulum state profiles for shared and independent control by human and IntelSys. The difference in the control behavior of human and IntelSys can be seen through the difference in the state profiles. The nature of the state profile of shared control is not only dependent on the human-IntelSys control behavior but also on the Q and R matrices used by the shared controller. The state profile in the case of shared control is better than that of independent control by human and IntelSys.

The control input profiles of human and IntelSys in Fig. 2.11 (with shared control) and Fig. 2.9 (without shared control) are different. In the case of shared control, through the final control input, the next state of the inverted pendulum is selected in such a way that the conflict state value would come closer to zero. The effect of the fusion system on the human and IntelSys behavior is clearly seen in these profiles.

Use case 2: IntelSys control model mismatches with that used for conflict model but its control inputs are admissible. Human control model parameters are same as in Use Case 1. IntelSys control model parameters (used in conflict model): $Q_{r1} = 2I$, $R_{r1} = 50$. IntelSys control model parameters (actual): $Q_{r_2} = 20I$, $R_{r2} = 6$. The simulation results for this use case are shown in Fig. 2.12, 2.13 and 2.14. The shared controller successfully resolves the conflict and brings the inverted pendulum to the zero state. The shared controller uses actual conflict state value.

Use case 3: In this use case, human control inputs are inadmissible while that of IntelSys are admissible. Hence, predicted conflict state is used to compute the final control input instead of actual conflict state. Inadmissibility is introduced by inverting the sign of human LQR optimal gain and hence that of control input. Simulation results are shown in Fig. 2.15, 2.16 and 2.17. Comparing the control input profiles of human in the case of shared control and individual control, it can be seen that the shared controller through its closed loop control manages the human control input in such a way that the inverted pendulum should remain stable and come to a zero state. This is possible because the shared controller uses the predicted conflict state $\hat{X}_d$ instead of actual conflict state X_d for the calculation of final control input. Thus, it ignores the inadmissible human behavior.

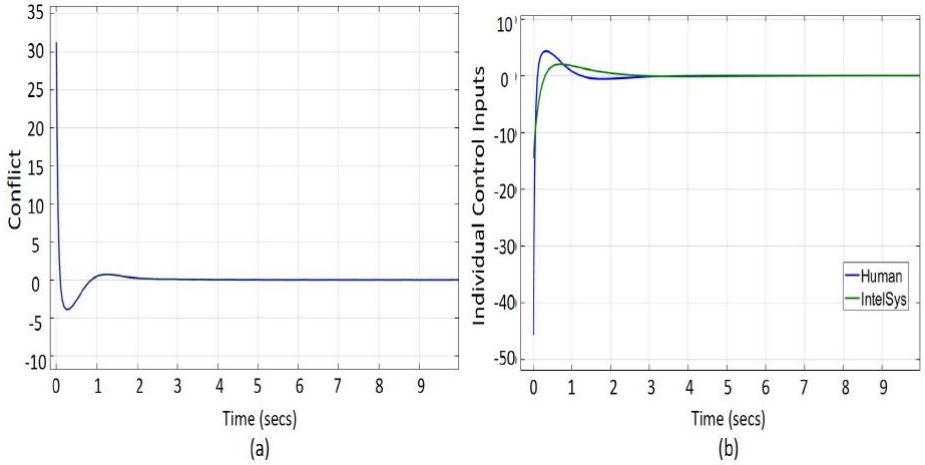

Figure 2.9 – Use Case 1: (a) Conflict (Actual) Profile. The conflict value is reduced to zero and remains steady at the zero level. The time required for the conflict state to come to zero is dependent on the Q and R matrices used by the Shared controller.

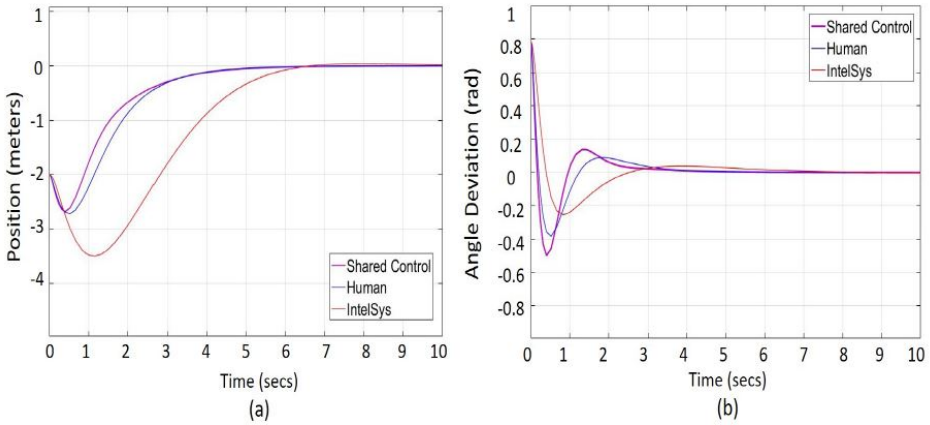

Figure 2.10 – Use Case 1: Position (state) Profiles (a) and angle deviation (state) Profiles (b) for the cases of shared control and independent control by human and IntelSys. State profile is improved in the case of shared control, (b) Individual control Inputs of human and IntelSys in the case of independent control.

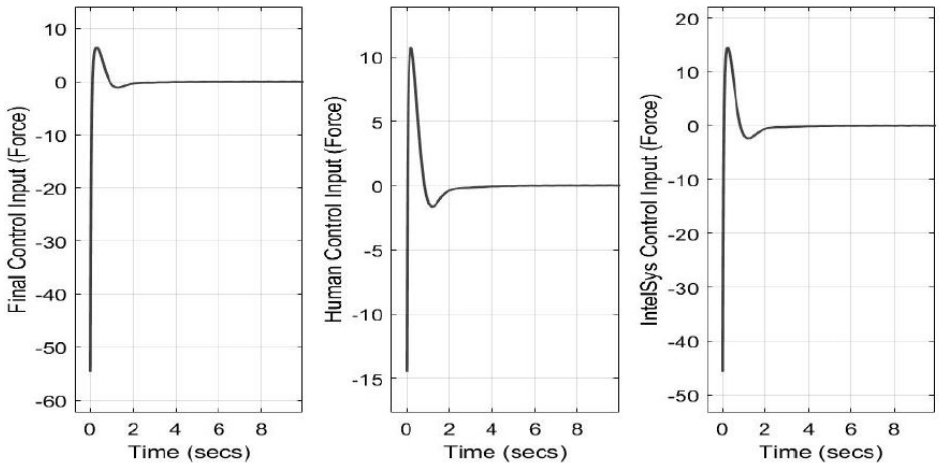

Figure 2.11 – Use Case 1: Shared Control input profiles of human, IntelSys and fusion system (final control input). Similarity in the profiles of human and IntelSys is due to the conflict resolution.

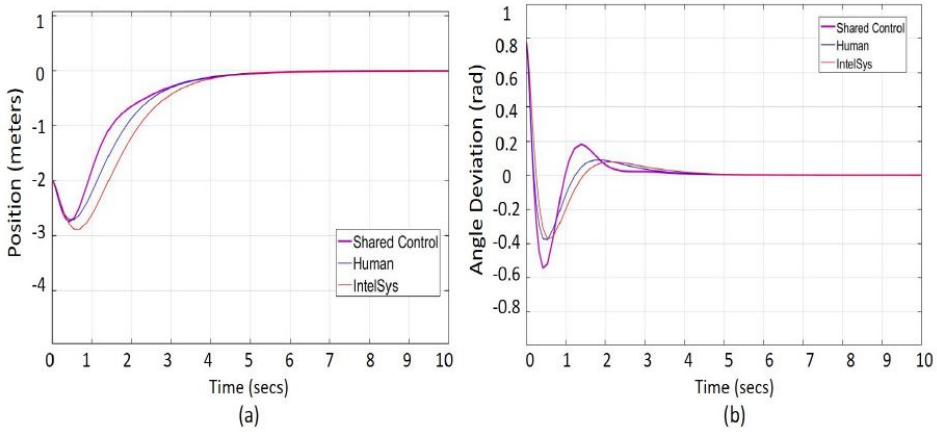

Figure 2.12 – Use Case 2: Position (state) (a) and angle deviation (state) (b) profiles for the cases of shared and independent control by human and IntelSys.

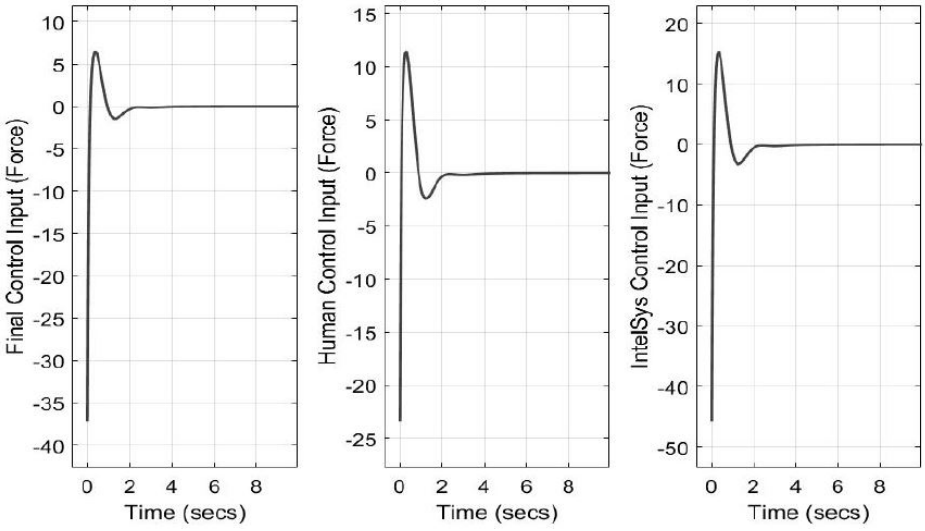

Figure 2.13 – Use Case 2: Shared Control input profiles of human, IntelSys and fusion system (final control input).

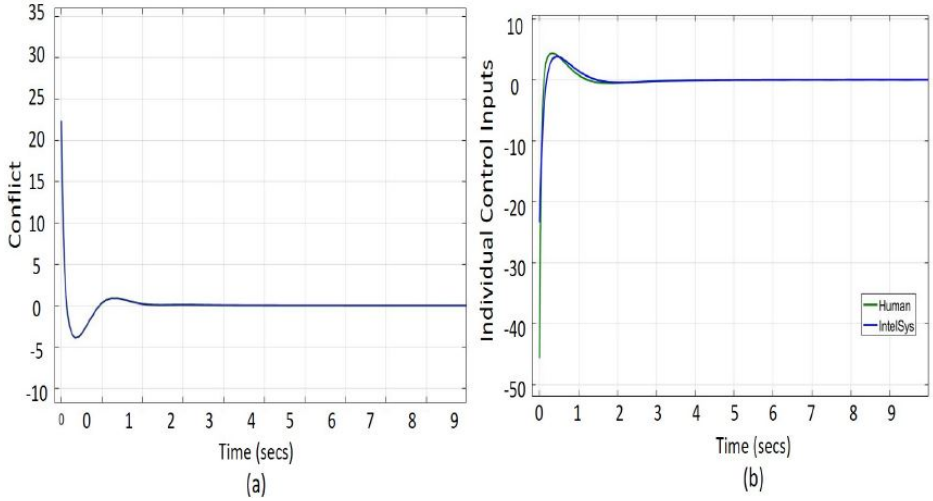

Figure 2.14 – Use Case 2: Conflict (Actual) Profile (a), Individual control Inputs of human and IntelSys in the case of independent control (b).

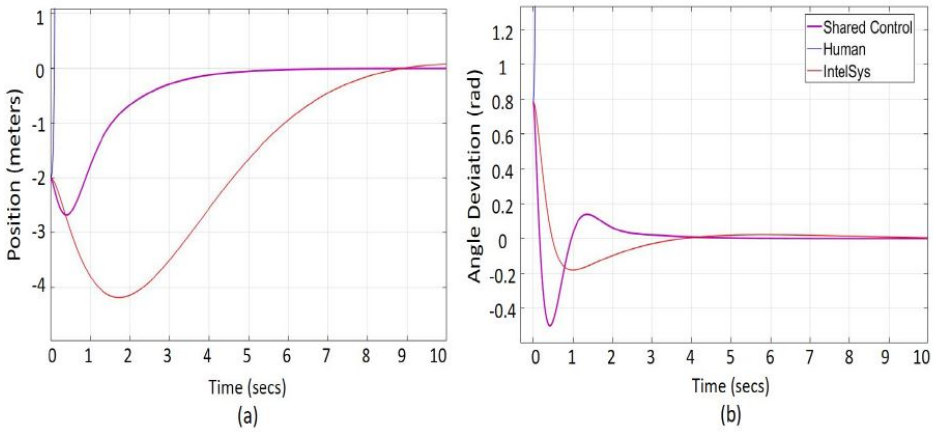

Figure 2.15 – Use Case 3: Position (state) (a) and angle deviation (state) (b) profiles for the cases of shared and independent control by human and IntelSys.

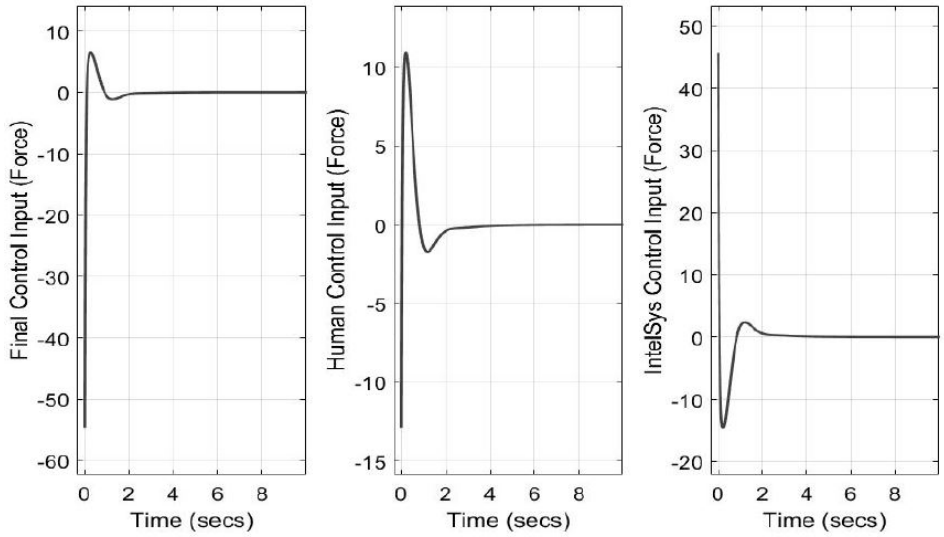

Figure 2.16 – Use Case 3: Shared Control input profiles of human, IntelSys and fusion system (final control input).

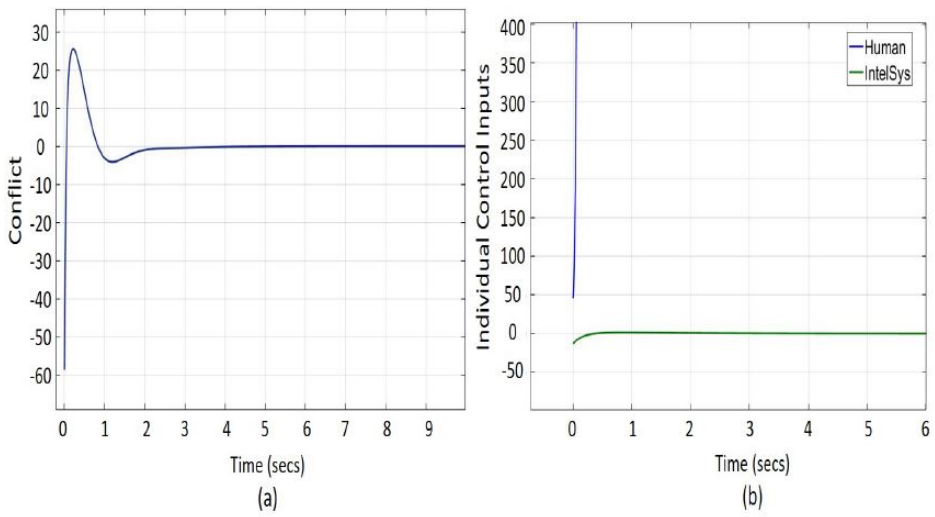

Figure 2.17 – Use Case 3: Conflict (Actual) Profile (a), Individual control Inputs of human and IntelSys in the case of independent control (b).

2.7 Conclusion

Conflict between the human driver and AutoSys is defined as the difference between the individual driving inputs. A shared control framework is developed with the aim to resolve the conflict over a time horizon. With the conflict as the state of a global system, the shared controller can be developed using state feedback control methods. The plant for this shared controller is an integrated system consisting of various subsystems such as vehicle dynamics, environment dynamics and the driving behavioral models for the human driver and AutoSys. A generic state space model is developed for the conflict plant system for the control analysis. The state feedback control law is assumed to be of the form $I = -Kx$ where x is the conflict state. The control gain K can be derived through different methods. As an example, the control gain K is computed using the LQR control method where the conflict resolution is posed as an optimal control problem. An application to the shared control of the inverted pendulum is presented.

The design and development of the shared controller i.e. the methodology to compute the control gain K is highly dependent on the vehicle and environment dynamics. The environment may consists of different vehicles. The state dynamics of the ego vehicle and the environment are correlated. Hence, the mutual interaction between the ego vehicle and other vehicles present in the environment need to be considered for modeling the plant dynamics. This is a very challenging problem and the dynamical model is prone to errors. The inaccuracy in the vehicle and environment dynamical model will directly affect the working of the shared controller. Hence, for the final design and development of the shared controller, decision making approach is used instead of classical control approach to compute the control input and gain K. Non-Cooperative Game theory is used to develop the shared control strategy. The details of this methodology are presented in Chapter 5. The updated shared control architecture is shown in Fig. 2.18.

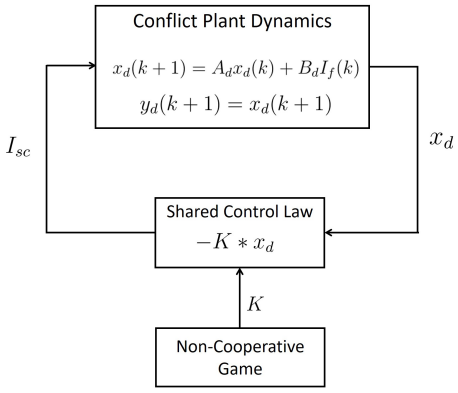

Figure 2.18 – Updated Shared Control Architecture

Driving Decision Admissibility

Contents

3.1 Introduction and Background

Shared control between human driver and autonomous driving system is achieved through the fusion of the individual driving inputs. For the effective fusion, it is necessary to assess the individual driving inputs with respect to various factors such as vehicle state, environment dynamics, individual driving intentions etc. This chapter mainly answers the question "Is the driving input acceptable for the vehicle safety?" with respect to collision risk, lane/road departure prevention, speed limit etc. The answer to this question (yes/no) is dependent on the environment perception which is uncertain. Hence, instead of simple yes/no i.e. 100/0 %, the answer is uncertain and expressed in terms of degrees of belief. This assessment is quantified into a metric for the use in the fusion methodology. The final driving input arising from the fusion is correlated to the assessment of individual driving inputs. The respective metric is termed as admissibility which implies the acceptability/validity of the individual driving decision. The driving decision admissibility is relative in nature and is influenced by various factors/contexts which are as follows:

- Collision Risk
- Road/Lane departures
- Driving intentions
- Speed limitations

One of the major objectives of the fusion system is to enhance the driving safety. Hence, collision risk is the most important context in which the individual driving inputs need to be assessed. In the traffic conflict techniques, various surrogate safety measures have been devised for the collision risk metrics. The calculation of any collision risk mainly involves three stages: estimation of the trajectories of the ego and surrounding vehicles, intermediate metric calculation (for e.g. Time-to-collision TTC) and calculating the collision risk from the intermediate metric. The relation between the collision risk and intermediate metric (mostly time metrics) is straightforward (inverse proportionality). Hence, the past researches have been focused mainly on the following:

- Deriving new methods for better trajectory prediction.
- Deriving new intermediate metrics for better identification and quantification of collision risk.

The main reason for the use collision risk metrics as the safety measures in the active safety systems is pro-activeness. The early identification of a collision helps the active safety system to take necessary action to either avoid or mitigate the collision. The accurate and early prediction of the vehicle future trajectory adds to the pro-activeness with respect to the collision risk assessment. Various methods have been developed in the past researches for the vehicle trajectory prediction. In [Schreier et al., 2016] and [Schubert and Wanielik, 2011], the vehicle trajectory is estimated using Bayesian inference. The measured states of vehicle and environment obtained from localization systems are used in the Bayesian network model. The prediction is in the form of joint probability distribution function. In [Kim and Kum, 2018], the prediction is done with respect to the lane changing scenarios. The predicted lane change trajectories are combined with the probability distributions of lane change. Time-to-Collision (TTC) metric is used to calculate the collision risk.

In [Houénou et al., 2014], [Eidehall and Petersson, 2008], [Berthelot et al., 2012] and [Berthelot et al., 2011], the uncertainty of the predicted vehicle trajectories is propagated to TTC. Also each sample time of prediction is considered to be potential TTC. The collision risk in terms of probability calculated for all sample times in the prediction time horizon using Monte Carlo Simulation. The collision risk assessment can be also made specific with respect to the scenario or conditions.

In [De Nicolao et al., 2007], the collision risk assessment is specifically targeted at pedestrian safety using stochastic pedestrian model. The methodology presented in [Kim et al., 2015] separates the probabilistic threat assessment for static and dynamic obstacles using particle filtering techniques. [Lefèvre et al., 2012] focuses on the risk assessment for the road intersections. The above mentioned methods have high dependency on the accuracy of the trajectory prediction of not only the ego vehicle but also the surrounding vehicles. The accurate prediction of the environment dynamics is very challenging since the driving intentions are unknown and the cooperative/reactive behavior of the drivers in the surrounding vehicles also need to be modeled.

Various risk indicators have been developed in the past researches such as time-to-collision (TTC), time-to-react, time-to-accident, post-encroachment time (PET), unsafe density (UD), proportion of stopping distance (PSD), gap time (GT), comprehensive time-based measure (CTM), rear-end collision probability (RECP) etc to assess the collision/threat accurately [Mahmud et al., 2017], [Lefèvre et al., 2014]. Time-to-collision is the most common indicator used in the past researches to calculate the collision risk. Several researches show different methods to calculate TTC [Jiménez et al., 2011], [Brannstrom et al., 2010], [Kaempchen et al., 2009],

but it is not consistent i.e. it doesn't always interpret the collision risk accurately. Hence, different collision risk assessment methods have been developed based on other indicators for e.g. time-to-react [Hillenbrand et al., 2006]. In [Nadimi et al., 2016], a new time based indicator/index was developed by combining TTC and PET using a fuzzy inference system. The mixed indicator helps in better risk assessment.

The vehicle and environment state data required for the collision risk assessment is usually obtained through the sensors in built sensors of the vehicle [Polychronopoulos et al., 2007]. [Li et al., 2016b] present a methodology in the case of connected vehicles, where the data is obtained from the roadside device through the vehicle-to-infrastructure (V2I) communications. The TTC warning messages can be conveyed to the other vehicles through V2V communications thus increasing the pro-activeness of the safety systems. This method has high dependency on connected vehicle technology and infrastructure.

TTC is not suited for the collision risk assessment in the driving decision admissibility with respect to fusion. The admissibility is developed with respect to the following properties:

- Generic nature i.e. to include collision risk, safe driving region with respect to road/lane boundaries, speed limit and individual driving intentions
- Minimum dependency on the accuracy of the trajectory prediction
- Assumption of environment dynamics to be random
- Inclusion of the uncertainty arising from the environment states (sensor data) and dynamics (randomness)

The driving decision can be classified as admissible or inadmissible only if there is absolute certainty in the sensor measurement data and environment dynamics which is practically not possible. Hence, instead of using a binary classification, the driving decision is assigned a degree of admissibility (0-100%), calculated using Belief Function theory.

3.2 Preliminaries

With respect to driving decision admissibility, input uncertainty play an important role. There are two major sources for these uncertainties. The environment is perceived through the sensors like LIDAR, Camera, Radar etc. The noise present in these sensor measurements create an uncertainty of the environment state which is quantified and expressed in the form of occupancy probabilities during grid mapping. The environment is dynamic in nature and it is difficult to accurately predict the future states of the environment. This also leads to the uncertainty in

the driving decision admissibility.

Any application (in general) with respect to the real world need to incorporate uncertainties. Uncertainty quantification is an important aspect in the uncertainty representation. The most common approach to quantify uncertainty is using probability theory. Based on the method of calculation, the probability is classified as either objective or subjective. When the probability of an event is calculated through a repeatable experiment, it is termed as an objective probability for e.g. the probability of the coin toss outcome as heads or tails. On the contrary, if the probability is calculated based on the information/evidence related to that event, then it is termed as subjective probability. For e.g. The chances of a rain for a given day is based on the information about the weather earlier.

Uncertainty can be classified into two types: aleatory and epistemic uncertainty. Aleatory uncertainty is statistical in nature and arise from the randomness of the process/experiment for e.g. uncertainty in coin toss, drawing a ball of particular color etc. Epistemic uncertainty are subjective in nature and arise from the lack of data or knowledge (often represented as ignorance) and are mostly represented by subjective probability. The probability theory is inadequate to model epistemic uncertainty i.e. using Bayesian model because of its incapability to represent ignorance and decision making based on the lack of data or knowledge.

3.2.1 Belief Functions Theory

Belief functions theory (BFT) also known as evidence theory or Dempster-Shafer theory was first proposed in [Beynon et al., 2000]. It was later extended in [Campos and Cavalcante, 2003]. It works with upper and lower probability instead of precise values, with the generalization of Bayesian theory of subjective probabilities (degree of belief). The main contents of this theory are the combination and representation of evidence or knowledge. Evidence can be represented by a basic probability (belief) assignment using various evidences and then combined using a combination rule. A model based on BFT is called an Evidential model.

3.2.2 Framework

Given a problem, a finite set of variables are used to model the uncertainty using BFT. These variables represent the outcome or different propositions related to the event given by the set $\{X_1, X_2, ..., X_n\}$. For a variable X, the frame Ω_X holds all the possible values of the variable. A frame of discernment consisting of all the mutually exclusive possible propositions of interest in the domain of interest given by Ω. For example, consider a variable X_1, and the frame of discernment is

given as: $\Omega_{X_1} = \{a_1, b_1\}$. The finite set for all the possible propositions of interest can be given in terms of a power set as: $2^{\Omega} = \{\emptyset, A, N, \Omega\}$, where $\emptyset$ indicates null proposition and Ω represents ignorance. For example, consider the event of the forecasting the rain tomorrow. The probability theory defines only two propositions of interest/events i.e. {rain, no rain}. The power set in this case is given as {null, rain, no rain, rain or no rain}.

For each proposition of interest in the power set, subjective probabilities also termed as mass values are assigned. These mass values are derived from the information/evidence using a mass assignment function $m : 2^{\Omega} \rightarrow [0, 1]$. In other words, it represents the knowledge/evidence in the form of mass values of the variables in the frame of discernment. The mass function satisfies the following condition:

$$\sum_{A \subseteq \Omega} m(A) = 1 \tag{3.1}$$

3.2.3 Combination of Evidences

The mass values of the propositions of interest are obtained from multiple evidences. Hence, it is necessary to combine the mass values to obtain a unique set of subjective probabilities. Some of the well known methods of combination are Dempster's rule of combination, Yager's rule, weight averaging rule etc. Dempster's combination rule is most commonly used for multiple applications. It considers the reliability and independence of the evidences (source of information). Let m_1 and m_2 be the mass functions, then the degree of conflict is given by:

$$k = \sum_{B,C \subseteq \Omega, B \cap C = \emptyset} m_1(B) m_2(C) \tag{3.2}$$

If k<1, then m_1 and m_2 can be combined using Dempster's rule as follows:

$$(m_1 \oplus m_2)(A) = \frac{1}{1-k} \sum_{B \cap C = A} m_1(B) m_2(C), \forall A \neq \emptyset \tag{3.3}$$

where $\frac{1}{(1-k)}$ is called the normalizing factor to handle small conflicts between the evidences. The degree of belief for a proposition of interest A is given as:

$$Bel(A) = \sum_{B \subseteq A, B \neq \emptyset} m(B) \tag{3.4}$$

Yager's rule is a modified form of Dempster's rule for the cases where the normalizing factor give counterintuitive results. In weighted averaging rule, different

weighting factors are assigned to the information depending on their reliability i.e. higher the reliability, higher the weight.

3.3 Evidential Model

For incorporating the collision risk in the driving decision admissibility, we have used the metric PSD (proportion of stopping distance). Let (v, ω) be the velocity and angular velocity (yaw rate) of the vehicle respectively, then the vehicle can safely be stopped before the collision if the following conditions are satisfied (One of the driving input/decision can be considered in terms of angular velocity as (v, ω) or steering wheel angle (v, θ)).

$$v \leq \sqrt{2 * D * \dot{v}_{bmax}} \tag{3.5}$$

$$\omega \leq \sqrt{2 * D * \dot{\omega}_{bmax}} \tag{3.6}$$

where D is the distance to the obstacle, $\dot{v}_{bmax}$ is the maximum deceleration, $\dot{\omega}_{bmax}$ is the maximum deceleration of angular velocity. If the above mentioned conditions are satisfied, then the driving decision is admissible with respect to the collision avoidance. The distance to the obstacle D is obtained from the sensor data. Hence, due to the sensor measurement noise, there is an uncertainty to the admissibility. Also the environment dynamics is unknown, thus adding additional uncertainty. The uncertainty related to the sensor measurement noise is assumed to be of the Gaussian nature while that related to the environmental dynamics is completely unknown and considered as ignorance. Hence, the method of BFT is used to quantify the uncertainty related to the driving decision admissibility in terms of degrees of belief.

For the application of BFT to the driving decision admissibility, the mutually exclusive possible propositions of interest are given by the finite set (frame of discernment) $\Omega = \{A, N\}$, where the propositions A and N state whether the driving decision is admissible and inadmissible respectively. The respective power set is given as $2^{\Omega} = \{\emptyset, A, N, \Omega\}$, where $\emptyset$ indicates null proposition and Ω represents ignorance about the admissibility. The driving decision admissibility is defined in terms of degrees of belief in decision admissibility i.e. degrees of belief in proposition A.

The uncertainty in the sensor data is reflected in the grid map in the form of probability of occupancy of each discrete cell. The discrete cells of the occupancy grid map form the source of evidence with their occupancy as the evidential

information. The mass values for different propositions given in the frame of discernment are calculated using this evidential information. In this methodology, we consider the obstacles within or in the vicinity of the vehicle path. Hence, not all the discrete cells are relevant with respect to the source of evidence i.e. all the occupancy information present in a grid map is not required to calculate the degrees of belief.

Given the occupancy grid map, a subset of cells is selected by superimposing the vehicle estimated trajectory (circular form) on the grid map. A sample of the vehicle path superimposition on the grid map is shown in Fig. 3.2.The width of this estimated trajectory is considered approximately equal to the lane width. The subset of discrete cells belonging to this superimposition is selected. Let the probability of discrete cell occupancy in the grid map be represented as $P(Occupancy)$. The subset is further reduced i.e. the discrete cells representing the free space ($P(Occupancy) \leq 0.1$) or the ignorant space ($P(Occupancy) = 0.5$) are filtered out because they are redundant with respect to providing information related to collision avoidance.

Consider the grid map shown in the Fig. 3.1. The region 'A' represent the free space between the ego vehicle and the other vehicles. The regions 'B' and 'C' represent the positions of other vehicles and the unknown occupancy region respectively. Let S_p be the discrete cell subset formed through the superimposition of estimated vehicle trajectory on the grid map. Let S_o be the discrete cell subset for the region 'B', then the discrete cell subset considered as the source of evidence is given by:

$$S_E = S_p \cap S_o \tag{3.7}$$

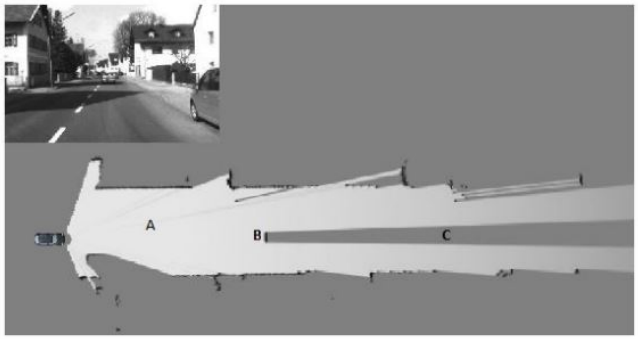

Figure 3.1 – Sample occupancy grid map divided into three regions: free space (A), positions of other vehicles (B) and unknown occupancy (C).

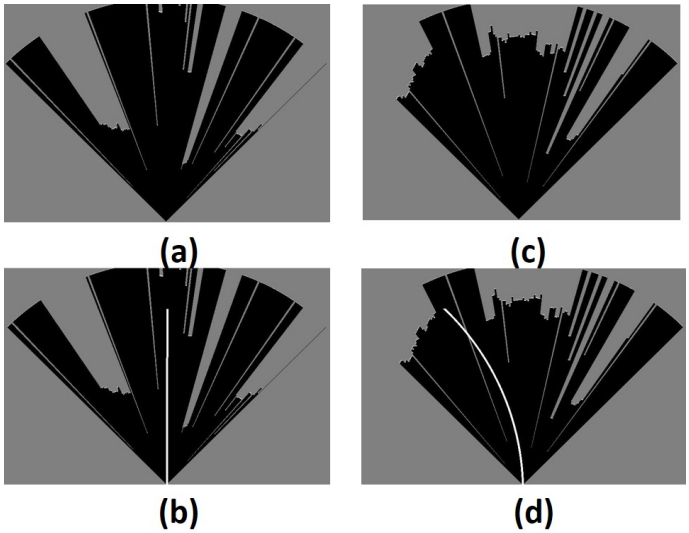

Figure 3.2 – Sample Occupancy Grid maps of single layer of LIDAR sensor. (a) and (c) show the probabilistic grid map at different time instants. (b) and (d) are the respective grid maps with the intended vehicle path superimposed on them.

3.4 Mass Value Computation

We have defined a mass assignment function to derive the mass values from the occupancy information obtained from the discrete cell subset S_E. This mass function is explained here in the form of an example. Consider the grid map shown in Fig. 3.3 with two occupied cells. This cell is in the path of the target vehicle at a distance 'D'.

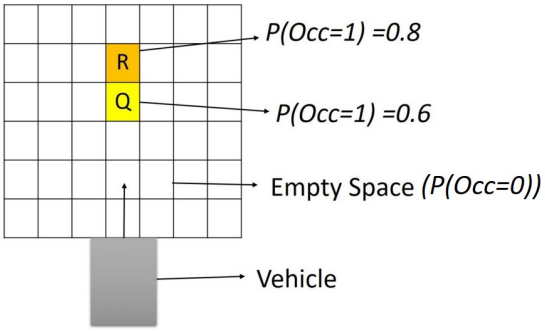

Figure 3.3 – Occupancy grid map for a sample scenario

$(P(Occ = 1) = 0.6) \implies (P(Occ = 0) = 0.4) \implies P$(Decision (v, ω) is admissible) = $P(A) = 0.4$. It can not be concluded that the probability of decision inadmissibility $(P(N))$ is 0.6 because the driving command may change with time. Another possibility is that the obstacle may move away because of the environment dynamics. These two possibilities are considered separately to analyze their impact

on the mass value assignment. As mentioned earlier, Equations 3.5 and 3.6 needs to be satisfied for the prevention of collision.

Maximum deceleration is not only dependent on the vehicle configuration but also on other factors such as road friction (dependent on road type, slippage etc), tire pressure and condition (wear and tear), brake condition etc. It is not always possible to attain maximum deceleration as per the vehicle configuration. This uncertainty is considered in terms of probability as P(Vehicle can stop before collision). The satisfaction of Equations 3.5 and 3.6 does not imply P(Vehicle can stop before collision) = 1. It only implies that this probability is high. The method to calculation of this probability is out of scope. For the mass function, we assume:

• P(Vehicle can attain maximum deceleration) = P(Vehicle can stop before collision) = 0.8.

The mass function can be divided into two use cases depending on the satisfaction of Equations 3.5 and 3.6 given as:

Use Case 1: Driving decision (v, ω) satisfies conditions given in Equation 3.5 and 3.6. The mass value of the proposition of decision admissibility is given as:

• $m_Q(A) = P$(Discrete cell is empty or Vehicle can stop before collision and Discrete cell is non-empty)

• $m_Q(A) = P$(Discrete cell is empty) + (P(Vehicle can stop before collision)* P(Discrete cell is non-empty).

Substituting the values we get, $m_Q(A)$ = 0.88. Substituting the value of $m_Q(A)$ in Equation 3.4, we get $m_Q(N) + m_Q(\Omega)$ = 0.12. Only if it was certain that the obstacle is static, the value 0.12 can be assigned fully to $m_Q(N)$. Equal mass values are assigned to the propositions N and Ω because of the ignorance of the environment dynamics i.e.

• $m_Q(N) = m_Q(\Omega) = (1 - m_Q(A)/2$

The final mass assignment for Use Case 1 is shown in the Table 3.1.

X	ϕ	A	N	Ω
$m_Q(X)$	0	0.88	0.06	0.06

Table 3.1 – Mass Assignment with the cell 'Q' as a source of evidence for Use Case 1

Use Case 2: Decision (v, ω) does not satisfy the conditions given in Equations 3.5 and 3.6 which implies:

• P(Vehicle stoppage before obstacle collision) = 0

The mass value of the decision admissibility is given as:

• $m(A) = P$(Discrete cell is empty) + (P(Vehicle can stop before collision)*P(Discrete cell is non-empty)

Substituting the values we get, $m_Q(A) = 0.4$. Similar to Use Case 1, we consider the ignorance of the dynamic nature of the obstacle. The final mass values of all the propositions for Use Case 2 are given in the Table 3.2.

X	ϕ	A	N	Ω
$m_Q(X)$	0	0.4	0.4	0.2

Table 3.2 – Mass Assignment with the cell 'Q' as a source of evidence for Use Case 2

Consider the cell 'R' as the source of evidence (shown in Fig. 3.3). Assuming that the Equations 3.5 and 3.6 are satisfied, the mass values are assigned as shown in Table 3.3.

X	ϕ	A	N	Ω
$m_R(X)$	0	0.84	0.08	0.08

Table 3.3 – Mass Assignment with the cell 'R' as a source of evidence

The mass assignment function can be generalized as follows:

$m(A) = P(Discrete\ cell\ is\ empty) + (P(Vehicle\ can\ stop\ before\ collision) * P(Discrete\ cell\ is\ non\ empty)$

if $Condition1(3.5)\ and\ Condition2(3.6)$ **then**

$P(Vehicle\ can\ stop\ before\ collision) = 0.8$

else

$P(Vehicle\ can\ stop\ before\ collision) = 0$

end if

$m_Q(N) = m_Q(\Omega) = (1 - m_Q(A)/2$

3.5 Degree of Admissibility Computation

The degree of admissibility is defined as the degree of belief in decision admissibility ($Bel(A)$). The mass values obtained from the evidential information, are combined using two combination methods which are Dempster's combination rule and Weighted averaging rule. The use of two different combination rules gives better accuracy for the calculation of degree of admissibility. Applying Dempster's

rule for the combination of mass values, the degree of belief in general can be given as:

$$Bel_D(A) = (m_1 \oplus m_2 \oplus \dots m_n)(A) \tag{3.8}$$

With reference to Tables 3.1 and 3.3, the degree of admissibility for the driving decision (v, ω) can be given as:

$$Bel_D(A) = (m_Q \oplus m_R)(A) = 0.97 \tag{3.9}$$

The Weighted Averaging rule is given as:

$$m_{1\dots n}(A) = \frac{\sum_{i=1}^{n} w_i * m_i(A)}{\sum_{i=1}^{n} w_i} \tag{3.10}$$

The uncertainty in the sensor measurement is commonly represented by Gaussian distribution (used in the inverse sensor model for grid map) around the obstacle position. Hence, the discrete cells closer to the real position of the obstacle i.e. closer to the mean of Gaussian distribution curve, are more reliable source of evidence. The weights assigned to the discrete cell evidence increase (in the order of 2) as they move closer to the real position of the obstacle. This is the reason for selecting the weights in the order of 2 is to substantially increase the impact of the occupancy of discrete cells closer to the real position of the obstacle. Applying this rule for the combination of mass values of given in Tables 3.1 and 3.3, the confidence level for the decision (v, ω) can be given as:

$$Bel_{WA}(A) = \frac{2^0 * m_Q(A) + 2^1 * m_R(A)}{3} = 0.85 \tag{3.11}$$

Consider the same scenario as shown in Fig.3.3 except the probabilistic occupancy of the discrete cell 'Q' is 0.2. Assuming that the Equations 3.5 and 3.6 are satisfied, the degree of admissibility computed using Dempster's combination rule $Bel_D(A)$ and Weighted averaging $Bel_{WA}(A)$ is given as follows:

$$Bel_D(A) = 0.98, Bel_{WA}(A) = 0.91 \tag{3.12}$$

The variation in the degree of admissibility computed using Dempster's combination rule and Weighted averaging is +0.01 and+0.7 respectively. With respect to the variation in the occupancy grid uncertainty, the sensitivity of the degree of admissibility computed using Weighted averaging is much more than that using Dempster's combination rule.

Different driving scenarios are simulated with dynamic obstacles to validate

the computation of degree of admissibility. The algorithm is implemented in MATLAB/Simulink and is integrated with the driving simulation software IPG CarMaker. The virtual LIDAR sensor of IPG CarMaker is used to acquire the environment data. The field of view (FOV) and the range of the virtual LIDAR sensor is set to 90 degrees and 100 meters respectively.

Driving Scenario (Dynamic Obstacle):

Consider the driving scenario shown in Fig. 3.4. The profiles of the vehicle speed and yaw rate are shown in Fig. 3.5 and 3.6 respectively. The vehicle is initially traveling on a curve road and then encounters a cyclist further.

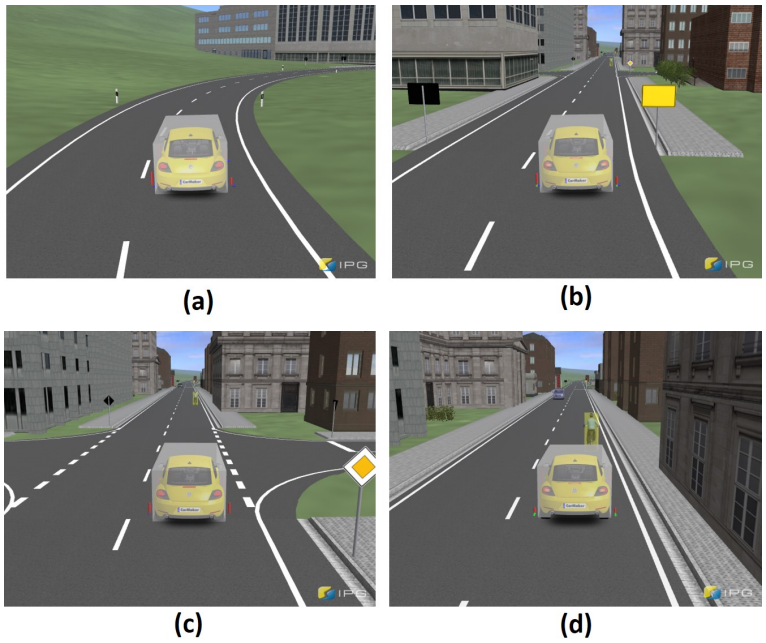

Figure 3.4 – Driving scenario 1 snapshots in the order from (a) to (d)

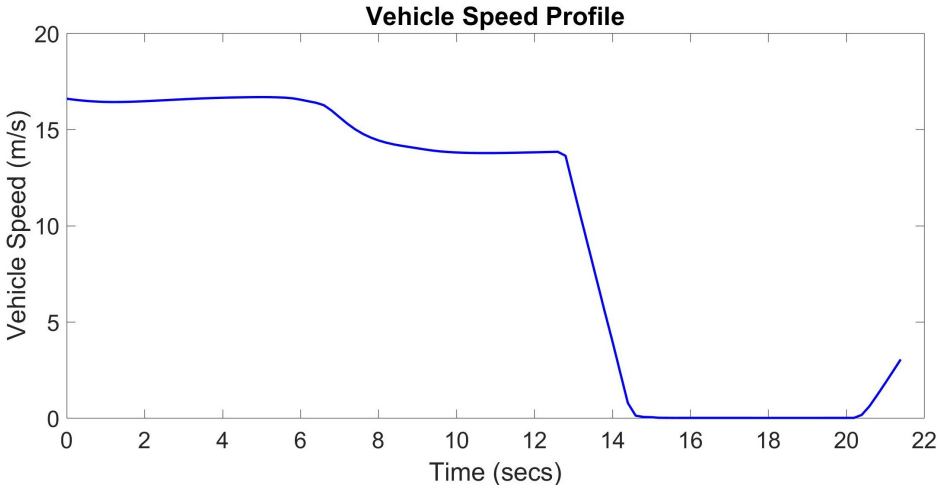

Figure 3.5 – Vehicle speed profile for Driving scenario 1

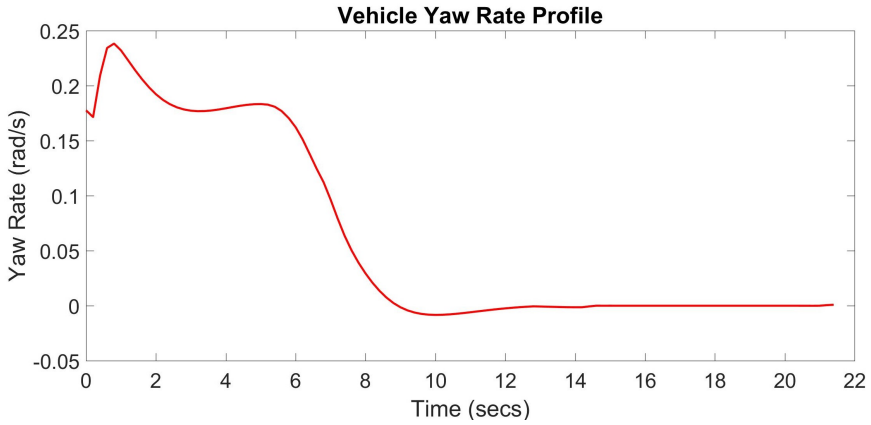

Figure 3.6 – Vehicle angular velocity (Yaw Rate) profile for Driving scenario 1

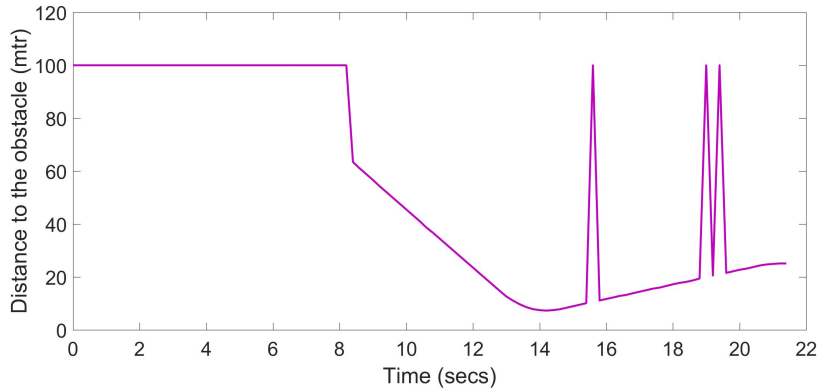

Figure 3.7 – Approximate distance to the obstacle for Driving scenario 1

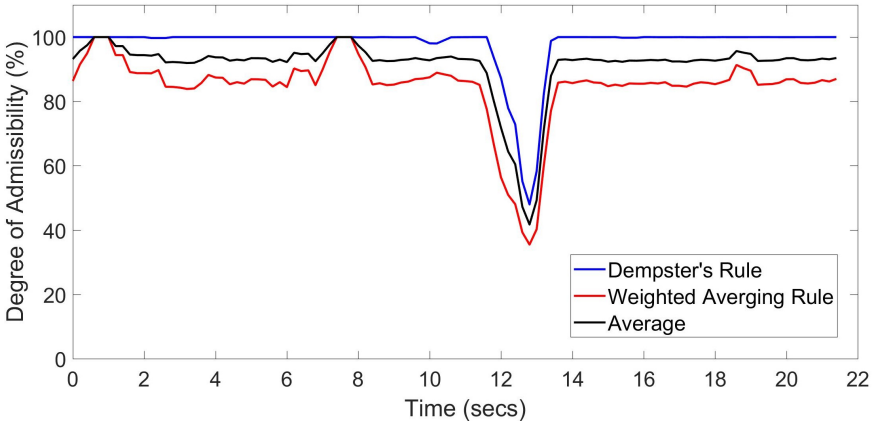

Figure 3.8 – Degree of Admissibility profiles for Driving scenario 1

The driving scenario snapshots are shown in Fig. 3.4. In this scenario, the driver encounters a cyclist and a hard braking action is taken. An occupancy grid map is formed using the sensor data. The approximate distance from the ego vehicle to the cyclist calculated from grid map is shown in Fig. 3.7.

The profiles of degree of admissibility using Dempster's combination rule and Weighted Averaging rule are shown in Fig. 3.8. The final degree of admissibility is computed as the average of the two profiles. Initially (till $t \leq 11$ secs) the driving decisions are admissible with respect to the collision avoidance and hence the degree of admissibility is high ($\geq 80\%$). The cyclist comes within the field of view and range of the virtual LIDAR sensor at $t \geq 8$ secs. The distance between the ego vehicle and the cyclist progressively decreases (Fig. 3.7). After $t \geq 11$ secs, the degree of admissibility starts decreasing reflecting the increase in the collision risk. At t=13 secs, the driver applies hard brakes to prevent collision. Hence, the degree of admissibility retains high value again.

3.6 Enhancement of Degree of Admissibility

As mentioned earlier, the time metric used for the calculation of degree of admissibility with respect to the collision avoidance/risk is PSD as shown in Equations 3.5 and 3.6 where the conditions are applied to both the driving inputs i.e. vehicle speed and angular velocity (yaw rate). Without the consideration of input uncertainties, the degree of admissibility can be expressed as a binary function [0/100]% using PSD conditions. This binary function applied to the vehicle speed is shown in Fig. 3.9. Similar function can be formed for the vehicle angular velocity.

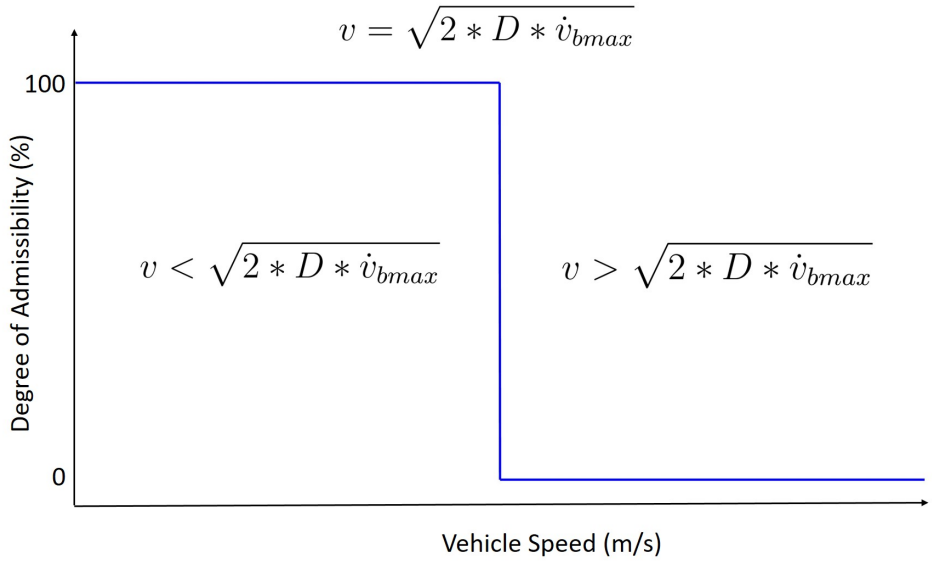

Figure 3.9 – Binary degree of admissibility with respect to PSD metric and vehicle speed (without uncertainty consideration)

As seen in Fig. 3.9, there is a hard boundary separating the admissible and inadmissible regions. Let the driving inputs be admissible at a given time instant.

The distance from the current driving input to the boundary i.e. the change required for the driving inputs to become inadmissible is not reflected in the degree of admissibility. This feature is significant especially when the driving inputs are near the boundary. Hence, to eliminate this limitation, we have modified the binary function (Fig. 3.9) as shown in Fig. 3.10. Similarly, the modified function can be applied to the other driving input (angular velocity).

In the modified function, a fuzzy characteristic with respect to the original function. The modified function is not binary and the degree of admissibility starts decreasing in a linear manner after the vehicle speed crosses the threshold speed. The main objective behind adding the fuzzy characteristic to the function is to provide an early intimation to the human driver. The fuzzy characteristic is defined using the parameter $V_{Threshold}$ which is the vehicle speed at which the function value changes. The transition slope from 100% degree of admissibility to 0% is also defined by $V_{Threshold}$. The requirement of linearity in the transition of degree of admissibility defined the choice of this type of function. The value of $V_{Threshold}$ is dependent on various factors such as current vehicle speed (V_C), relative speed of surrounding vehicles (V_S), human reaction time (T_{React}) ($\approx$ 2 secs), severity of possible collision (S_{Col}) and maximum possible deceleration (A_{decmax}) as shown in Equation 3.13. In the presented methodology, we have used $V_{Threshold}$ as a tuning parameter with a difference of 5 km/hr between $V_{Threshold}$ and boundary speed ($\sqrt{2 * D * \dot{v}_{bmax}}$) as shown in the Equation 3.14.

$$V_{Threshold} = f(V_C, V_S, T_{React}, S_{Col}, A_{decmax}) \tag{3.13}$$

$$V_{Threshold} = \sqrt{2 * D * \dot{v}_{bmax}} - 1.4 \tag{3.14}$$

The methodology for calculating the degree of admissibility (using BFT) is modified with respect to the new fuzzy conditions (PSD). The methodology is validated on the same driving scenario (using Dempster's rule) presented earlier to compare the results. The profiles of degree of admissibility computed using both the methodologies is shown in Fig. 3.11.

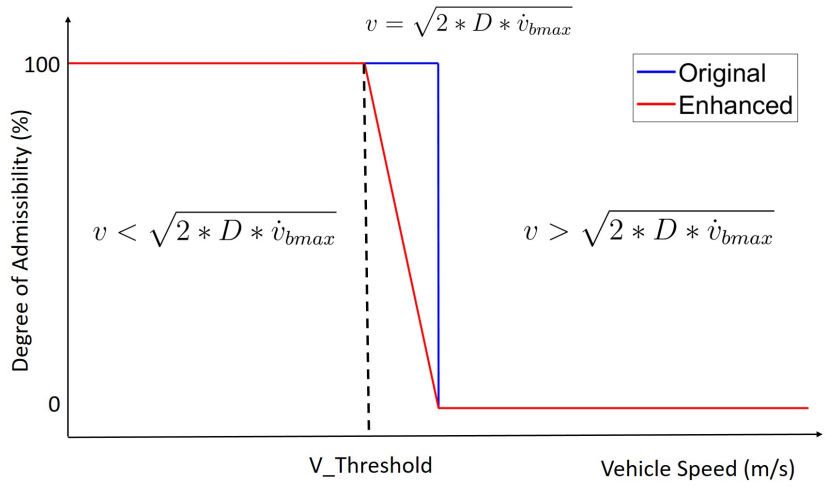

Figure 3.10 – Enhanced function for degree of admissibility with respect to PSD metric and vehicle speed (without uncertainty consideration)

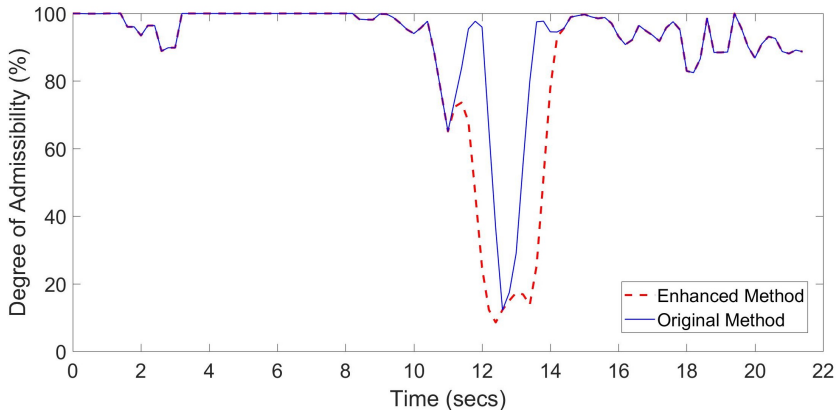

Figure 3.11 – Driving Scenario 1: Profiles of degrees of admissibility using original and enhanced methodologies

Consider Fig. 3.11. Till T$\approx$ 11 secs, the two profiles are very similar. After t=11 secs, the enhanced degree of admissibility starts decreasing earlier. The lowest values of admissibility of the two profiles are very close (difference$\leq$ 5%). Also during the other phase ($t \approx$ 13-15 secs), the recovery of the enhanced degree of admissibility is slower. Thus, the comparison of the two profiles show that the enhanced degree of admissibility provides an early intimation of a possible collision.

3.7 Incorporation of Road/Lane Boundaries

The driving decision (v, ω) can be inadmissible/unacceptable with respect due to various reasons such as high collision risk, road/lane departure prevention, legal speed limit, driving intentions etc. Earlier the degree of admissibility for a given

driving decision was computed with respect to the collision risk. The method can be extended to incorporate the lane/road departure scenarios. In such cases, the lane/road boundaries are presented in the occupancy grid map and considered to be another set of obstacles. An example of the inclusion of the road boundaries in the occupancy grid map is shown in Fig. 3.12.

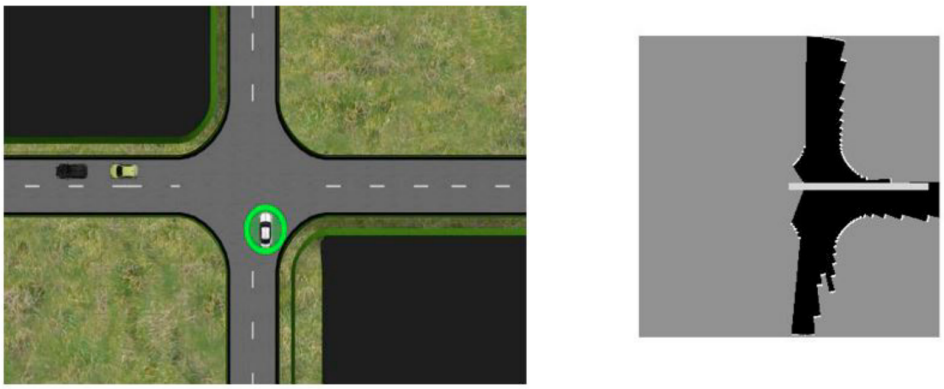

Figure 3.12 – An example of inclusion of road boundaries in the occupancy grid map with superimposed vehicle path (estimated).

3.8 Incorporation of Speed Limit

Intelligent speed adaptation (with respect to the speed limit) is an important ADAS functionality. The vehicle speed greater than the speed limit is certainly inadmissible/unacceptable. Hence, we include this factor in the degree of admissibility. Given the speed limit as V_{max}, the degree of admissibility is given by the function as shown in Fig. 3.13. The hard boundary present limitation similar to that explained in Section 3.6. Hence, a similar solution is applied to overcome this limitation. The modified function for degree of admissibility is shown in Fig. 3.14.

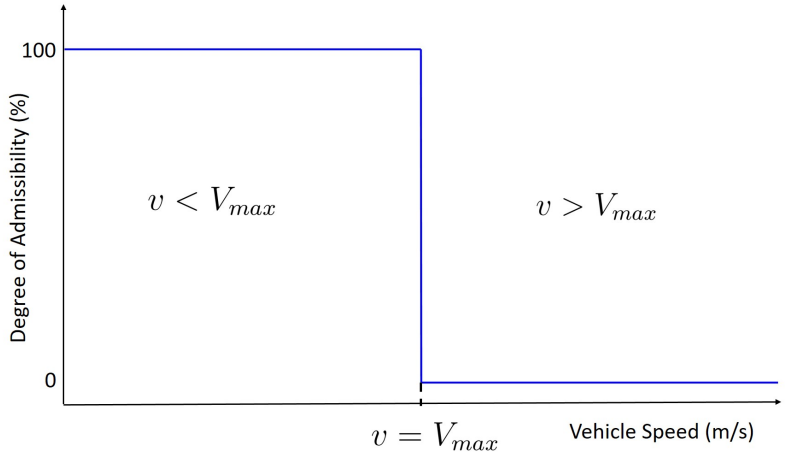

Figure 3.13 – Driving decision admissibility function with respect to speed limit

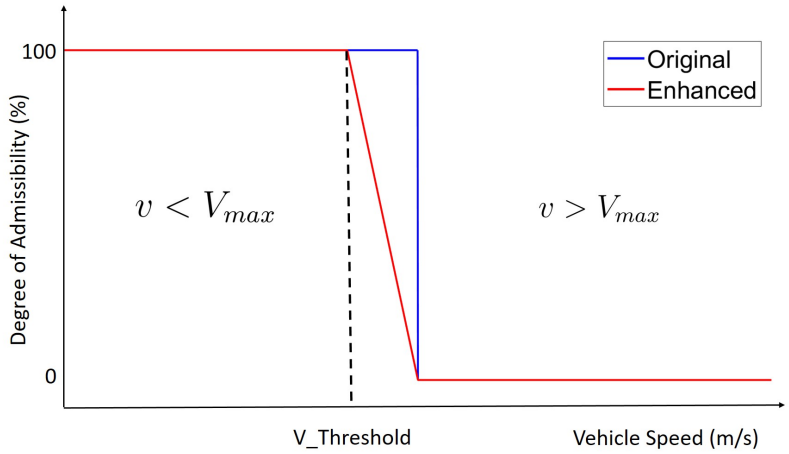

Figure 3.14 – Modified Driving decision admissibility function with respect to speed limit

3.9 Incorporation of Conflict and Driving Intentions

The main objective of the shared driving is to provide assistance to the human driver for the betterment of driving safety and performance. Hence, one of the important characteristic of the shared driving system is to be human centric. The nature of being human centric is correlated to the conflict and the individual driving intentions (explained in detail in Chapter 5). Hence, the factor of the high conflict or dissimilar driving intentions need to be reflected in the driving decision admissibility of autonomous system. For example, if the driving intentions of human and autonomous system are dissimilar, then the driving decisions of autonomous system are unacceptable to the human driver i.e. the degree of admissibility of autonomous driving decisions is low with respect to the human driving intentions i.e. it is inversely proportional to the conflict. The incorporation strategy is presented in detail in Chapter 5.

3.10 Application to Velocity Search Space

Autonomous navigation strategies are dependent on the vehicle and environment states. The main two approaches for the navigation control strategy are position based (optimal path planning) and speed based etc. The speed based strategies rely on the velocity search space. A velocity search space is a two dimensional search space (vehicle speed and angular velocity) conveying the admissibility information (binary) for each pair of (v, ω). As seen in the previous sections, we have computed the decision admissibility profile with respect to the collision avoidance for the vehicles present in the path or vicinity of the ego

vehicle. We applied our decision admissibility algorithm to the velocity search space thus introducing uncertainty information. The main aim for this application is to compute decision admissibility profile with respect to the collision avoidance for the scenarios where the obstacles (other vehicles) are not in the path or vicinity of the ego vehicle without estimating the path/trajectory of other vehicles.

Consider the following driving scenario where there is a collision risk at the intersection junction. Fig. 3.15 shows the vehicle speed and angular velocity profiles respectively. Fig. 3.16 shows the driving scenario snapshots for different time instants along with the respective velocity search space computed using the methodology presented earlier for each (v, ω). The velocity search space is discretized in two dimensions. The vehicle speed dimension has the range of [0,20] m/s with the resolution of 1 m/s. The angular velocity dimension has the range of [-2.4,2.4] rad/s with the resolution of 0.2 rad/s.

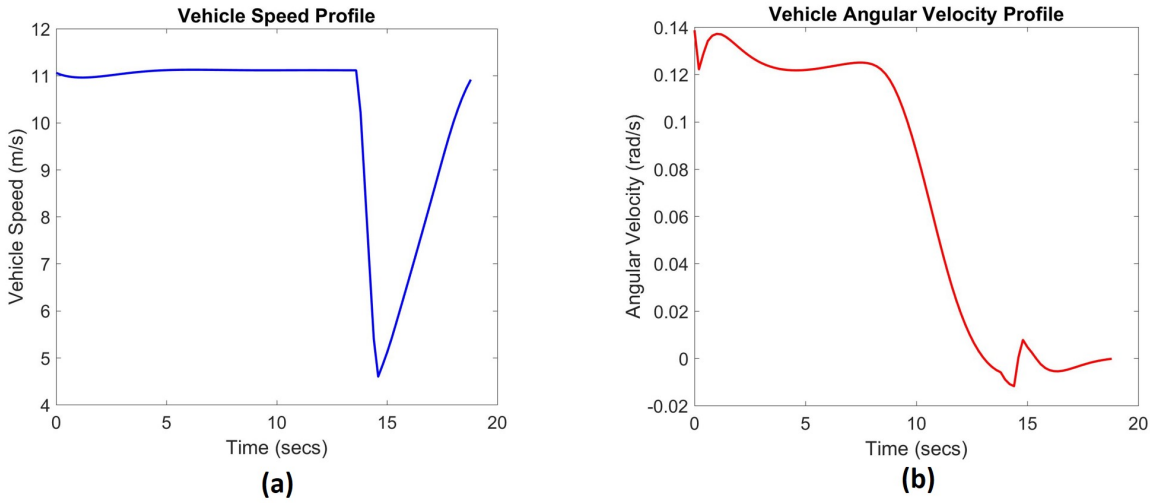

Figure 3.15 – a: Vehicle Speed Profile, b: Angular Velocity Profile

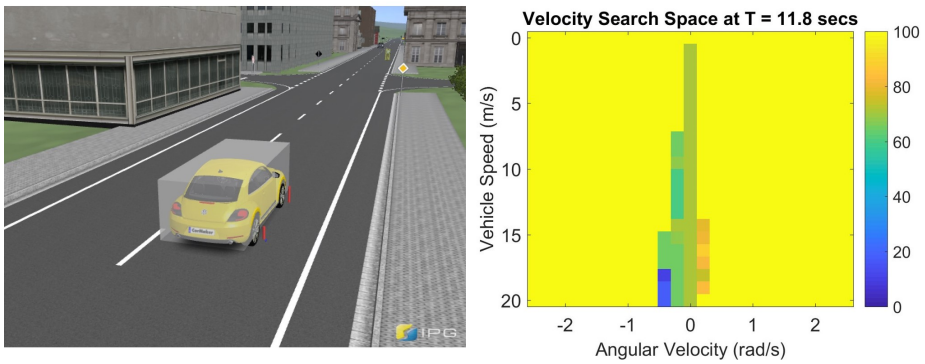

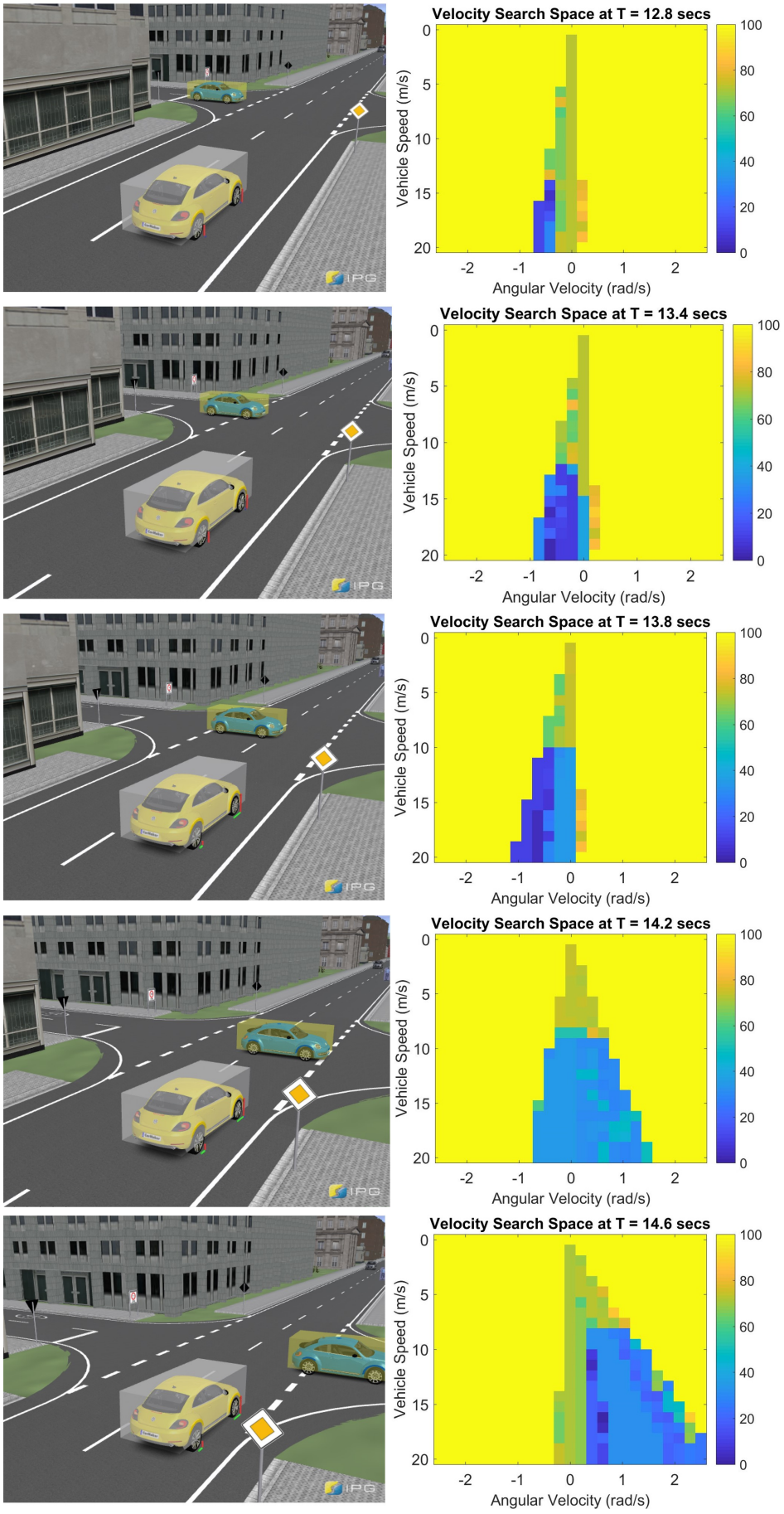
Velocity Search Space at T = 12.8 secs
Velocity Search Space at T = 13.4 secs
Velocity Search Space at T = 13.8 secs
Velocity Search Space at T = 14.2 secs
Velocity Search Space at T = 14.6 secs
Vehicle Speed (m/s)
Angular Velocity (rad/s)
0
5
10
15
20
-2
-1
0
1
2
100
80
60
40
20
0
IPG

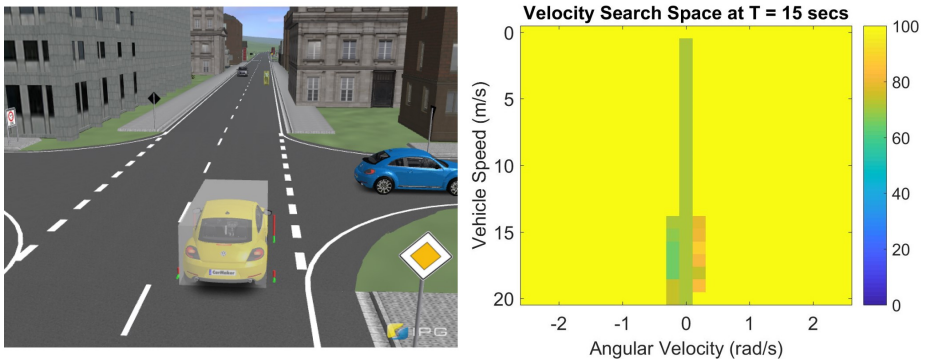

Figure 3.16 – Snapshots of a driving scenario with collision risk at the intersection junction along with velocity search space (showing degree of admissibility) at respective time instants

The velocity search space consists information of degree of admissibility for each (v_i, ω_i). Let (v_t, ω_t) be the driving decision at time t secs. The new degree of admissibility is computed by averaging the degree of admissibilities of surrounding to the driving decision (v_t, ω_t). Hence, the change of environment dynamics is incorporated. The new degree of admissibility profile for the driving scenario (Fig. 3.16) is shown in Fig. 3.17. The degree of admissibility decreases as the other vehicle approaches intersection i.e. the distance between the ego and other vehicle decreases.

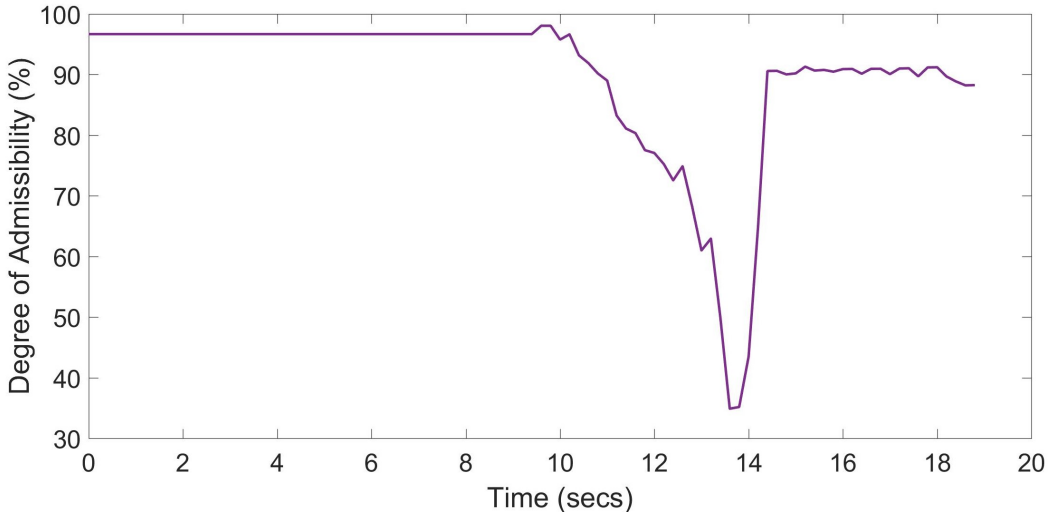

Figure 3.17 – Degree of Admissibility Profile for Driving Scenario shown in Fig. 3.16

3.11 Conclusions

The admissibility/acceptability of driving decisions (v, ω) (or (v, θ)) is viewed as a relative term. Different factors considered for the admissibility are collision

avoidance/risk, lane/road boundary departure, speed limit adaptation, driving intentions etc. Input uncertainties arising from sensor measurement and unknown environmental dynamics are propagated to the driving decision admissibility using Belief functions. The driving decision admissibility is represented as degrees of belief in admissibility). The method can be tuned to the requirements using the parameters: maximum acceleration and deceleration (linear and angular). Also the distribution of probabilities in the area of unknown dynamics can be tuned to the requirements. The original method was then enhanced using a fuzzy function for an early indication of any collision risk. Degree of admissibility is incorporated in the velocity search space. This incorporation is used to compute the degree of admissibility for the scenarios where the other vehicles are not within the ego vehicle path or in the vicinity. Apart from the shared driving control, the driving decision admissibility can be applied and used for various ADAS functionalities.

Driving Behavior Prediction using Feed-forward Neural Networks

Contents

4.1 Introduction and Background

One of the important factors in achieving shared driving control is to handle the conflict between human driver and Autosys. The final driving command is calculated with respect to the conflict resolution over a period of time. The prediction of the driving inputs/behavior of both human driver and AutoSys is necessary for this purpose. Considering the definition of conflict, prediction of driving inputs is equivalent to the prediction of conflict profile/trajectory. There are several aspects of predicting the human driving behavior. One of the aspects is to identify patterns and classify the driving behavior [Takano et al., 2008],[Li et al., 2018b],[Meng et al., 2006]. This helps for the automated driving to understand the behavior of human drivers in other vehicles.

Vehicle trajectory prediction is another major aspect of modeling human driving behavior. The prediction of trajectory is either in generalized form using deep neural networks [Kim et al., 2017], [Altché and de La Fortelle, 2017] or specific to some scenarios for e.g. lane change [Yao et al., 2013]. These trajectory prediction methods are well suited for the behavioral cloning [Kuefler et al., 2017] or assessment of automated driving [Roesener et al., 2016]. However, neural networks requires lot of data for the training and validation purpose, and second the knowledge of the future trajectory of the vehicle does not directly provide the information about the vehicle speed and steering profiles. Hence, it is difficult to identify human driving commands. Another related work, with the prediction of vehicle speed and steering wheel angle is presented in [Zhao et al., 2017] which uses deep belief nets and predicts the commands only for one time step in the future.

The presented methodology predicts the human driving decisions in the form of vehicle speed and steering wheel angle with prediction horizon of medium size (4 secs). Supervised machine learning methodology (non-linear regression) is used to develop the model based on multi-layer feed-forward neural networks. The advancements in the field of machine learning not only assist in formulating this prediction problem but also provide the ease of implementation because of the available software tools. The general architecture of feed-forward neural networks is customized to adopt to the complexity of data fitting. In order to avoid the problems associated to the deep neural networks (demanding lot of data for the training and validation), we have developed data transformation functions such as feature extractor, accumulator etc to filter relevant data and process it before sending it to the neural network. The validation of the model is carried out on the driving platform at Heudiasyc laboratory for different driving scenarios.

4.2 Model Architecture

Human driving decisions can be expressed in terms of intended vehicle speed and steering wheel angle. These are sufficient to determine the driving behavior and to predict the vehicle trajectory for the future time instants. The presented model will predict the driving command profiles for a particular time horizon based on the environment perception, human intention and current vehicle state. The predictions will be updated at each time sample i.e. the model is of the receding horizon type. The maximum possible time horizon for the vehicle speed profile prediction is 4 secs while that for the steering wheel angle profile is 2 secs. The rapid changes in the steering wheel angle for a given scenario restricts the prediction capability of the model to a shorter time horizon. Hence, the prediction time horizon considered later for the shared control strategy is 2 secs. This time horizon can also be correlated to the human reaction time ($\approx$ 2 secs). The model is of the open loop form i.e. the predictions of the model at current time instant are not fed back for the next prediction. This allows the model to be dependable on the inputs rather than the past predictions. The main objective of this strategy is to eliminate the error propagation of the past predictions.

The model architecture (shown in Fig. 4.1) shows different components each having a unique functionality. The main function of the prediction is performed by a multi-layer feed-forward neural network. It is trained on the input-output driving data collected separately for the training purpose. The inputs shown in the architecture are selected based on the human approach towards driving decision-making and can be classified into three categories namely: environmental state, vehicle state and the human intention. Past information of the inputs is used to identify the variation with respect to time. This adds a time series perspective to the model.

The environment perception of the human driver can not be captured directly. Hence, we have to rely on sensors for environment perception which may differ a bit from that of the human driver. The model is designed to be robust to such errors/differences. The obstacles are identified using LIDAR sensor and environment perception techniques. The presented modeling methodology uses LIDAR sensor with 4 vertical layers, 90 degrees field of view and has a range of 110 m. The methodology can be extended to any other configuration of LIDAR sensor. The sensor data contains lot of information which needs to be processed and filtered before sending it to the neural network. This function is performed by the feature extractor. It identifies the obstacles relevant to the driving decision, calculates the relative distance to the closest obstacle in a given direction (that is the predicted

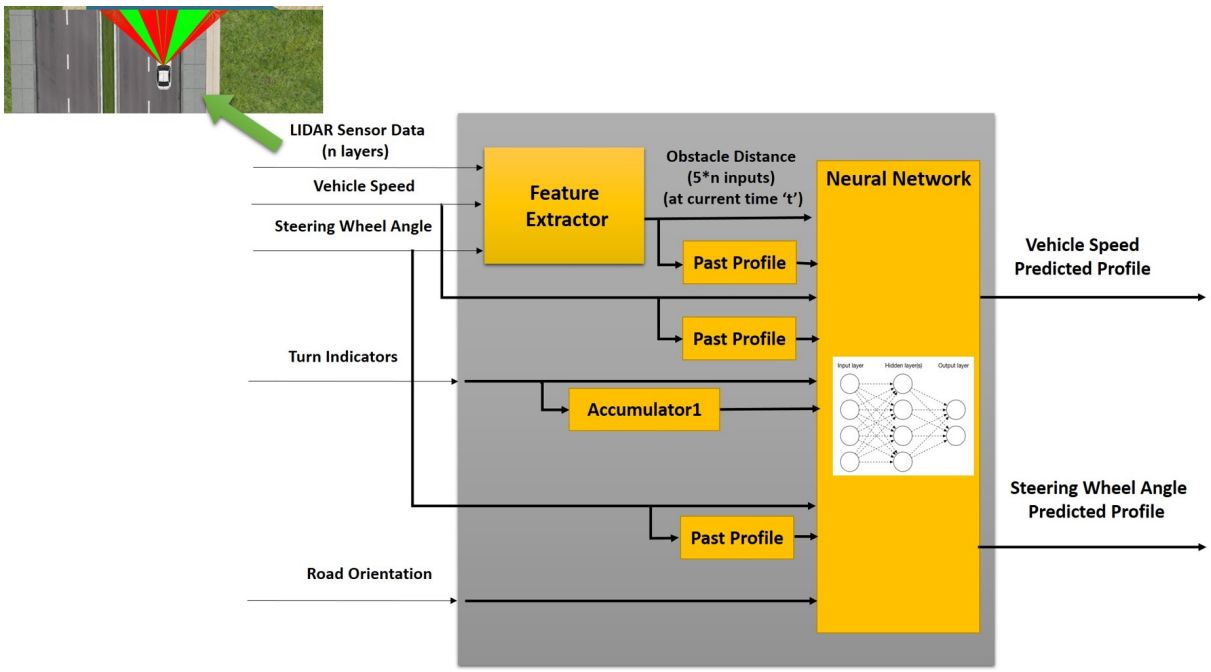

Figure 4.1 – Model architecture for the prediction

ahead path for the vehicle: explained later) and processes it further. This processed data is then sent to the neural network.

The human driving decisions are not always dependent on the environmental factors for e.g. the human driver may slow down the vehicle because of a reason other than the state of the obstacles. Such intentions are very hard to predict in some difficult maneuvers but can be identified in the form of time series. Hence, the model uses the past information of the vehicle speed for the predictions. The past input variation information can be represented in the form of the polynomial coefficients obtained through polynomial regression (quadratic). Such a representation reduces the number of inputs of the neural network. The past information of the feature extractor data is also represented in the form of polynomial coefficients. The function for the polynomial regression and extraction of the coefficients is shown as “Past Profile" block in the Fig. 4.1. For the model, the past input information is limited to 2 secs. This time period is selected through trial and error with respect to the relevance of the past driving information for the prediction. An application of the past profile function to the turn indicator signal is shown in Fig. 4.3.

The driving decisions related to the vehicle speed are also affected when the human driver is about to take a turn for e.g. depending on the current vehicle speed and turning radius, the human driver slows down the vehicle before taking a turn. Hence, the signals like turn indicator (left and right) and road orientation (inverse of road radius curvature) is considered to be the inputs to the model. The

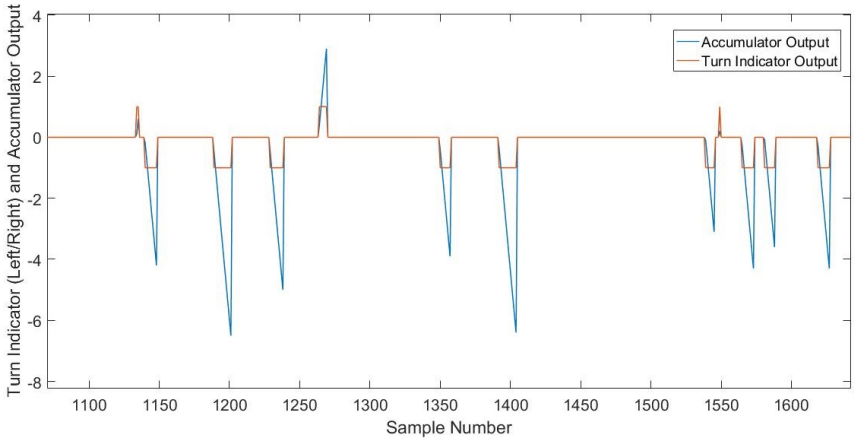

Figure 4.2 – Accumulator function applied to turn indicator signals

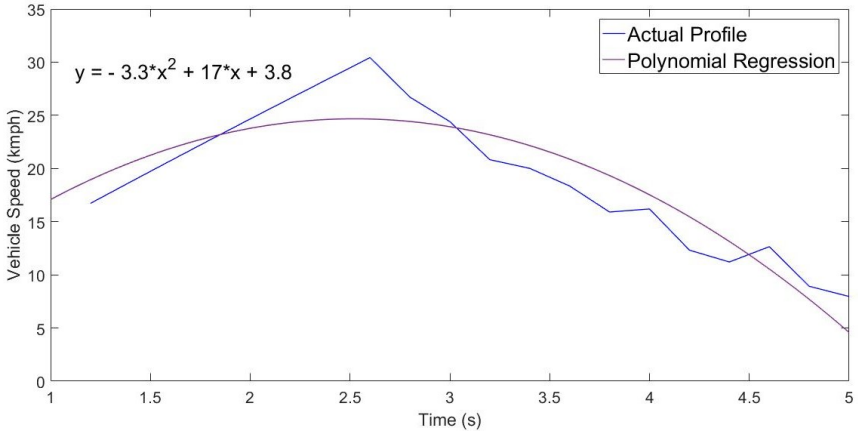

Figure 4.3 – Past profile function applied to steering wheel angle signal

accumulator (shown as Accumulator in Fig. 4.1) is a sample counter from the instant when the turn indicator is on. This signal is relevant for this model because the human driver does not turn the vehicle immediately after the turn indicator signal is on. Hence, the probability of the human driver taking the turn increases with the accumulation signal. The accumulator value resets after each cycle of the turn indication.

The vehicle steering future decisions are dependent mainly on the road curvature, human intention to take the turn or change the lane or overtake another vehicle. The main inputs correlated to the future steering wheel angle decisions are the turn indicators signal, the past values of the steering wheel angle etc. These decisions are partially dependent on the environmental state. Hence, the neural network uses all the inputs to find the correlations.

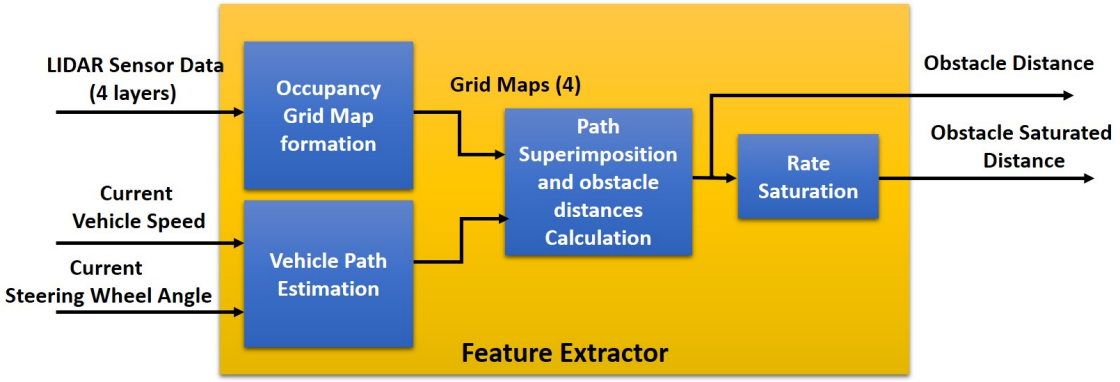

Figure 4.4 – Block diagram of Feature Extractor

4.2.1 Feature Extractor

Feature extractor (as shown in Fig. 4.4) is used for processing the LIDAR sensor data and filtering out relevant information. For the prediction of speed profile, relative distances (between the target vehicle and the obstacles) and their variation with time is of main interest. For e.g. if the target vehicle is approaching a static obstacle (another vehicle, pedestrian etc), the relative distance decreases with time. In case of proper driving, it can be predicted that the human driver will slow down the vehicle to avoid collision. The LIDAR sensor data is used to form a probabilistic occupancy grid map (one grid map for each layer of LIDAR). The grid maps contain information related to all the objects and other vehicles in the environment around the target vehicle. With respect to the variation of the vehicle speed, the driving decisions are influenced only by the obstacles present in the path of the vehicle. Thus, not all the information present in the grid maps is relevant to the prediction of the future vehicle speed profile.

The relevant information is filtered out of grid maps by superimposing the estimated path of the vehicle onto the map. The vehicle trajectory in general is considered to be of circular form. Given a time instant, approximate angular velocity of the vehicle is computed from its speed and wheel angle (computed through the steering ratio). The turning radius of the vehicle is computed from the speed and angular velocity and the estimated circular trajectory of the vehicle is superimposed on the grid maps. An example of the grid maps with and without superimposition of the vehicle's estimated path is shown in Fig. 4.5. The width of the path is approximately equal to the vehicle's width. The intersection of the estimated path and the obstacle present in the grid maps implies that the obstacle is present in the intended path and is thus considered to be relevant. The distance (straight line) between the target vehicle and the relevant obstacle is calculated for

each grid map. In the case of multiple intersections, obstacle closest to the target vehicle is considered.

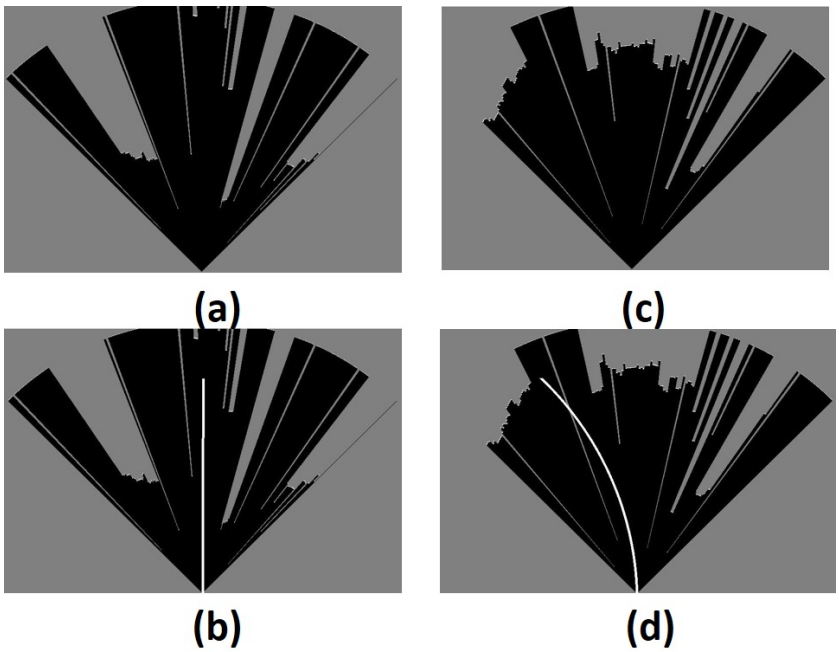

Figure 4.5 – Sample Occupancy Grid maps of single layer of LIDAR sensor. (a) and (c) show the probabilistic grid map at different time instants. (b) and (d) are the respective grid maps with the intended vehicle path superimposed on them.

The uncertainties in the sensor data is reflected in the grid map which affects the relative distance profile. Also, the variation in the vehicle's pitch create additional uncertainties in the sensor data and hence in the grid map. These uncertainties give rise to the impulses in the profile of the relative distance (for each grid map). These impulses will affect the training as well as performance of the neural network. The impulses are created mainly due to the false detection of the objects and during quick turns. Rate saturation is applied to the variation of relative distances. This gives the information to the neural network about the impulses. The upper and lower threshold values for the rate saturation are 1000 m/s and 10 m/s. The lower limit of the rate saturation is concerned with the false obstacle detection or to ignore obstacles during the transition phase of quick turns. The upper limit is concerned with the increase in free space in the intended vehicle's path. Hence, the lower rate saturation limit is kept much less as compared to the upper limit. These are selected by trial and error method. An example of the relative distance profile and its rate saturated profile is shown in Fig. 4.6.

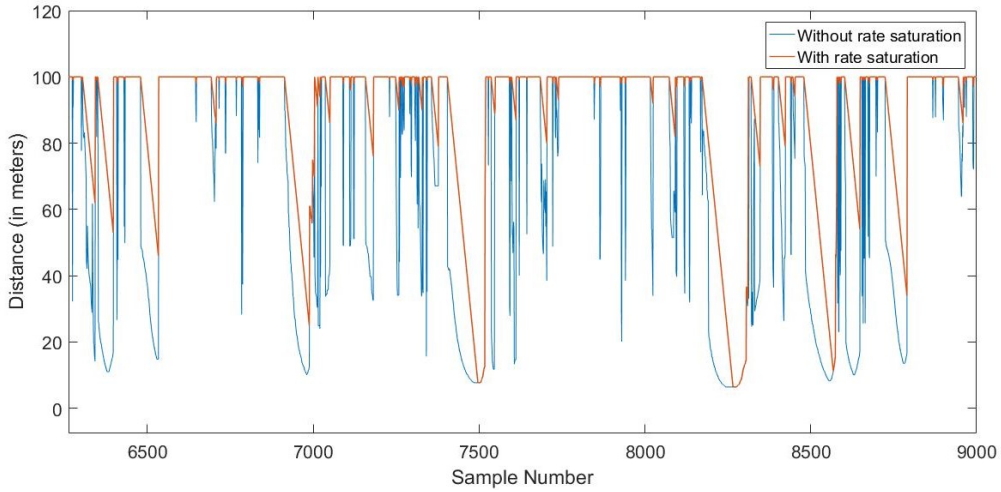

Figure 4.6 – Relative Distance profile (one LIDAR layer) with and without rate saturation

4.3 Neural Network Design

4.3.1 Architecture

As mentioned before, multi-layer feed-forward neural network is used in the model development to predict the vehicle speed and steering wheel angle profiles. The architecture of the neural network is shown in 4.8. The neural network model can be divided mainly into three parts with respect to the type of layers i.e. input layer, hidden layers and output layer. The layers are connected in a sequential manner. The input layer is the first layer followed by the hidden layers and output layer at the end. Each layer consists of perceptrons also called as neuron nodes. The number of nodes in each layer vary according to the design. Each perceptron in each layer is connected to every perceptron of the next layer thus forwarding the data from one layer to the next. Hence, these neural networks are called feed-forward networks. There is no connection between perceptrons of the same layer (More information can be found at http://www.cs.toronto.edu/ hinton/nntut.html). A general architecture of the feed forward neural network is shown in Fig. 4.7 (https://www.oreilly.com/library/view/deep-learning/9781491924570/ch04.html).

In the proposed neural network based predictive model, the number of input and outputs are 30 each. The number of future profile samples (output) of vehicle speed and steering wheel angle are 20 and 10 respectively (4 and 2 secs time horizon respectively with 0.2 secs sampling time interval). This predictive model is used later in the fusion process during which only first 10 outputs of each signal are considered i.e. the time horizon is 2 secs. The neural network used has 20 outputs (or 4 secs time horizon) for the intended vehicle speed signal only to explore the

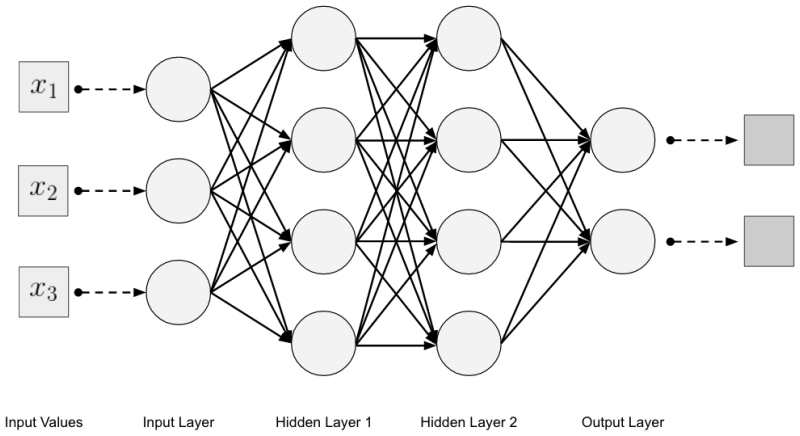

Figure 4.7 – General Neural Network Architecture

full potential of the model. Because of the complexity and non-linearity of the correlation between inputs and outputs, two hidden layers with 40 neurons each are considered. The number of hidden neurons is based on the number of inputs and outputs. The number of neurons in the hidden layers are considered to be on the higher side than necessary to keep the provision for model expansion in the future with additional inputs. The neural network trained using supervised machine learning techniques (regression). Hence, given the vehicle and environment state (inputs) at a time instant, the neural networks will predict the driving decisions. The neural network is implemented in the Neural Network Toolbox of Matlab.

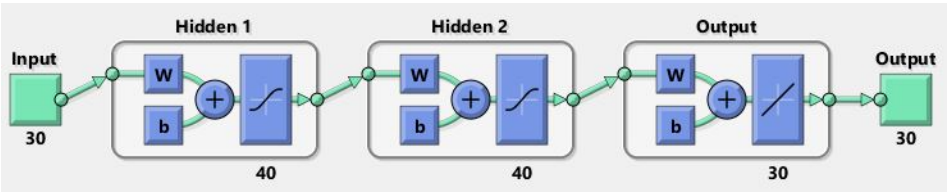

Figure 4.8 – Neural Network Structure

4.3.2 Training

For the purpose of training and offline validation of the neural networks, data is collected using the driving simulator and SCANeR studio software as shown in Fig. 4.9 from a city map inbuilt in this software. This map has various structures and objects for e.g. buildings, multi-lane roads, trees, bridge etc. The varied scenarios available in the map provides the data close to the real world.

Data is collected at the sampling rate of 5 Hz for the duration of 2 hours. This choice of sampling rate helps in the removal of impulsive disturbances in the data without lose of any important information. Virtual LIDAR sensor is mounted on the

Figure 4.9 – Driving Simulator Platform at Heudiasyc Laboratory

vehicle. The variation in the pitch and roll of the vehicle affects the sensor data, along with the built in disturbances. These factors help in getting sensor data close to that of the sensor in the real world.

Given the vehicle and environment state, the prediction horizon for the vehicle speed and steering wheel angle profiles are 4 and 2 secs respectively. The sharp and consecutive turns lead to the fast variation of the steering wheel angle which makes it difficult to predict for a larger horizon. The steering wheel angle varies mainly during curved roads, lane changes and turns, all of which last for a shorter duration. Labeled data for the training and validation of neural networks are created accordingly. Simulink and SCANeR studio software are integrated for the data collection and validation. Feature extraction algorithm is implemented in Matlab/Simulink which processes the collected data and forms input/output data sets.

The data set is divided into two parts (ratio 2:1) for the purpose of training and validation respectively. Back propagation technique is used to train neural networks [HECHT-NIELSEN, 1992]. Levenberg-Marquardt optimization method is selected specifically for this purpose. It is the fastest back propagation algorithm and gives the best training results when compared to the application of other algorithms. The performance of the neural networks are computed in the form of mean squared error (MSE). The validation is performed using the testing data. The validation results for the prediction of intended vehicle speed and steering wheel angle for different time sample steps (sampling interval = 0.2 secs) is shown in Fig. 4.10 and 4.11 respectively. It is evident that the prediction accuracy decreases with increase in the time horizon. To avoid over-fitting, we have used the regularization techniques which constraints the optimization parameters during neural network training.

4.3.3 Outlier Detection and Elimination

The uncertainties in the data set (for e.g. measurement noise in the LIDAR sensor data) creates outliers, thus affecting the learning performance of the neural networks. A higher threshold is set for the output error to identify the outliers. The training samples identified as outliers using this threshold are assigned a zero weight and the rest are assigned non-zero weight. The neural networks are trained again using weighted MSE as the performance function which ignores the training samples with zero weight. The detection and elimination of outliers improves the neural network performance. The total number of outliers eliminated is kept under 10% of the training data set. The training and offline performance of both the neural networks are provided in Table 4.1.

Table 4.1 – Neural Network Prediction Performance

	Intended Vehicle Speed	Intended Steering Wheel Angle
	MSE (kmph)	MSE (rad)
Training	5.2	0.06
Validation	6.5	0.1

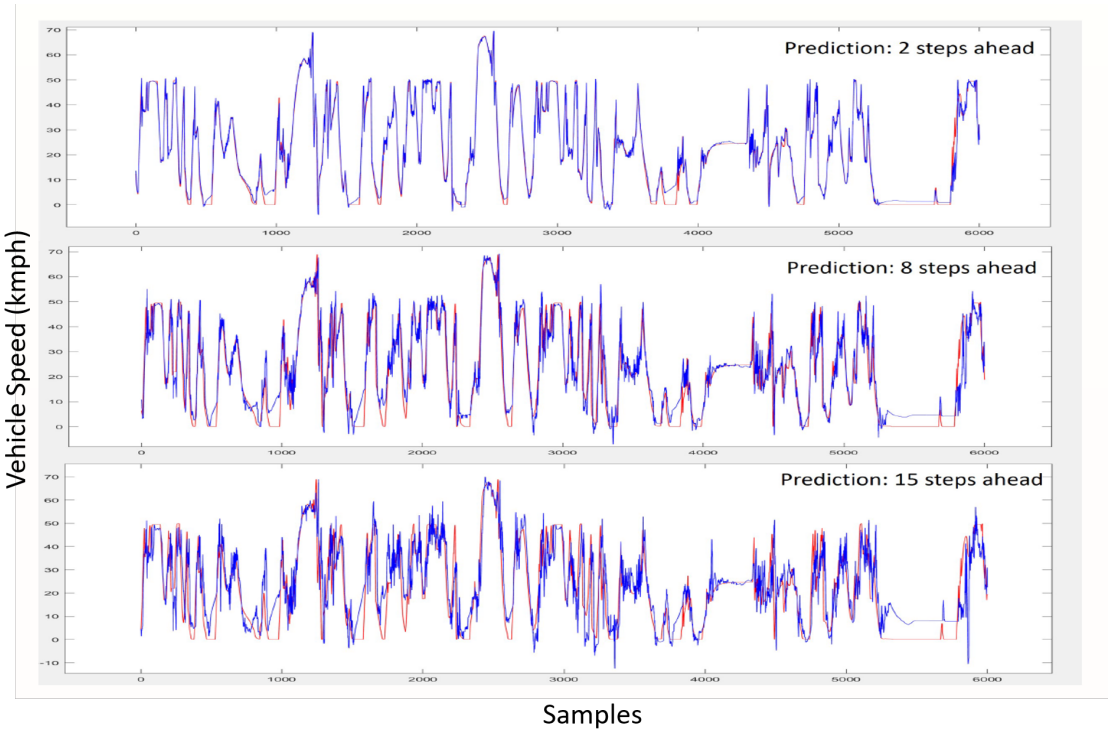

Figure 4.10 – Validation results for intended vehicle speed prediction at different sample steps with sampling interval of 0.2 secs. Actual intended speed is shown in red while the prediction is shown in blue.

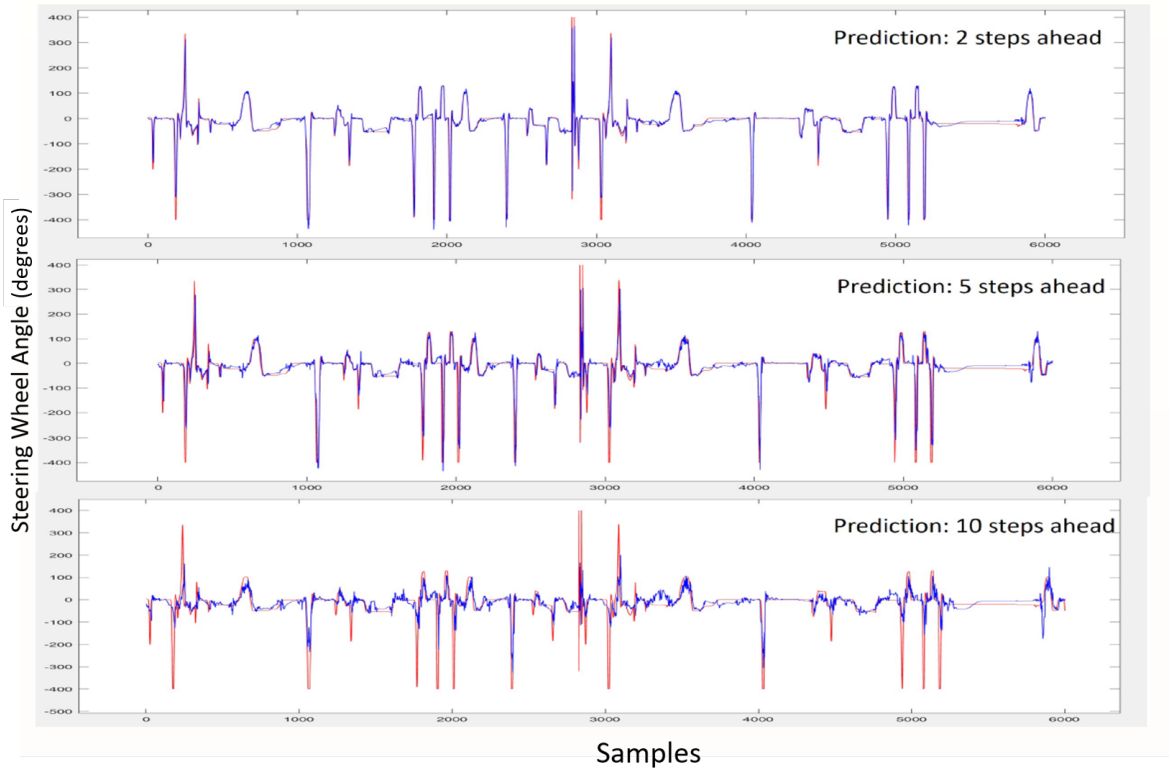

Figure 4.11 – Validation results for intended steering wheel angle prediction at different sample steps with sampling interval of 0.2 secs. Actual intended steering wheel angle is shown in red while the prediction is shown in blue.

4.4 Simulation Results and Analysis

The validation using SCANer studio has been carried out for various use cases and the test performance is as given in Table 4.1. We present the results and analysis of three of those use cases.

Use Case 1: This use case is related to the basic collision avoidance. At the start of the use case, the obstacles are dynamic and they come to a halt due to a traffic light. Since the target vehicle is driving in the same lane, the driver applies brakes and stops the vehicle smoothly. The snap shots of the use case are shown in Fig. 4.12 in a summarized form.

The profile of vehicle speed and brake pedal force is shown in Fig. 4.13. The brake pedal force is not used by the model and is considered for the analysis of the results only. Since the human driving model uses receding horizon, it is not possible to show the entire prediction in one graph. Hence, for the analysis, critical instants from the use case are considered and shown. In this use case, the driver applies brakes at around 11 secs. It is expected from the model to predict the decrease in the vehicle speed profile (due to obstacles) before the driver applies brakes.

This phenomenon is of early prediction is shown in Fig. 4.15. For the purpose of analysis, we have shown the profile of the relative distances (given as outputs by Feature Extractor) in Fig. 4.14. The graph clearly shows the decrease in the relative distance between the target vehicle and relevant obstacle due to which an early prediction is possible. The model continues with the correct prediction in the future as shown in Fig. 4.16. There is no change in the steering angle profile because of which it is not shown here.

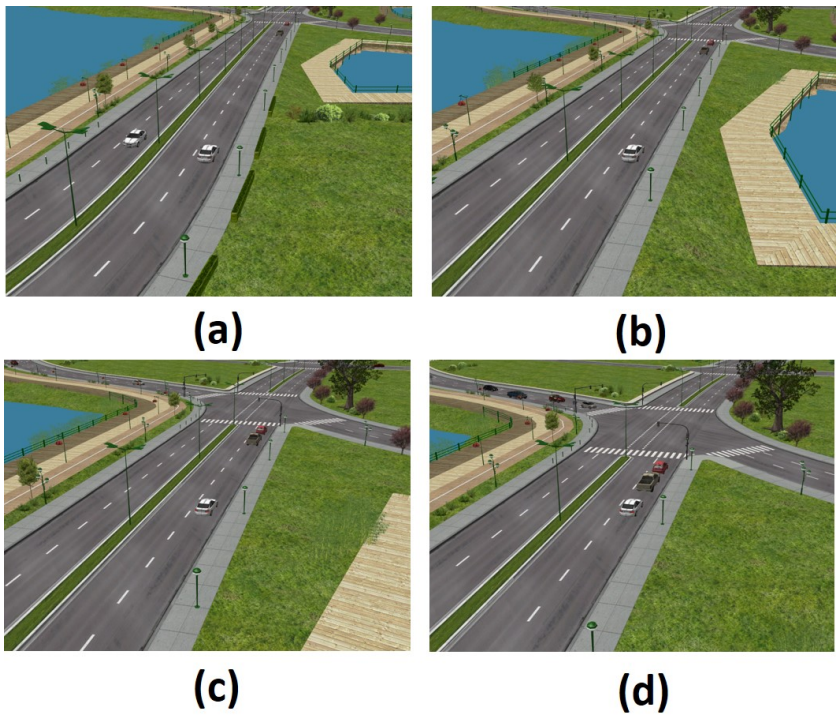

Figure 4.12 – Use Case 1: Snap shots of the test scenario in the order from ‘a’ to ‘d’

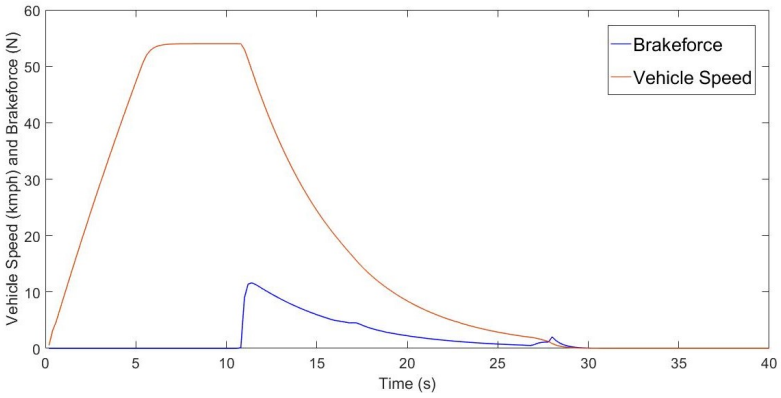

Figure 4.13 – Use Case 1: Profiles of vehicle speed and brake pedal force

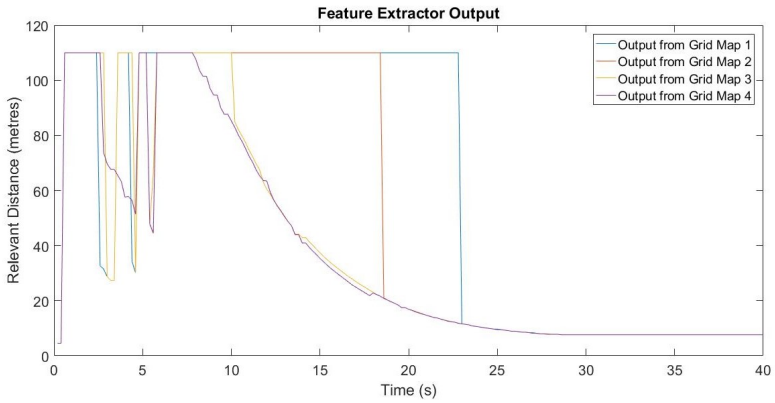

Figure 4.14 – Use Case 1: Relative distance outputs from Feature Extractor

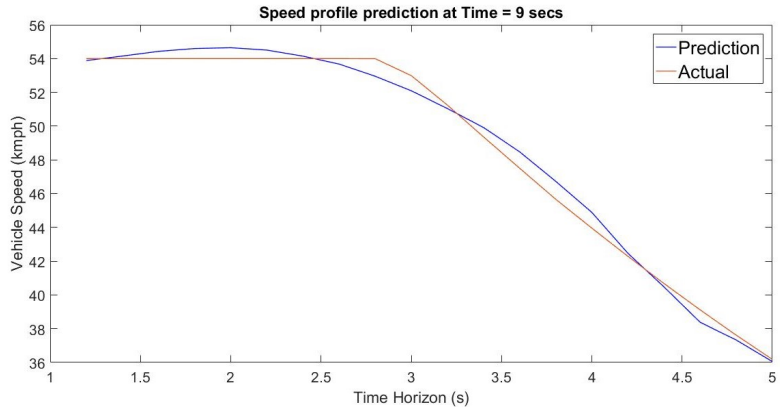

Figure 4.15 – Use Case 1: Vehicle Speed Profile prediction at time = 9 secs

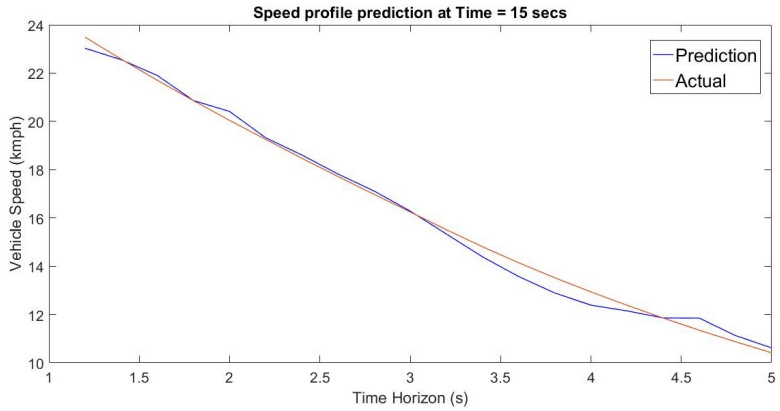

Figure 4.16 – Use Case 1: Vehicle Speed Profile prediction at time = 15 secs

Use Case 2: In this use case, the target vehicle accelerates, take a turn and then almost comes to a halt due to a bus (dynamic obstacle). The snapshots of this use case are shown in Fig. 4.17. The vehicle speed and brake pedal force profiles are shown in Fig. 4.18. The steering wheel angle profile is shown in Fig. 4.19.

The vehicle speed profile prediction at time instants 7.5 and 20 secs are critical since the model is expected to predict the decrease in the vehicle speed before the application of the brakes. These predictions are shown in Fig. 4.20 and Fig. 4.23 respectively. The selected critical time instants for the steering wheel angle prediction are 12, 13 and 15 secs. These time instants cover the part of the scenario where the vehicle takes a turn. The model predicts the variation in the steering wheel angle accurately as shown in Fig. 4.21 and 4.22 respectively.

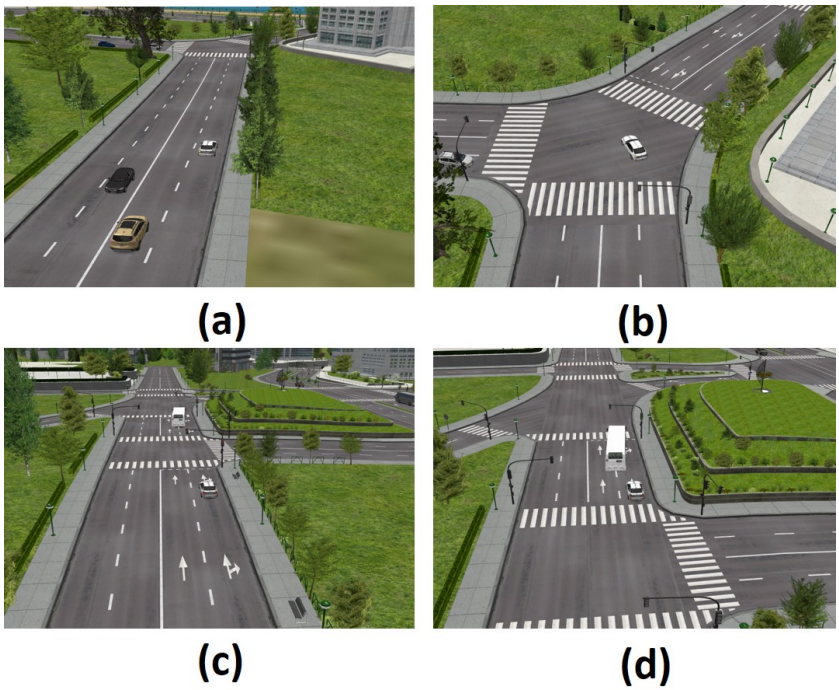

Figure 4.17 – Use Case 2: Snap shots of the test scenario in the order from 'a' to 'd'

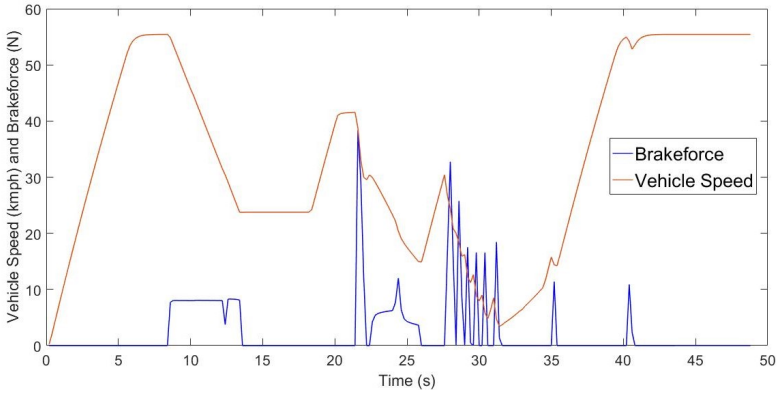

Figure 4.18 – Use Case 2: Profiles of vehicle speed and brake pedal force

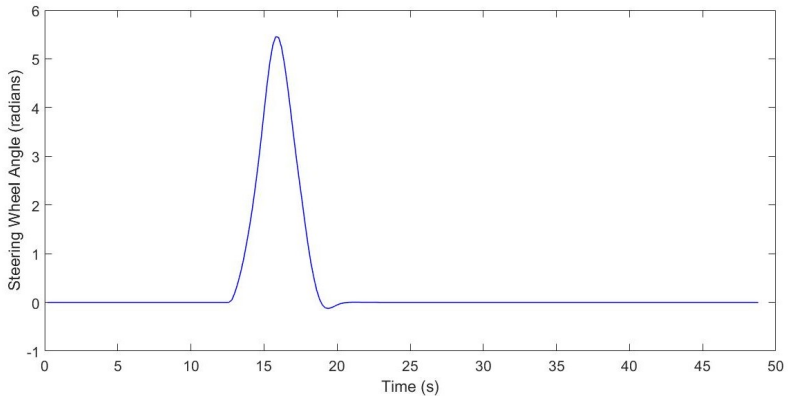

Figure 4.19 – Use Case 2: Steering wheel angle profile

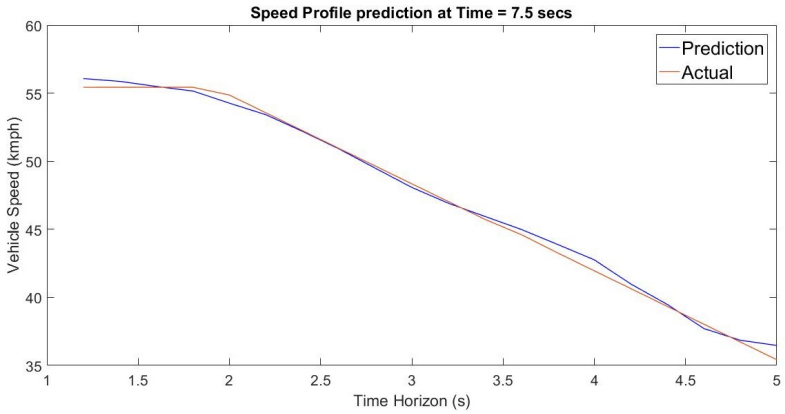

Figure 4.20 – Use Case 2: Vehicle Speed Profile prediction at time = 7.5 secs

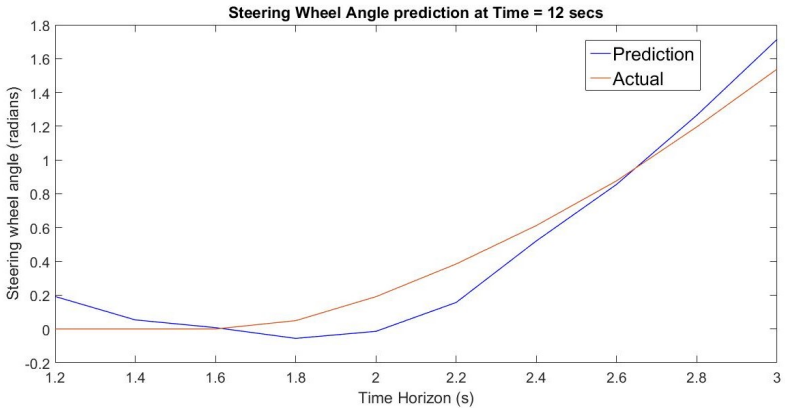

Figure 4.21 – Use Case 2: Steering Wheel Angle Profile prediction at time = 12 secs

Use Case 3: In this use case, the target vehicle overtakes a dynamic obstacle and comes back to its previous lane. To add complexity, another dynamic vehicle is present in the same lane which overtakes the same obstacle before the target vehicle. Hence, the human driver has to wait before overtaking the obstacle. The snapshots

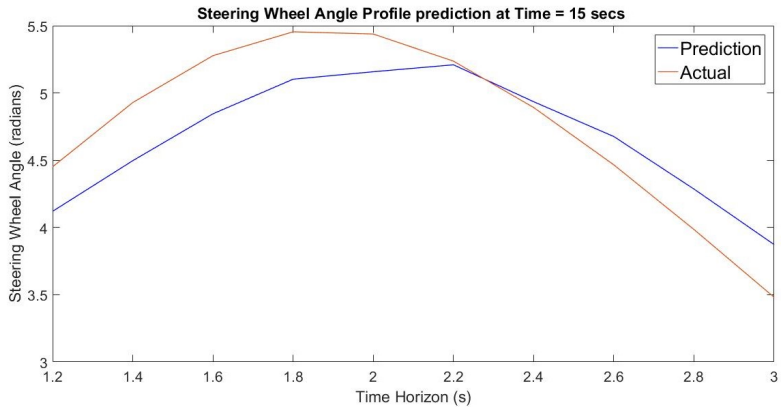

Figure 4.22 – Use Case 2: Steering Wheel Angle Profile prediction at time = 15 secs

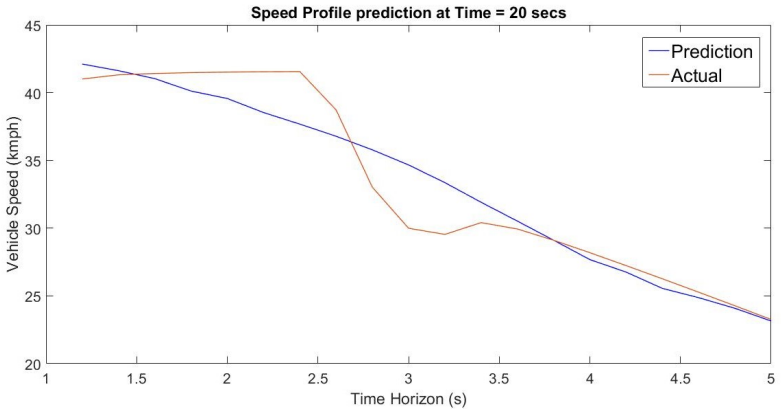

Figure 4.23 – Use Case 2: Vehicle Speed Profile prediction at time = 20 secs

of the scenario are shown in Fig. 4.24. The vehicle speed, brake pedal force and the steering wheel angle profiles are shown in Fig. 4.25 and 4.26 respectively.

Similar to the previous use cases, the critical time instants considered from the point of view of vehicle speed prediction are 5.5 and 26 secs. The critical time instant for the steering wheel angle prediction considered is 15 secs. The model predictions have less accuracy as compared to the previous use cases due to the complex nature of driving in this scenario as shown in Fig. 4.27, 4.28 and 4.29. The model predicts the future profile (output) in the form of samples. During the prediction, the neural network does not consider these samples to be correlated and predicts them independently. Hence, polynomial regression (quadratic) can be performed to these predicted future samples (for both vehicle speed and steering wheel angle) to increase the prediction accuracy. This phenomenon is shown in the Fig. 4.27, 4.28 and 4.29. The regression is applied to the prediction only when the predicted outputs do not form a smooth profile. This polynomial regression is different than that applied in the model architecture for representing the past information of the inputs.

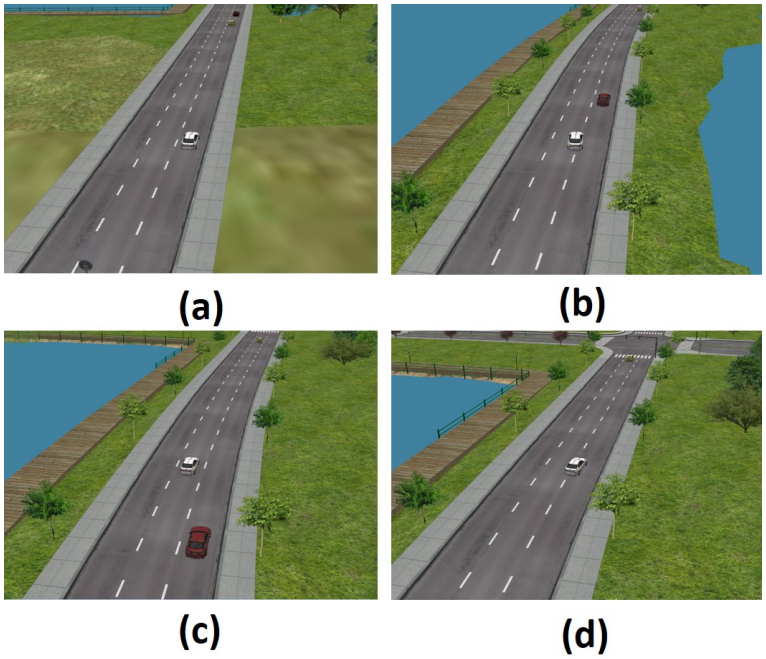

Figure 4.24 – Use Case 3: Snap shots of the test scenario in the order from ‘a’ to ‘d’

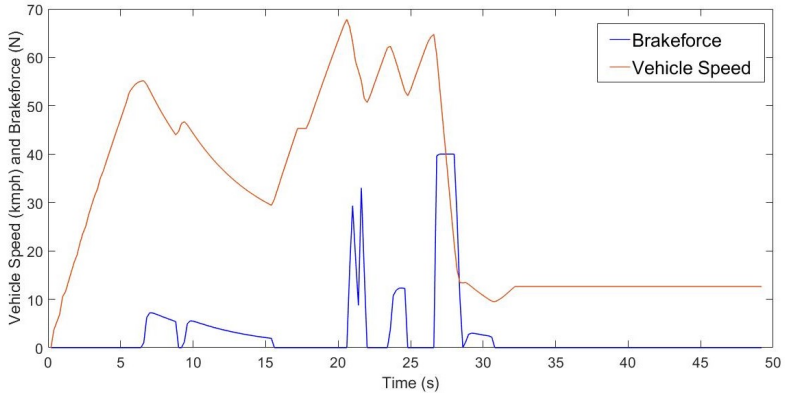

Figure 4.25 – Use Case 3: Profiles of vehicle speed and brake pedal force

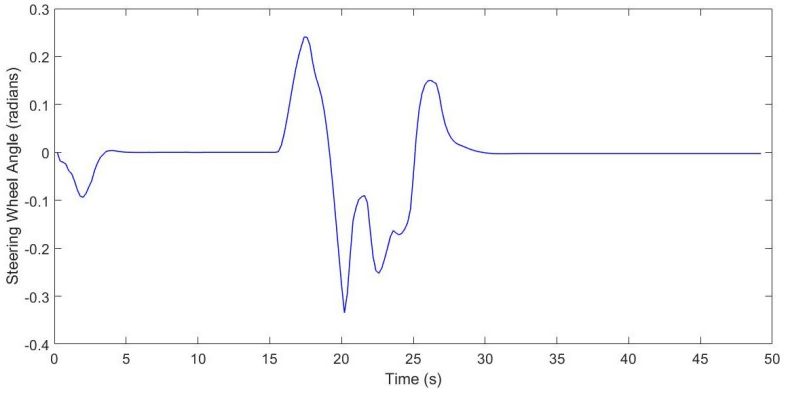

Figure 4.26 – Use Case 3: Steering wheel angle profile

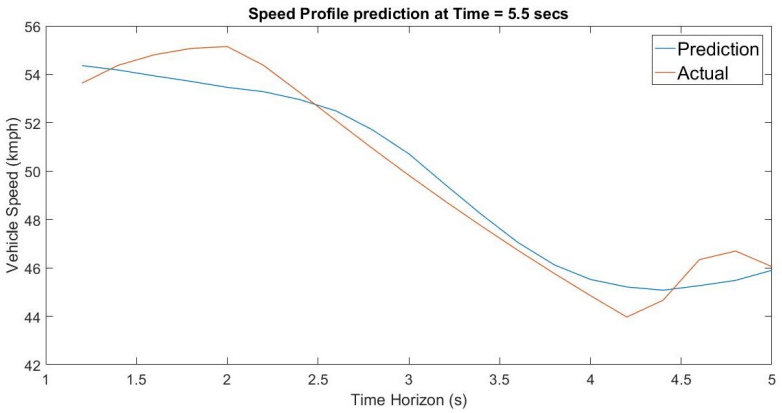

Figure 4.27 – Use Case 3: Vehicle Speed Profile prediction at time = 5.5 secs

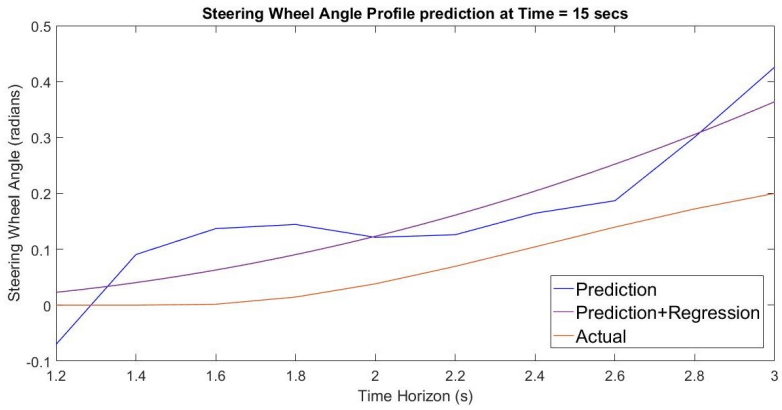

Figure 4.28 – Use Case 3: Steering Wheel Angle Profile prediction at time = 15 secs

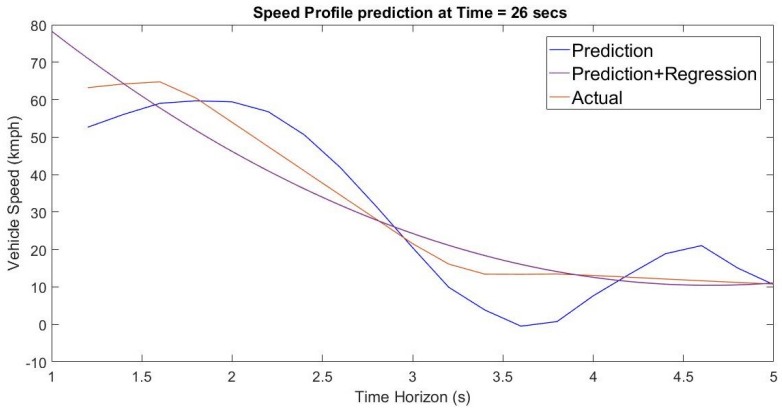

Figure 4.29 – Use Case 3: Vehicle Speed Profile prediction at time = 26 secs

4.5 Conclusion

For an effective driving inputs fusion, it is necessary to identify and quantify the driving intentions of human driver and AutoSys. For this purpose, the prediction of

the driving input profiles is important. Future conflict profile can be calculated from these driving input profiles. Multi-layer feed-forward neural network is used for the prediction of the human driving decisions (vehicle speed and steering wheel angle) for a particular time horizon. Environment perception, vehicle state and human intention are majorly the three input categories considered in the methodology. The inputs related to the environment perception are derived from the LIDAR sensor data. Training and validation of the neural network is performed using the driving simulator platform at Heudiasyc laboratory integrated with SCANeR studio software.

Decision Making using Non-Cooperative Game Theory

Contents

5.1 Introduction and Background

In the past researches, even though shared driving control mainly target road safety and driver assistance, its methodology vary with respect to the type of vehicle control, feedback to the driver, decision making technique, implementation etc. These factors define the overall intelligent driving strategy. In general, the methodology usually take the form of the haptic control where a single controller (directly linked to the vehicle) is controlled by both human driver and AutoSys. Most of the past researches are focused on the haptic shared control of the steering wheel where the steering torques of the human driver and AutoSys are combined leading to shared lateral control of the vehicle. This way the communication between them is established. In [Mars et al., 2014], different degrees of haptic shared control have been defined and their respective effects have been investigated through various subjective and objective indicators under different driving conditions. An aspect is ensured in this study that the human driver can always override the system.

Obstacle collision avoidance strategy is developed using the haptic shared control especially for the cases of human driver distraction in [Jensen et al., 2011]. Similarly, [Borroni and Tanelli, 2018] presents an adaptive weighted strategy to dynamically change the control authority for the driver assistance in the lateral vehicle control. A lateral vehicle dynamics model is used along with the steering system and vehicle positioning. This strategy is developed with the objective of lane keeping assistance. In [Soualmi et al., 2014b], the autonomous driving mode is considered to be the default driving mode and the shared control strategy is developed with respect to the human driver intervention in the case of undetected obstacles.

Two major approaches have been used in the past researches for the shared control development which are classical control and game theory. A differential game approach is used in [Mosbach et al., 2017] for the development of cooperative longitudinal driver assistance system. Here, the human driver is expected to work in a cooperative manner with the AutoSys with respect to an objective function which is unlikely. Model predictive control is used in [Guo et al., 2017] (for the lane keeping application) using the vehicle model for the dynamic control allocation with respect to the hazards. A shared fuzzy controller is presented in [Li et al., 2018d] incorporating the driving intentions and situation assessment using the Time to Collision (TTC) metric. Here, the vehicle and environmental state information is assumed to be available without any uncertainty. A fuzzy Takagi-Sugeno (T-S) optimal control method is used for the shared controller in [Soualmi et al., 2011]. The approach of traded control i.e. switched shared steering control is presented in

[Guo et al., 2018]. [Li et al., 2017] present a very different approach where the final controller and the AutoSys are combined forming indirect shared control. The final steering input is decided by the AutoSys by considering the human driving input.

Conflict between the human driver and AutoSys is an important factor in the shared control strategy. It arises mainly from the difference in the individual driving intentions. A driver model including the interaction factor has been presented in [Wang et al., 2018] with the aim of improvement in the prediction accuracy of the driving intentions. The degree of driver reliance on the haptic steering feedback is also considered. The effects of conflict (arising due to the difference in perception or individual driving intentions) on the overall driving performance are studied in [Johns et al., 2016]. The application of torque on the steering wheel without any warning to the human driver is often observed as a failure of the shared control. Hence, the human-machine interaction and the way the conflict is handled play an important role from the point of view of human factors. Similarly the control authority transition effects with respect to the human factors are presented in [de Winter and Dodou, 2011]. Analysis of the effects of online adaptation on the driving performance are studied and presented in [Benloucif et al., 2019]. The concept of shared control is also of interest in the field of robotics [Alonso-Mora et al., 2014]. Considering the past research in the shared control, following are the limitations observed:

- Shared control development for specific driving scenarios such as lane keeping, lane assist, longitudinal control, lateral control etc.
- No consideration of uncertainties in the vehicle and environmental states.
- Dependency on the vehicle and environment dynamics model which are highly non-linear.
- The way conflict is handled with respect to the individual driving intentions.
- Haptic feedback to the human driver thus introducing intervention in the driving. This might be uncomfortable for the human driver.
- Lack of communication of information to the human driver to understand the status of the shared controller.

The shared control strategy presented in this chapter is focused not only on the improvement of the driving safety and performance but also to generalize the fusion system with respect to the observed limitations mentioned above.

5.2 Driving Intention Quantification

Given a vehicle and environmental state, there exist a difference in the driving behavior of the human driver and AutoSys. From the point of view of decision making, the main objective of the shared driving is to utilize this difference to improve the safety and performance. Hence, handling conflict between the human driver and AutoSys is an important aspect of shared driving control. If $u_1 = (v_1, \theta_1)$ and $u_2 = (v_2, \theta_2)$ are the individual driving inputs of human driver and AutoSys respectively, then the conflict at any time t is given by

$$Conflict(t) = u_1(t) - u_2(t) \tag{5.1}$$

Conflict at any given time is dependent directly on the individual driving intentions. As shown in the previous chapter, a neural network based model is developed for the prediction of the driving behavior of human driver and AutoSys. The model predicts the profiles of intended vehicle speed and steering wheel angle for the time horizon of 2-4 secs. For the shared driving methodology, the prediction time horizon considered is T secs considering the accuracy of the model output. These predicted profiles represent the quantification of individual driving intentions.

We have developed a method to compare the individual driving intentions using similarity measure proposed in this work. The comparison of the predicted profiles is equivalent to finding the similarity between two trajectories which can be directly correlated to the shape of the trajectories. Hence, the shape of the predicted profiles need to be quantified. The polynomial regression is performed for the predicted profiles of intended vehicle speed and steering wheel angle. The coefficients of the regression quantify the shape of the profile. Hence, the comparison of the polynomial regression coefficients of two different profiles is equivalent to the comparison of their individual shapes.

Consider the sample predicted profiles of intended vehicle speed shown in Fig. 5.1. The polynomial regression (2nd order) coefficients are scaled and plotted on a Cartesian coordinate plane as shown in Fig. 5.2. Consider a quadratic function $y = ax^2 + bx + c$. The output y is more sensitive to the coefficient value a than b. Hence, both the axis need to be scaled accordingly. Considering the time horizon as T secs, the coefficient a is scaled to Ta. The value at $t = 0$ is considered the current vehicle speed or steering wheel angle i.e. the coefficient c for both human driver and AutoSys. Hence, the coefficient c is not considered in the mapping. The distance between the two profiles can be represented by the Euclidean distance between

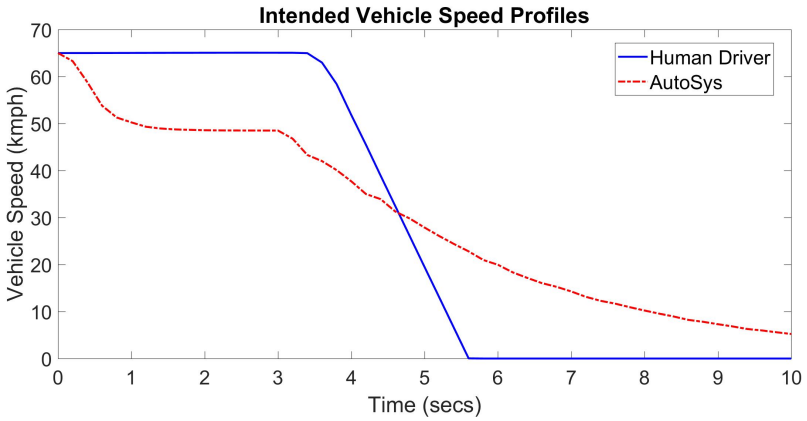

Figure 5.1 – Sample profiles of intended vehicle speed with the time horizon of 12 secs

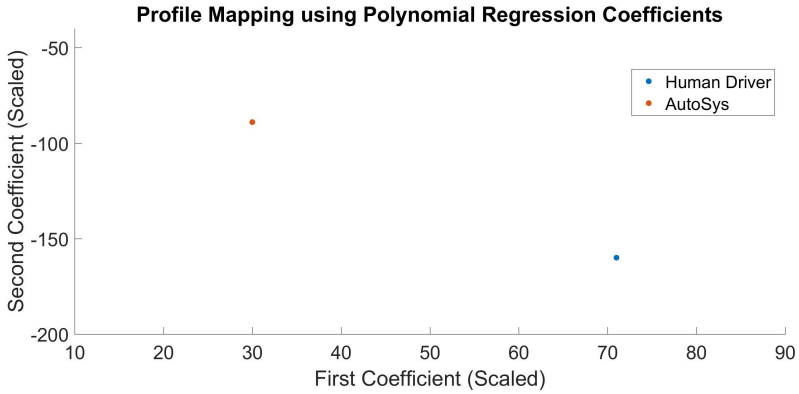

Figure 5.2 – Mapping of scaled coefficients of polynomial regression (2nd order) of profiles shown in Fig. 5.1 on a 2D plane

their respective mapped points. Let D be the Euclidean distance between the mappings in Fig. 5.2. The similarity between the profiles is inversely proportional to the square of distance between given as:

$$Sim(P_H, P_A) \propto \frac{1}{D^2} \tag{5.2}$$

where P_H, P_A represent the predicted profiles of human driver and AutoSys respectively. The similarity function is defined with respect to a context in the later section. Similarly, the predicted profiles of steering wheel angle can be mapped on to the 2D plane using polynomial regression. Thus, both the predicted input profiles (intended vehicle speed and steering wheel angle) can be mapped in a 4 dimensional space.

The mappings of the predicted profiles represent the individual driving intentions. Since the mapping function is continuous, the individual driving intentions are also of the continuous nature. The 2D mapping plane can be divided into different regions representing different high level driving intentions such as acceleration,

braking, turn right or left, constant speed etc as shown in Fig. 5.3 and Fig. 5.4.

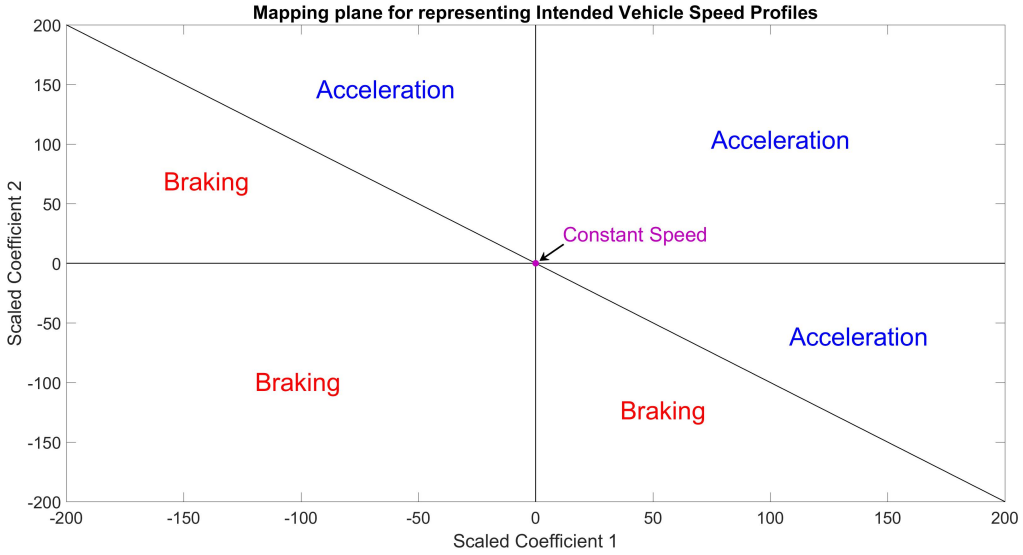

Figure 5.3 – Different regions representing high level intentions (Intended Vehicle Speed)

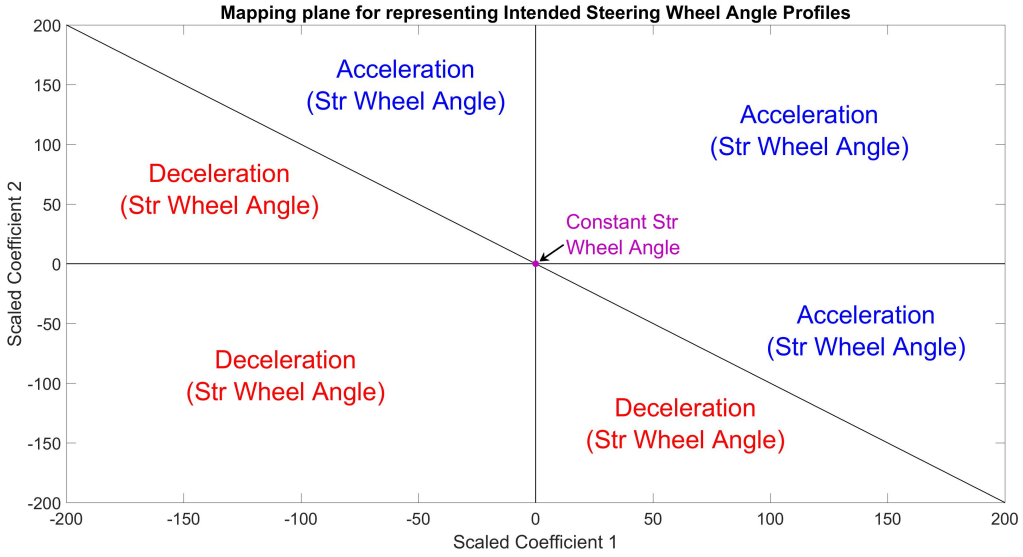

Figure 5.4 – Different regions representing high level intentions (Intended Steering Wheel Angle)

5.3 Decision Making Strategy

In this section, we define a 2 player non-cooperative game as a bargaining problem. The game is defined with the aim of conflict resolution i.e. the bargaining solution or the Nash equilibrium will resolve the conflict between the human driver

and AutoSys. The fusion system analyzes this game and the bargaining solution represent the final driving input $(v_{final}, \theta_{final})$ for the vehicle.

5.3.1 Two Player Non-Cooperative Game

In the field of decision making, strategy and interaction play an important role in the case of multiple participants. These decisions lead either to a gain or loss for the participants. A mathematical theory related to the study of rational strategy making in interactive situations is called Game Theory [Watson, 2001]. It has wide range of applications in the field of economics, social situations, computer science, business strategies etc. For the purpose of decision making, the problem is represented in terms of a game. A game consists of at least two players and are broadly classified as Cooperative and Non-Cooperative games. In a cooperative game, the outcome either gain or loss is common to all the players. Hence, it is expected to work together in a cooperative manner. The mathematics of a cooperative game is related to find a decision making strategy to maximize the gain for all the players. Similarly, in a non-cooperative game, the outcome is different for all the players. For e.g. In a game of chess, only one player can win. Hence, the mathematical strategy is focused on maximizing the gain of individual player. The solution to a non-cooperative game is often referred to as an equilibrium point.

Both human driver and AutoSys provide the driving inputs independently without any interaction with respect to their driving behavior and intentions. Only the fusion system has the direct control of the vehicle. Hence, shared driving can be seen as a 2 player non-cooperative game between the human driver and AutoSys. The conflict resolution is considered as a bargaining problem. Hence, its solution is the final driving input for the vehicle (low level controller). The bargaining solution to this 2 player non-cooperative game is given by the Nash equilibrium [Rusinowska, 2003]. Nash equilibrium is a stable solution to a non-cooperative game with multiple players, in which no player can obtain higher payoff/gain by deviating unilaterally from the individual strategy if the strategy of other players remain unchanged.

5.3.2 Loss Utility Function

The strategies of the non-cooperative game are related to maximizing the gain/payoffs. Similarly, the strategies can also be related to minimizing the loss of the players. The final driving input computed by the fusion system can be different than the individual inputs. In other words, the final driving intention can be different than the individual intentions. This deviation of the driving intention

can be seen as a loss to the human driver and AutoSys and is equivalent to their resistance against the final driving intention. This loss utility is represented in the form of a function over the 2D plane where the predicted driving profiles are mapped using scaled coefficients of polynomial regression as described in Section 5.2.

The resistance of the human driver to the final driving intention is dependent on the situation (for e.g. good/bad weather, drowsiness, distraction), confidence/driving skills and tolerance/flexibility towards modification of intention. For e.g. Given a deviation from the driving intention for a situation, the resistance shown by multiple human participants will be different. Hence, the loss utility is very subjective in nature. Similarly, in the case of AutoSys, the resistance is dependent on perception and navigation ability. The only objective factor of the loss utility function is that the loss value and its rate of change (derivative) are directly proportional to the deviation from the individual driving intention. Hence, the loss utility function is considered to be paraboloid in nature without loss of generalization. A sample loss utility function in shown in Fig. 5.5. The loss utility is a hypothetical parameter since it is non-measurable and subjective with respect to different human drivers and autonomous driving systems. Let the predicted profile be mapped to the point (A, B). Then the loss utility function is given as

$$f(x, y) = (x - A)^2 + (y - B)^2 \tag{5.3}$$

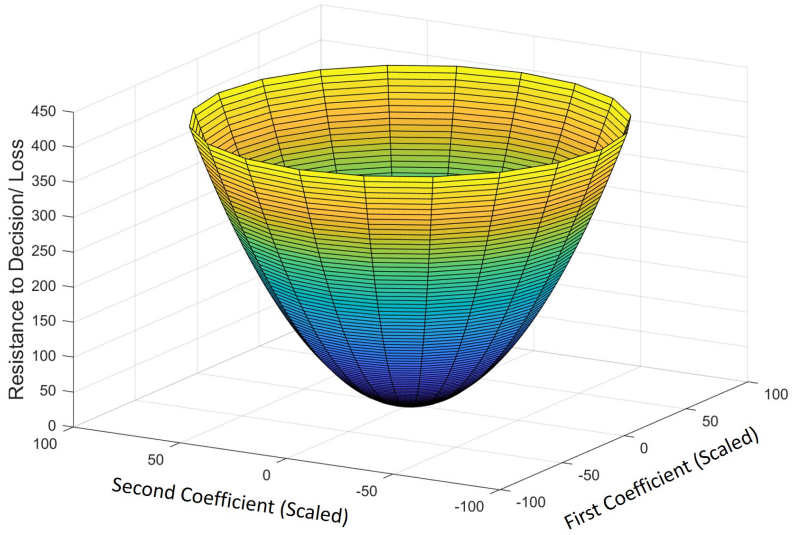

Figure 5.5 – Sample Loss Utility Function

The loss utility parameter defined previously for both human driver and AutoSys can be correlated to the conflict between the two. Consider the sample mapping of

predicted intended speed profiles of human driver and AutoSys as shown in Fig. 5.2. Let the mapped points be (A_h, B_h) and (A_a, B_a) respectively. The respective loss utility functions are plotted on both the mapped points. The loss utility functions for the human driver and AutoSys can be given as follows:

$$f_{Human}(x, y) = (x - A_h)^2 + (y - B_h)^2 = 0 \tag{5.4}$$

$$f_{Auto}(x, y) = (x - A_a)^2 + (y - B_a)^2 = 0 \tag{5.5}$$

The fusion system has to select a point on this 2D plane representing the final driving intentions. The predicted profiles of intended vehicle speed and steering wheel angle is the collection of the individual driving inputs over a time horizon. Hence, the difference in the respective predicted profiles of the human driver and AutoSys is the predicted conflict profile. Consider a predicted conflict profile (discrete) at time t over a certain time horizon consisting of N sample points. The Euclidean distance (E_D) between the mapped points not only represent the following:

- Quantification of the difference in shape of the profiles.
- Area between the profiles i.e. summation (discrete case) of the conflict values over the time horizon. This relation is given in the following equation.

$$\sum_{k=t+1}^{t+N} Conflict(k) \propto E_D \tag{5.6}$$

For any point (x_i, y_i) on this 2D plane, the loss utilities for the human driver and AutoSys will be $f_{Human}(x_i, y_i)$ and $f_{Auto}(x_i, y_i)$. Let the difference in the loss utilities with respect to (x_i, y_i) be δL_i, then its relation to the Euclidean distance E_D with respect to the loss utility function is given as follows:

$$\delta L_i \propto E_D^2 \tag{5.7}$$

Comparing Equations 5.6 and 5.7, we get

$$\sum_{k=t+1}^{t+N} Conflict(k) \propto \sqrt{\delta L_i} \tag{5.8}$$

In the non-cooperative game, let the two players i.e. human driver and AutoSys select a point each on the 2D plane representing the final driving intention. This selection is hypothetical in nature. Let the respective selected points be (x_H, y_H)

and (x_A, y_A) and the difference in the loss utilities for these selections be δL_H and δL_A respectively. The minimum of the two loss utility difference i.e. $min\ (\delta L_H, \delta L_A)$ wins the game.

Consider the sample predicted profiles (intended vehicle speed) as shown in Fig. 5.6(a). These profiles are mapped on the 2D plane as shown in Fig. 5.6(b). Respective loss utility functions are plotted on the mapped points as shown in Fig. 5.6(c). With respect to the game defined above, the intersection of the loss utility functions are of interest. As mentioned earlier, the conflict resolution between the human driver and AutoSys is correlated to the minimization difference in the loss utilities. Along with the minimization of the loss utility difference, the two players will also try to minimize their individual loss utility thus closing the difference between the final and their individual driving intentions. Hence, the final bargaining solution/Nash equilibrium state corresponds to the minimum value on the intersection curve. Hence, this bargaining solution will always lie on the line joining the mapped points representing individual driving intentions of the human driver and AutoSys respectively.

To simplify the analysis, consider the Fig. 5.7. The bargaining solution lie on the line joining the mapped points A and B. Consider a plane passing through the mapped points A and B as shown in Fig. 5.7a. The intersection of the plane with the loss utility functions is shown in Fig. 5.7b. The point on the x axis corresponding to the intersection of the two parabolas i.e. point C as shown in Fig. 5.7c is the bargaining solution between the human driver and AutoSys. Using the reverse mapping, the final driving profile (intended vehicle speed) can be derived from the bargaining solution as shown in Fig. 5.7d. The final driving input to be given to the vehicle can be derived from this fusion system profile. The fusion using the non-cooperative game is a receding horizon method. The predicted driving input profiles of both human driver and AutoSys are of discrete form. Considering the discrete values from both the input profiles are different time instants, the final driving input profile can be viewed as an output of a form of nonlinear regression applied to the discrete input profiles. The fusion process performs some form of polynomial data fitting with respect to the predicted driving input data.

The loss utility represents the approximation of the driver resistance or quantification of the driver reaction to the deviation from the intention which is subjective in nature. Without loss of generalization, the shape of this function is assumed to be parabolic but the function can be scaled to improve the quantification of the driver reaction. An example of the scaled function is shown in Fig. 5.7. The Nash equilibrium or the bargaining solution remains unchanged. Hence, no scaling of the loss utility function is considered in the strategy.

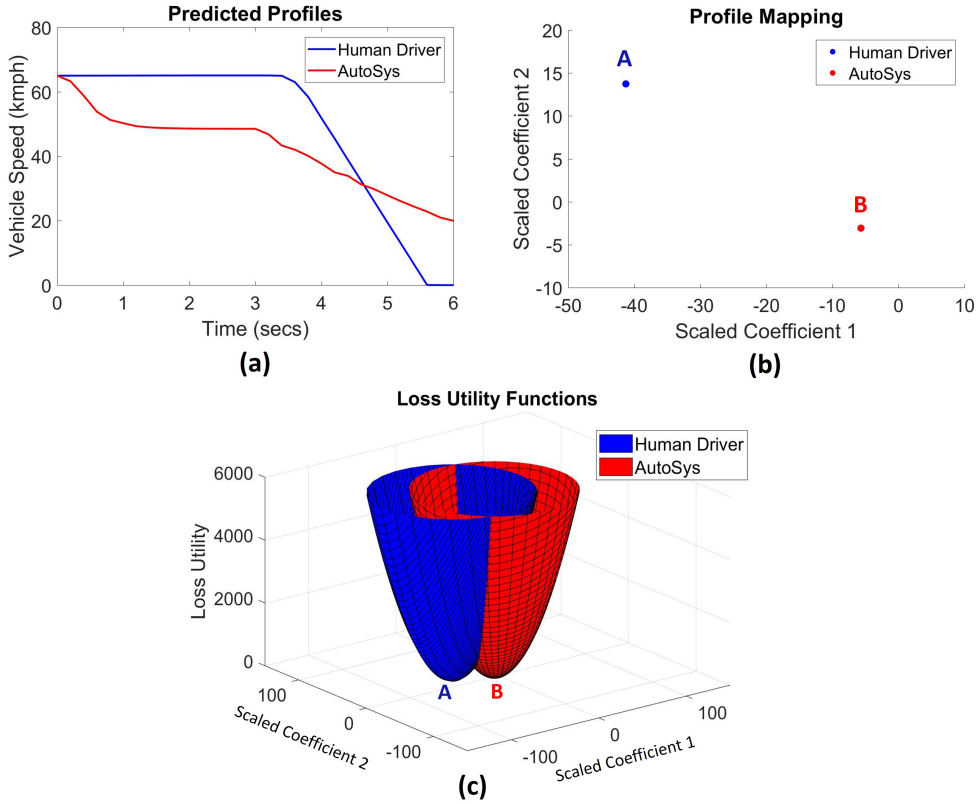

Figure 5.6 – (a) Sample predicted profiles (intended vehicle speed) of human driver and AutoSys, (b) Mapping of predicted profiles, (c) Loss Utility functions plotted over the mapped points.

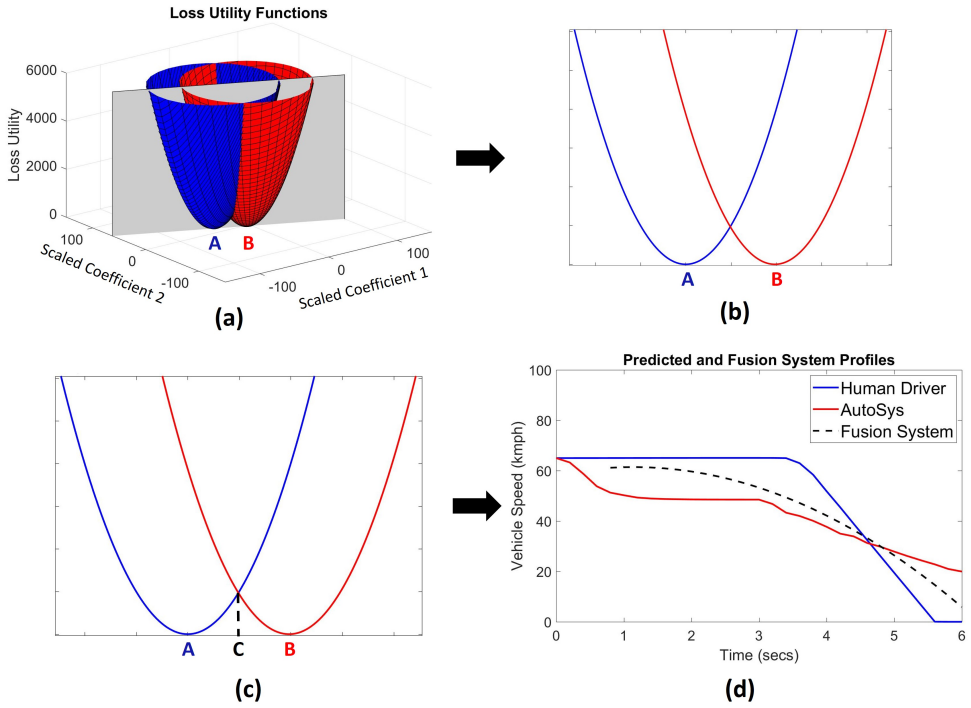

Figure 5.7 – (a) Sample predicted profiles (intended vehicle speed) of human driver and AutoSys, (b) Mapping of predicted profiles, (c) Loss Utility functions plotted over the mapped points, (d) Vehicle speed profile of the fusion system using the bargaining solution C.

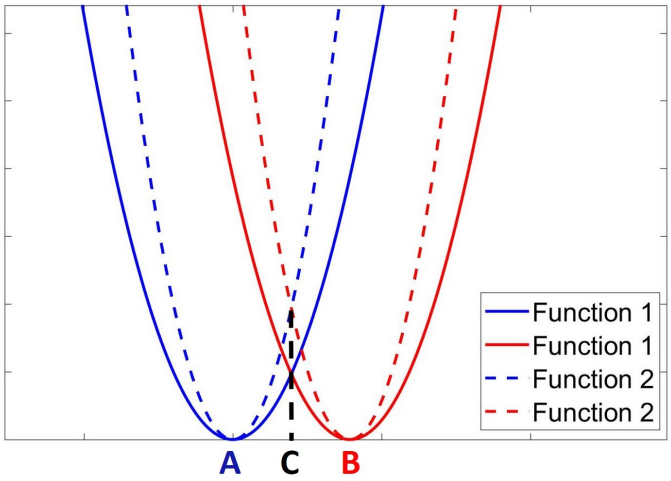

Figure 5.8 – Bargaining solution robustness to different steepness of loss utility functions

5.3.3 Incorporation of Driving Decision Admissibility

As seen in the previous chapter, the individual driving decision are assessed for the admissibility with respect to the collision risk, speed limit etc. The input certainties arising from the environment perception and dynamics are propagated to the driving decision admissibility. Consider a driving situation where the human driver is not driving efficiently i.e. the degree of decision admissibility is low. In such a situation, the human driver will expect the fusion system to take the corrective action. In other words, the human driver is more negotiable with respect to the bargaining problem i.e. the resistance shown by the human driver to the deviation from the individual driving input/intention will decrease as compared to the driving situation of high degree of decision admissibility.

The change in the degree of driving decision admissibility is reflected in the loss utility function as shown in Fig. 5.9. In the previous section, the loss utility function was defined to be of the parabolic nature. The degree of decision admissibility for that function was considered to be 100%. When the degree of decision admissibility decreases, the output of the loss utility function for a given input decreases. If the degree of decision admissibility is zero of either human driver or AutoSys is 0%, then the fusion system is expected to completely ignore this individual driving input. In terms of the loss utility function, the output will be zero for all inputs. Thus, the loss utility functions are defined for the 100% and 0% degrees of admissibility respectively. The loss utility functions for the degree of admissibility between 0 and 100% are uniformly distributed/calibrated as shown in Fig. 5.9.

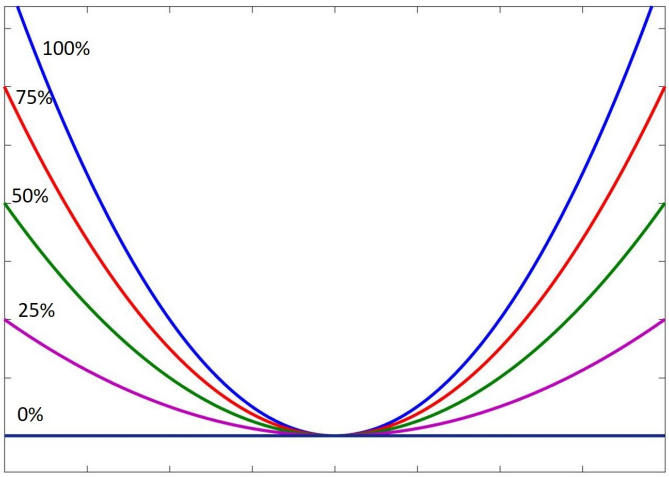

Figure 5.9 – Loss Utility Functions for different degrees of driving decision admissibility

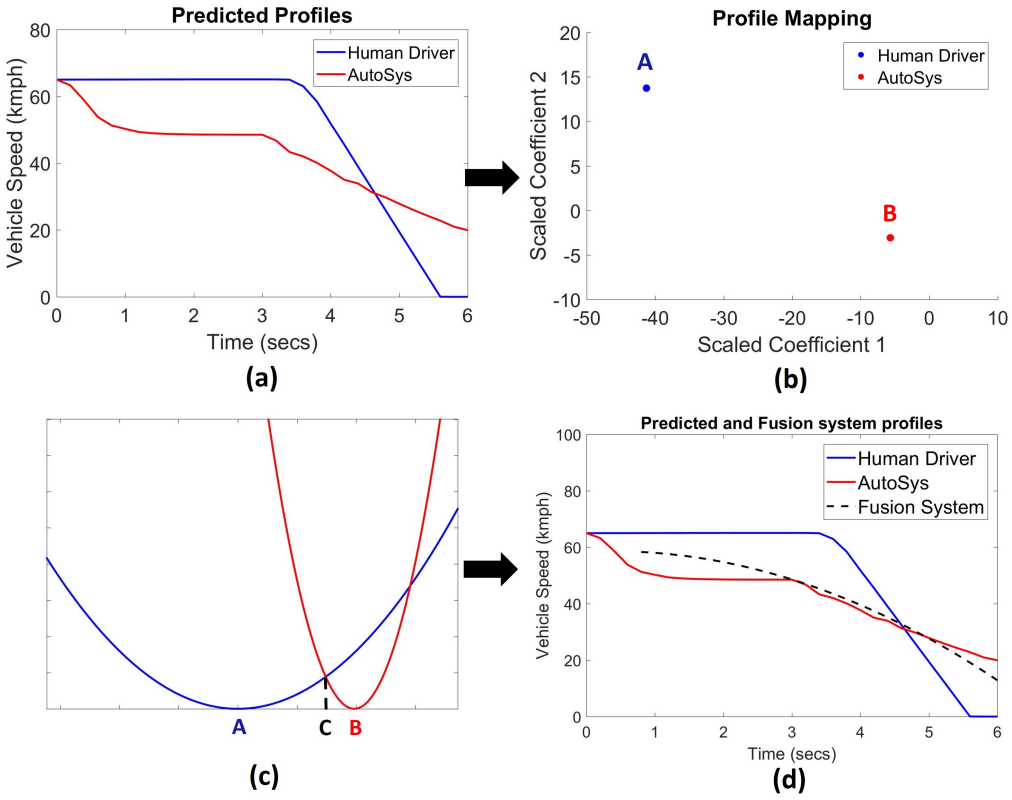

Figure 5.10 – An example of fusion process in the case of low degree of decision admissibility

Consider the predicted intended vehicle speed profiles shown in Fig. 5.7a. Let the degree of decision admissibility of human driver and AutoSys be 10% and 95% respectively. In such a situation, it is expected that the final driving input will be more inclined towards the individual driving input having higher degree of decision admissibility. The loss utility functions, bargaining solution and the resultant final

driving profile (intended vehicle speed) is shown in Fig. 5.10. Comparing the fusion system driving decision (intended vehicle speed) profiles of Fig. 5.7d and 5.10d, it is observed that the final decision profile in the 2nd case is more inclined towards the profile of AutoSys with higher degree of admissibility.

5.3.4 Incorporation of Driving Intention Similarity

Using the mapping of the predicted profiles, the driving intentions of human driver and AutoSys can be quantified and compared. Considering the fusion process, the resultant final driving input (vehicle speed and steering wheel angle) is dependent on individual driving intentions. Given the degree of decision admissibility with respect to collision avoidance, speed limit etc is high ($\geq$70%) for both human driver and AutoSys, there are some situations where the fusion of the driving inputs may not result in a better final driving input. These are the situations where the individual driving intentions are highly dissimilar for e.g. human driver intend to accelerate while AutoSys intend to decelerate, human driver intend to head straight while AutoSys intend to turn the vehicle etc. The high dissimilarity in such situations is evident from the different regions shown in Fig. 5.3 and Fig. 5.4. Hence, if the predicted profile mappings of human driver and AutoSys lie in different regions of driving intentions, then the fusion system follows the human driving input.

Given the high degree of driving decision admissibility for both human driver and AutoSys, assume that the predicted profile mappings lie in the same region. The difference in the individual driving intentions is quantified by the Euclidean distance between the mapped points. The similarity between the driving intentions is inversely proportional to this distance given by Equation 5.2. This similarity measure need to be incorporated in the fusion process. One of the major objectives of the fusion system is to assist the human driver. Hence, to be human centric is one of its characteristic. A similarity measure in terms of percentage of the AutoSys driving intention can be computed with respect to the human driving intention. This similarity measure can be incorporated in the loss utility function of the AutoSys. In other words, as the difference between the driving intentions increase, the acceptability of the Autosys driving intention for the human driver will decrease.

5.3.4.1 Similarity Function

The similarity between the predicted profiles is inversely proportional to the euclidean distance between their respective mappings on the 2D plane. The

individual driving intentions of human driver and AutoSys can be compared through these mappings. Since, the non-cooperative game is based on the loss utility function, the driving intentions are compared in the context of their respective loss utilities i.e. the loss utility functions of the respective mappings are compared to calculate the similarity measure.

Consider the predicted profiles (intended vehicle speed) and respective mappings shown in Fig. 5.6a and Fig. 5.6b. Consider the respective projection of the loss utility functions as shown in Fig. 5.7b. The comparison of these projections is equivalent to the comparison of the loss utility functions. The interpretation of the similarity measure with respect to the comparison of these projections can be made as follows. Given a mapping selected on the 2D plane, the projected functions can be compared through the difference in the respective loss utilities. In other words, as the mapping B approaches the mapping A, the overlap of the loss utility functions increase. If the mappings A and B match, the overlap of the loss utility functions is 100% i.e. the loss utility functions match. In this case, the similarity measure is considered to be 100%. The similarity measure is inversely proportional to the euclidean distance between the mappings. Let D be the Euclidean distance, then the similarity measure between the profiles P_H and P_A is given in Eqn. 5.9 where α is the scaling and tuning parameter. Using Equation 5.9 (α=0.001), the similarity measure function with respect to human driving intention can be plotted around point A as shown in Fig. 5.11. Since the similarity measure is defined with respect to the loss utility functions, the similarity function has the same form.

$$Sim(P_H, P_A) = \frac{1}{(1 + \alpha D^2)} \tag{5.9}$$

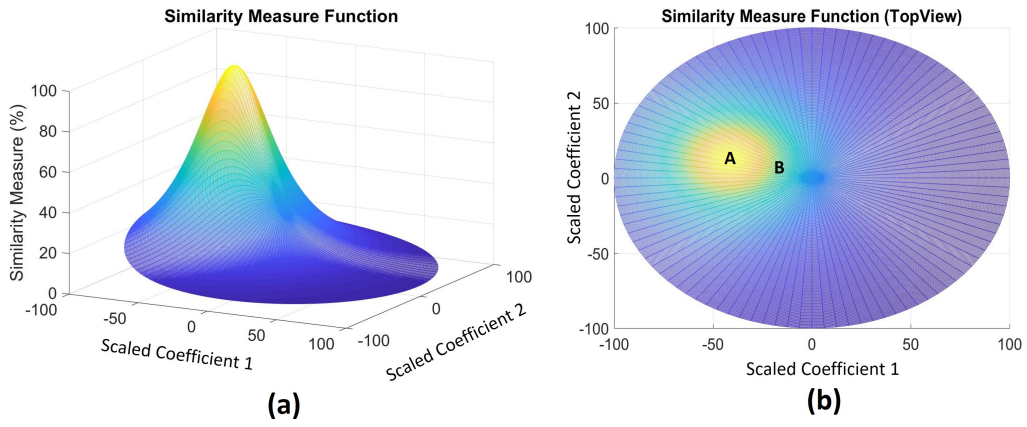

Figure 5.11 – Similarity Measure function plot over point A (representing human driver intention)

Consider the sample loss utility function projections as shown in Fig. 5.11. In the considered use case, the similarity between the driving intentions of human driver and AutoSys is 40%. Hence, the decision admissibility of AutoSys is considered to be 40%. The fusion process is then applied as shown in the previous section. Thus, using the similarity measure function, the individual driving intentions can be incorporated in the fusion strategy.

5.4 Experimental Validation

There are different functions performed by the fusion system to improve the driving safety and performance. The experimental setup, validation process and test scenarios are defined with respect to the validation of these multiple functions. The test scenarios cover both longitudinal and lateral navigation control. Following are the high level functional aspects of the fusion system:

- Human Centered
- Collision Avoidance
- Switching between manual and autonomous driving mode
- Manual driving refinement

5.4.1 Validation Setup

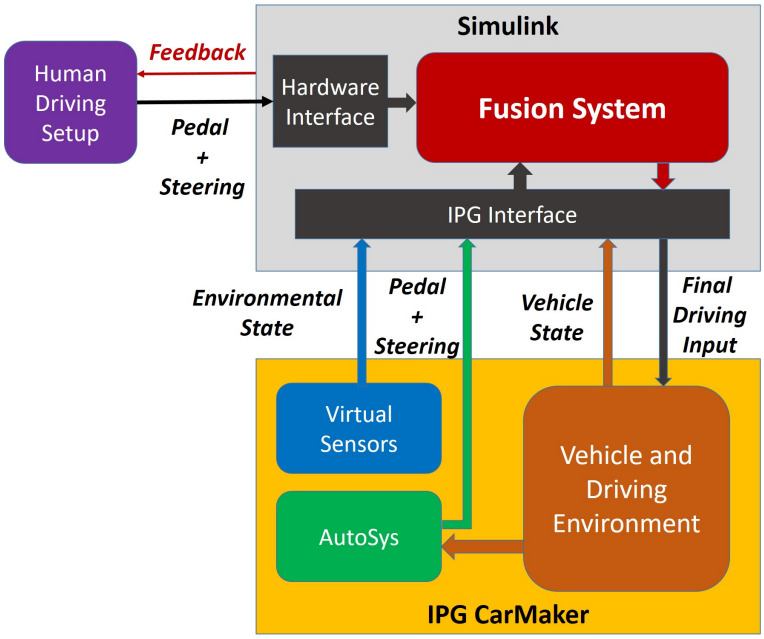

Figure 5.12 – Validation Setup: Integration of test rig, MATLAB/Simulink software and IPG CarMaker simulation software

The shared driving strategy is performed in the closed loop consisting of elements like human driver, autonomous driving system, vehicle and environment etc. The validation setup is shown in Fig. 5.12. The setup can be divided into three major components i.e. test rig and the softwares MATLAB/Simulink and IPG CarMaker. The human driver input is acquired through a test rig consisting of steering wheel and pedals. These were connected to a computer through a hardware interface. The fusion system architecture is implemented in the Simulink model. Separate simulink blocks were designed to incorporate the human driving input signals into the Simulink model. A feedback was generated in the Simulink model to provide the human driver relevant information necessary to operate in the closed loop environment of the shared driving control without any ambiguity and thus avoid any confusion. The objective of the project and validation was not the HMI i.e. interaction with the human driver since that is a challenging problem which need to be dealt with separately from a human factors perspective. Following are the signals fed back to the human driver:

- Actual Pedal Input
- Human Intended Pedal Input
- Actual steering wheel angle (from Fusion System)
- Human intended steering wheel angle
- Degree of Admissibility (0-100%) of the human driving input

These signals are selected for the feedback to update the human driver about the admissibility and deviation in the driving inputs. Conveying this information through mere numbers will make the assessment for human driver much difficult. Hence, a graphical user interface (GUI) is designed in Simulink for the purpose of validation. Some examples of this GUI are shown in Fig. 5.13. The pedal inputs (accelerator, brake) are presented in the form of percentage. To calculate the brake pedal input in terms of percentage, maximum value of brake force considered is 40 N. Consider the GUI in Fig. 5.13a. This is a GUI state at a time instant when the human driving input admissibility is low (50%). The deviation in the pedal input is high while that in the steering wheel angle input is low. The human driver can compare these deviations with the driving input admissibility to assess the situation and correct himself.

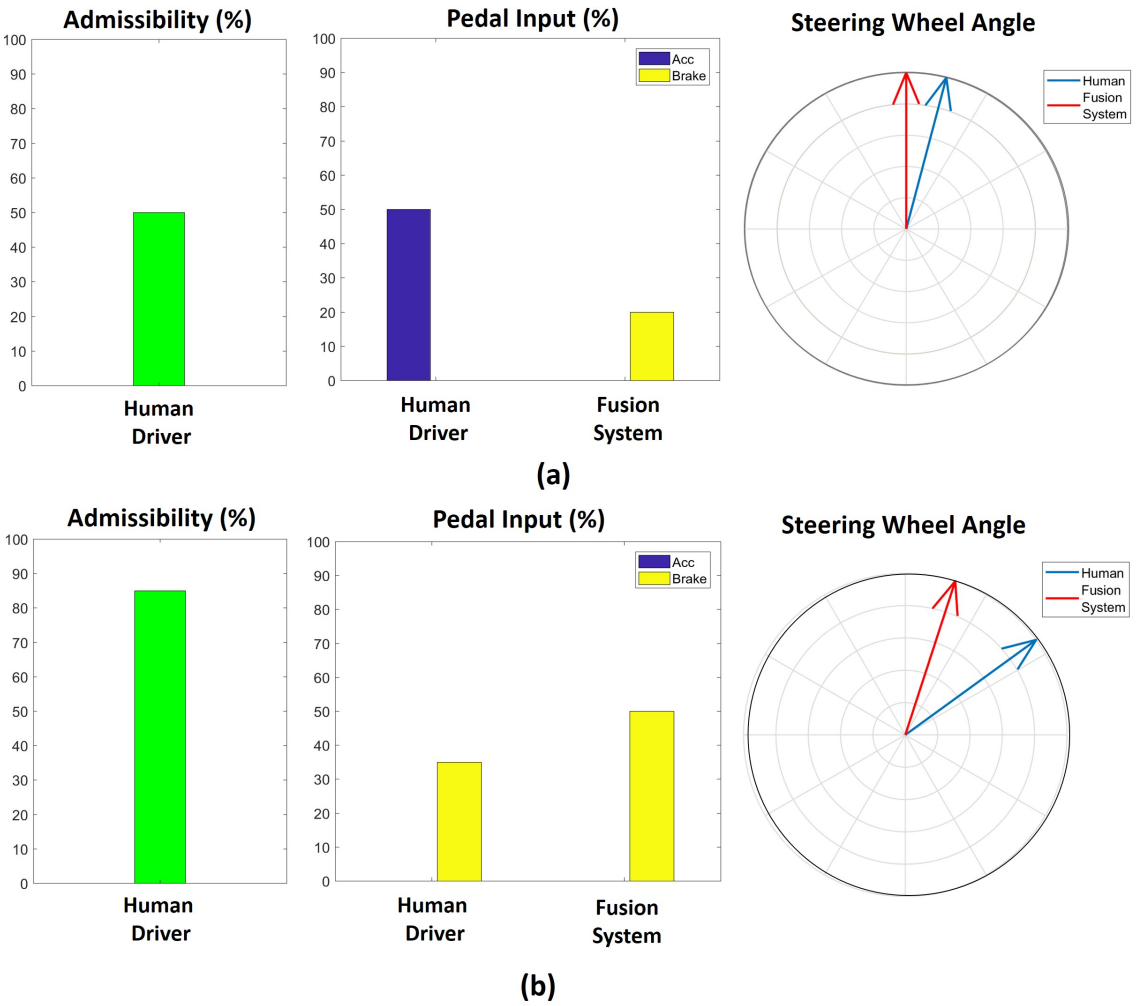

Figure 5.13 – Examples of the feedback to the human driver using GUI at different time instants in a driving scenario.

IPG CarMaker is used to simulate the vehicle and environment. Virtual sensors in IPG CarMaker like LIDAR etc is used to perceive the surrounding vehicles. The information related to the road orientation is also acquired from the IPG CarMaker which is used in the driver behavior prediction model in MATLAB/Simulink. There is an inbuilt autonomous driving system in IPG CarMaker which acts as another driver for the shared driving control. Some snapshots of the IPG CarMaker software is shown in Fig. 5.14.

The sensor data and the autonomous driving input is acquired by the Simulink model through the input interface simulink blocks of the IPG CarMaker. Computation of driving decision admissibility, driving behavior prediction and the fusion of the driving inputs is performed in Simulink. The final driving input is sent to the IPG CarMaker using output interface Simulink blocks. The vehicle and the environment state dynamics are obtained internally by the inbuilt autonomous

driving system. The human driver can observe the same in the graphics window of IPG CarMaker on a LED screen. The validation was performed during a placement at Jaguar Land Rover. The test rig used for the validation can not be shown in this report due to proprietary reasons.

Figure 5.14 – IPG CarMaker snapshots (ipg-automotive.com)

5.4.2 Validation Process

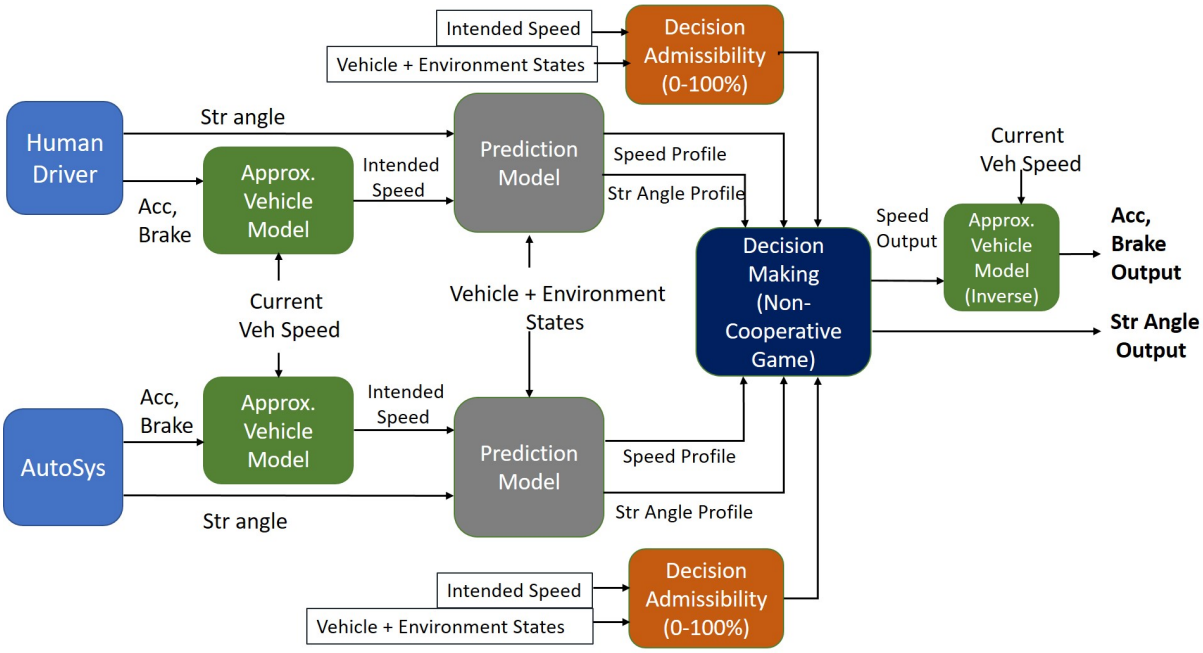

Figure 5.15 – Block Diagram of Shared Driving Control Implementation

The block diagram of the fusion system model implemented in Simulink is shown in Fig. 5.15. The human driver and AutoSys provide driving inputs in the form of pedals and steering wheel angle. The shared driving control methodology uses intended vehicle speed as one of the driving input. Hence, a neural network based model is developed to convert the pedal input and current vehicle speed to the intended vehicle speed. The final driving input is computed by the decision

making subsystem in the form of vehicle speed and steering wheel angle. The vehicle speed in the simulation tool IPG CarMaker is controlled only through the pedal input. Hence, a neural network based model convert the intended vehicle speed to a pedal input.

The driving test scenarios are categorized with respect to different aspects as shown in the table below. The categorization of the decision admissibility (High/Low) is only for the explanation purpose but is considered as a continuous variable during calculations. The high level driving intention comparison is also presented in the table below. The mismatch of the individual driving decision admissibilities directly implies the mismatch of the high level driving intentions.

Type	Human Driver Admissibility	Auto Sys Admissibility	Driving Intentions
A	high	high	match
B	high	high	mismatch
C	high	low	mismatch
D	low	high	mismatch

5.4.3 Driving Scenarios

For the purpose of validation, driving scenarios for the categories A, B, C and D are designed as shown in Figures 5.16, 5.17, 5.18, 5.19, 5.20 respectively.

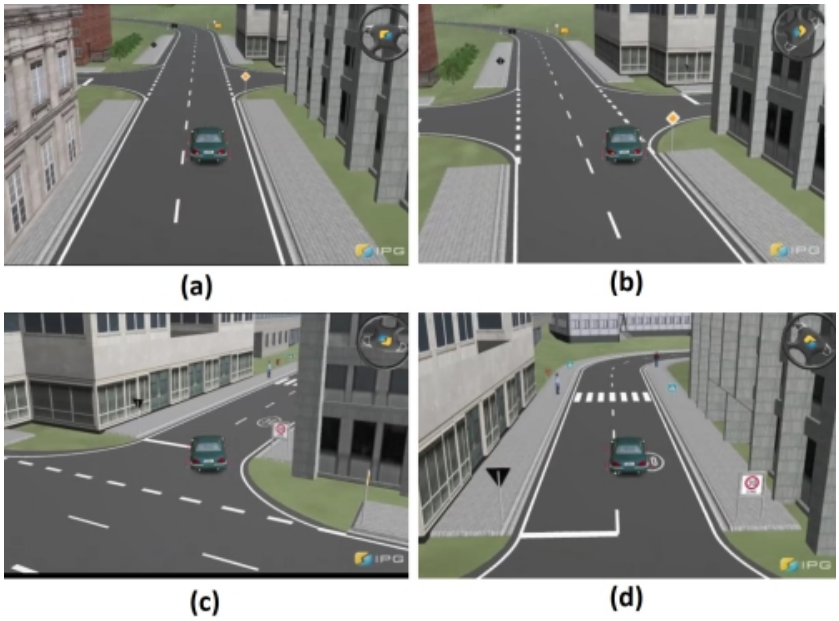

Figure 5.16 – Driving Scenario Type A: Sharp turn. The driving intentions of human driver and autosys match but the nature of vehicle trajectory differs. Individual driving inputs are admissible.

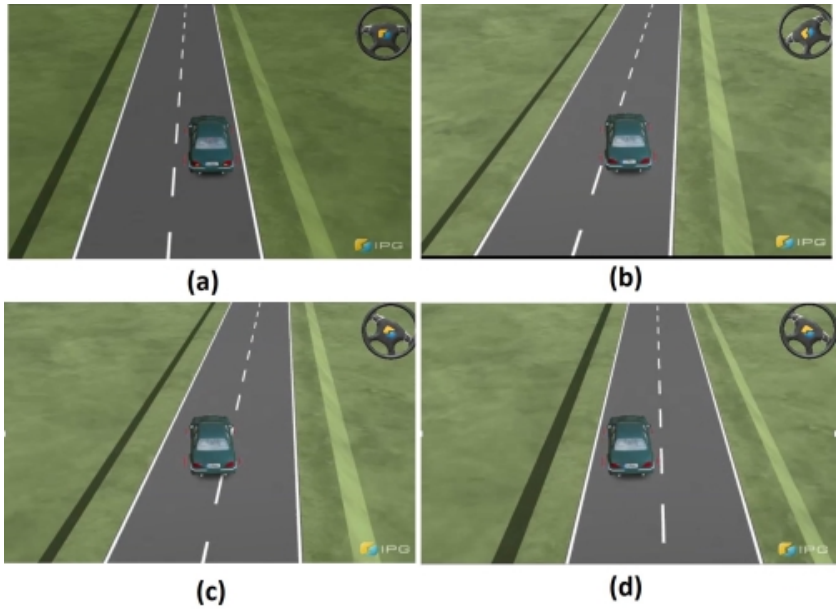

Figure 5.17 – Driving Scenario 2 Type A: Lane Change. The driving intentions of human driver and autosys match but the nature of vehicle trajectory differs. Individual driving inputs are admissible.

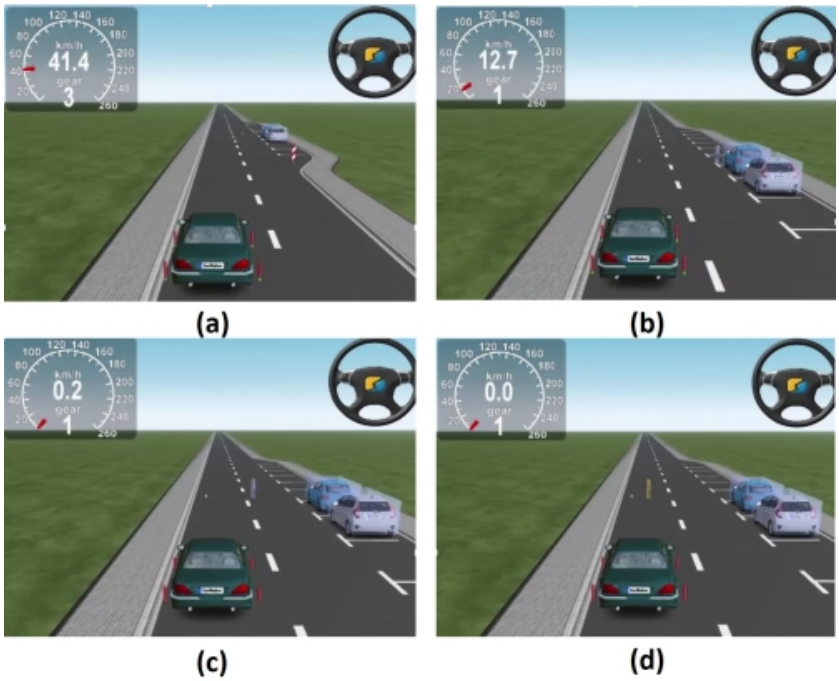

Figure 5.18 – Driving Scenario Type B: Target Vehicle encounters a rolling ball but the child is not visible. Human driver decelerates the vehicle to avoid probable collision, while the Auto Sys continues with the same speed. Individual driving inputs are admissible but the driving intentions do not match.

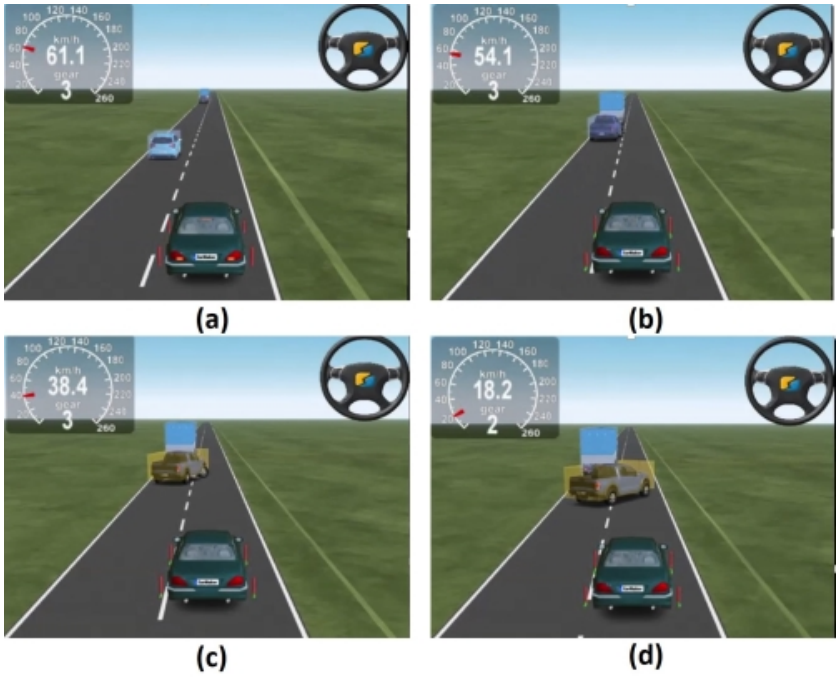

Figure 5.19 – Driving Scenario Type C: Stationary vehicle (in blue) suddenly sets in motion. Human driver interprets the situation pro actively and applies brakes to avoid collision (admissible decision). Auto Sys initially does not track the stationary vehicle and continues with the same speed (inadmissible decision)

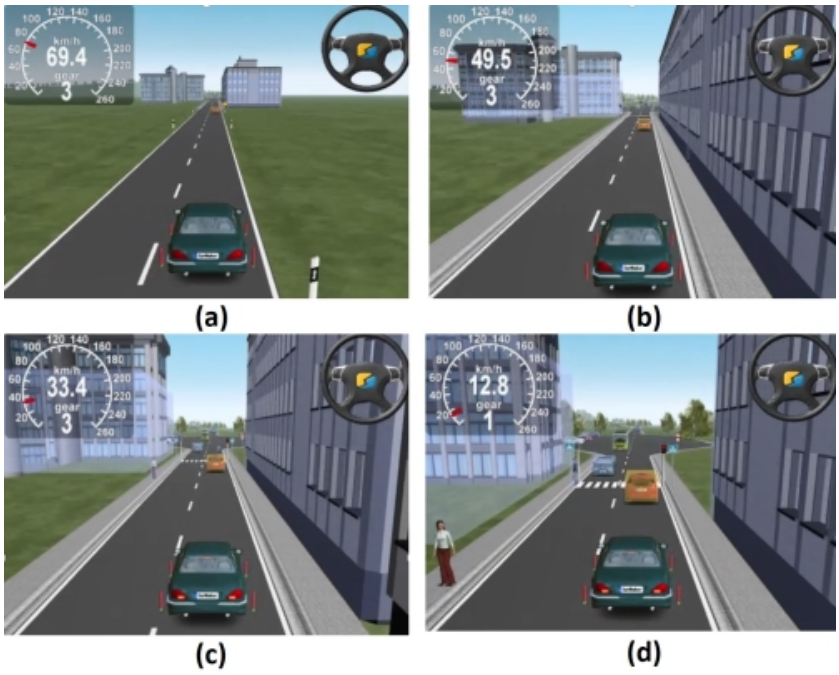

Figure 5.20 – Driving Scenario Type D: Human driver continues to accelerate leading to a possible collision (inadmissible decision) while AutoSys intends to decelerate the vehicle to avoid the collision (admissible decision)

5.4.4 Experimental Results and Analysis

The driving inputs fusion is done with respect to individual decision admissibilities and driving intention similarity. With respect to the driving safety, the decision admissibility has higher priority than the driving intentions.

The validation results related to Scenario type A (Fig. 5.16) are shown in Fig. 5.21, 5.22 and 5.23. Both the driving input profiles are highly admissible ($\geq$70%) throughout the scenario. Till t=25 secs, the conflict between the human driver and AutoSys is low. At t$\geq$25 secs, the conflict with respect to the steering wheel angle input starts increases and again decreases at t=31 secs. The fusion of the driving inputs is done with respect to the driving decision admissibility and similarity measure of the individual driving intentions.

The human driving profile (Fig. 5.23) is refined through the final profiles of vehicle speed and steering wheel angle. The fusion thus can assist the human driver in the situations of over-steering and under-steering. Comparing the steering wheel angle profiles of the human driver and the fusion system, the steering ratio for the human driver is variable. The variation in the steering ratio is felt by the human driver on the steering wheel i.e. the human driver participant felt resistance (during under/over steering) or assistance in steering indirectly because of the fusion system. It is thus possible to create this feel factor at the steering wheel without using a haptic feedback.

Scenario 2 (Fig. 5.17) is a test case of Type A. In this scenario, both the drivers have the intention to change the lane. The respective validation results are shown in Fig. 5.24, 5.25, 5.26. Similar to the earlier scenario, the human driving profile is refined using the fusion with that of Autosys. The fusion of the driving inputs (speed and steering wheel angle) result in the fusion of the intended vehicle trajectories. Given the high degree of driving decision admissibilities of both human driver and AutoSys, the influence of the similarity measure on the fusion process can be seen in Fig. 5.25. Similar to the earlier scenario, the fusion of the driving profiles (intended vehicle speed and steering wheel angle) is nonlinear.

The validation results related to Scenario type B (Fig. 5.18) are shown in Fig. 5.27 and 5.28. As seen in Fig. 5.28, the individual driving actions are admissible but the driving intentions are different (Fig. 5.27). Hence, the fusion system gives more preference to the human driver (human-centric). In such critical scenarios, it is always safe to follow human driver. In Fig. 5.27, the individual speed profiles are same till t=1 sec and then start differing but the fusion system smoothly follows the human driver without any transients. This phenomenon is seen because of the consideration of future driving behavior predictions during decision making.

During the fusion process (Fig. 5.15), the pedal inputs from the human driver and AutoSys are converted to speed inputs termed as intended speed. If either the human driver or AutoSys intend to jump to the actual vehicle speed profile, they can stop giving pedal inputs momentarily. This is an add-on provision in the test setup. Hence, at around t=7secs, there is a jump/transient in the intended speed profile of AutoSys.

The validation results related to Scenario type C (Fig. 5.19) are shown in Fig. 5.29 and 5.30. In this scenario, just before t=8 secs, the driving actions of AutoSys become inadmissible while that of human driver remain admissible as seen in Fig. 5.30. Hence, the fusion is done with more inclination towards human driving actions to avoid collision. Also, the AutoSys corrects its driving action at t=8 secs (Fig. 5.29).

The validation results related to Scenario type D (Fig. 5.20) are shown in Fig. 5.31, 5.32. Till t=7.5 secs, the individual driving intentions are similar and the fusion takes place accordingly. For t=7.5 secs to 16 secs, the individual driving intentions are dissimilar (similarity measure $\leq 60\%$) and hence, the fusion system becomes human centric and follows human driver.

The fusion is also dependent on the individual driving decision admissibility. Hence, at t=16 secs, the vehicle speed is decreased sensing the collision risk. Thus, the fusion system smoothly brakes the vehicle. Here, the admissibility of human driving is low and the driving intentions do not match. Hence, the fusion system follows AutoSys to avoid collision.

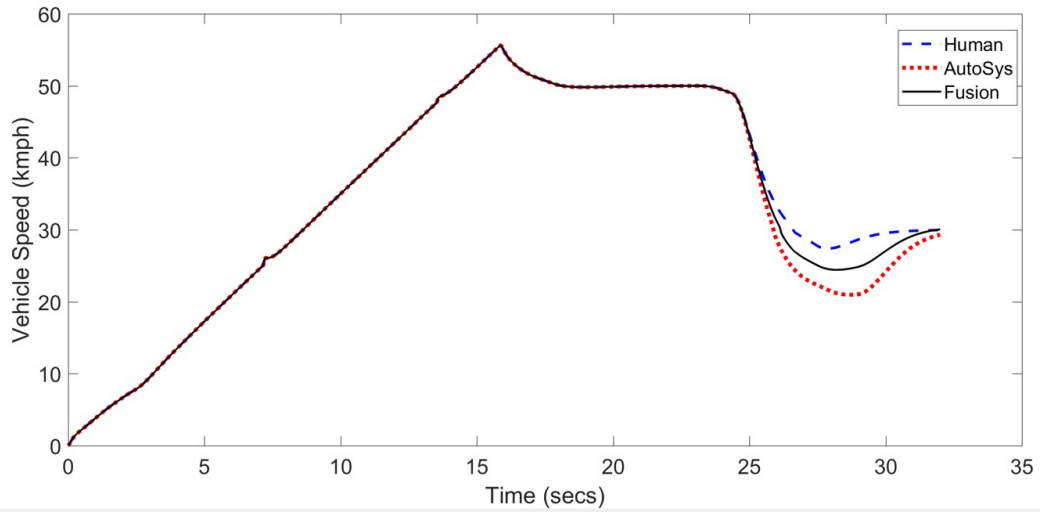

Figure 5.21 – Scenario Type A: Intended and Final Speed profiles

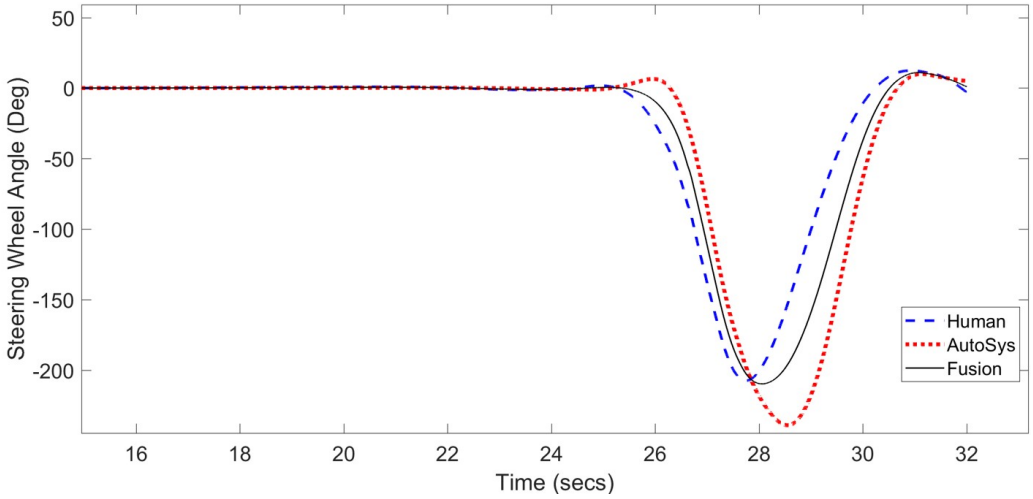

Figure 5.22 – Scenario Type A: Steering wheel angle profiles

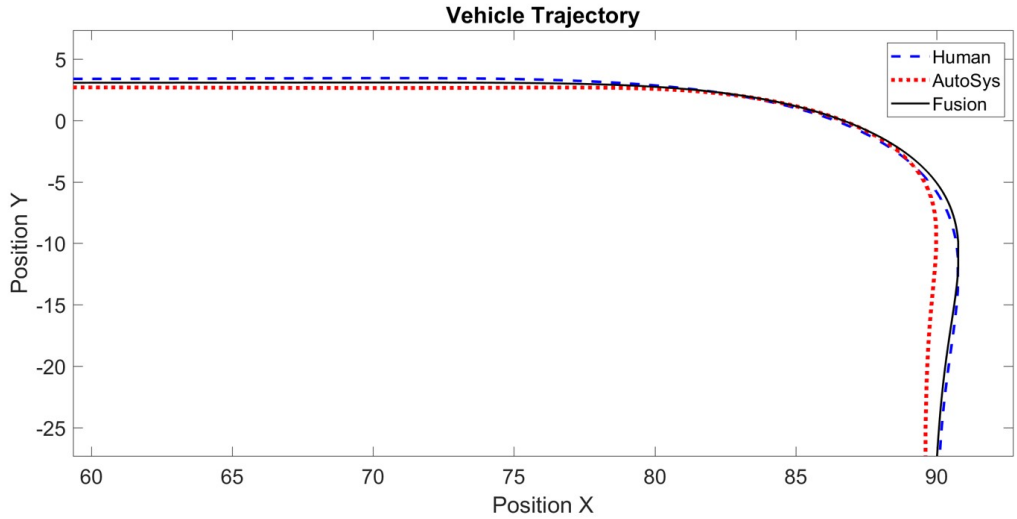

Figure 5.23 – Scenario Type A: Intended and Final vehicle trajectory profiles

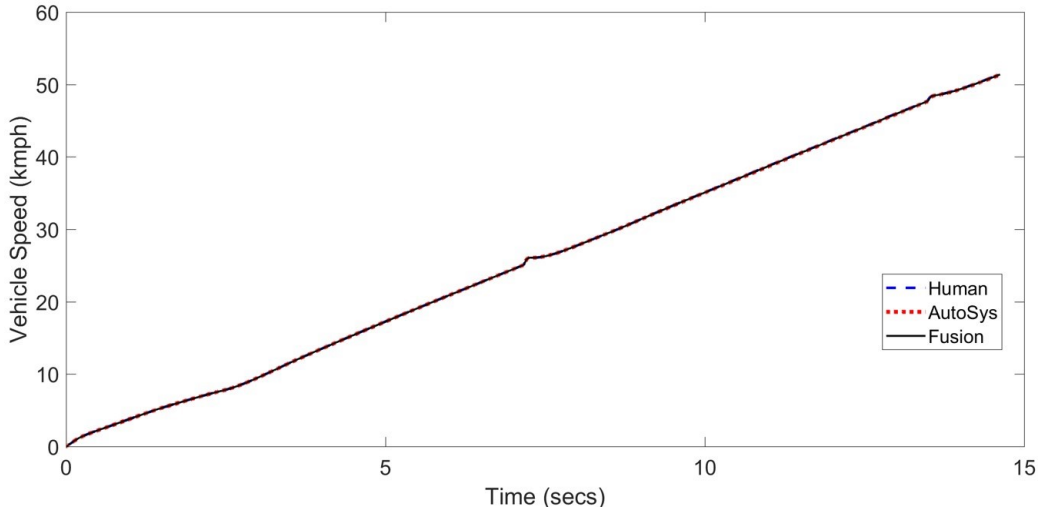

Figure 5.24 – Scenario 2 Type A: Intended and Final Speed profiles

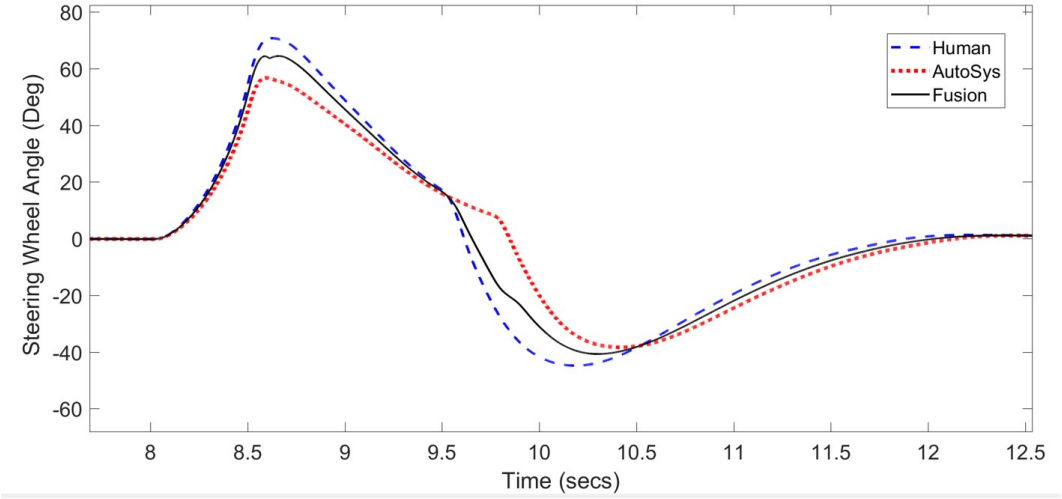

Figure 5.25 – Scenario 2 Type A: Steering wheel angle profiles

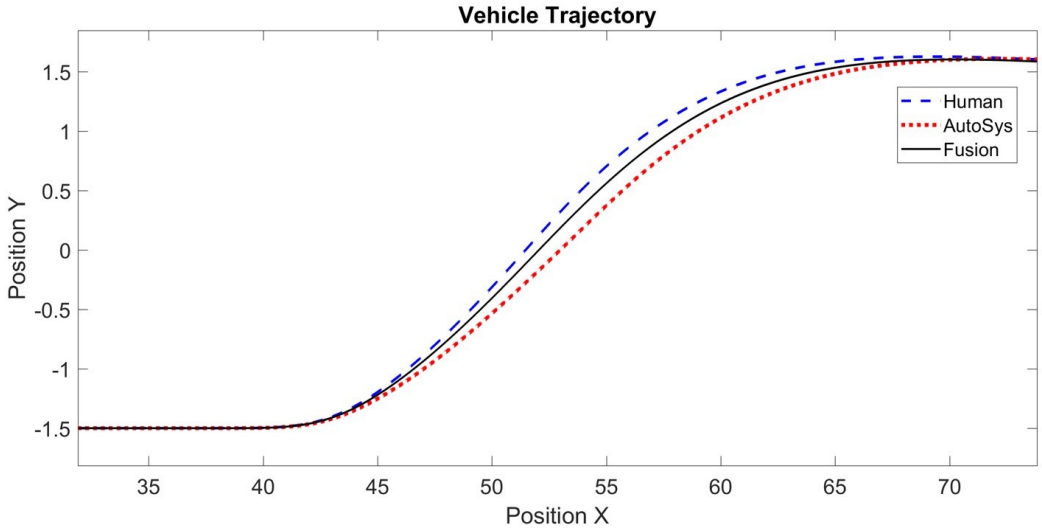

Figure 5.26 – Scenario 2 Type A: Intended and Final vehicle trajectory profiles

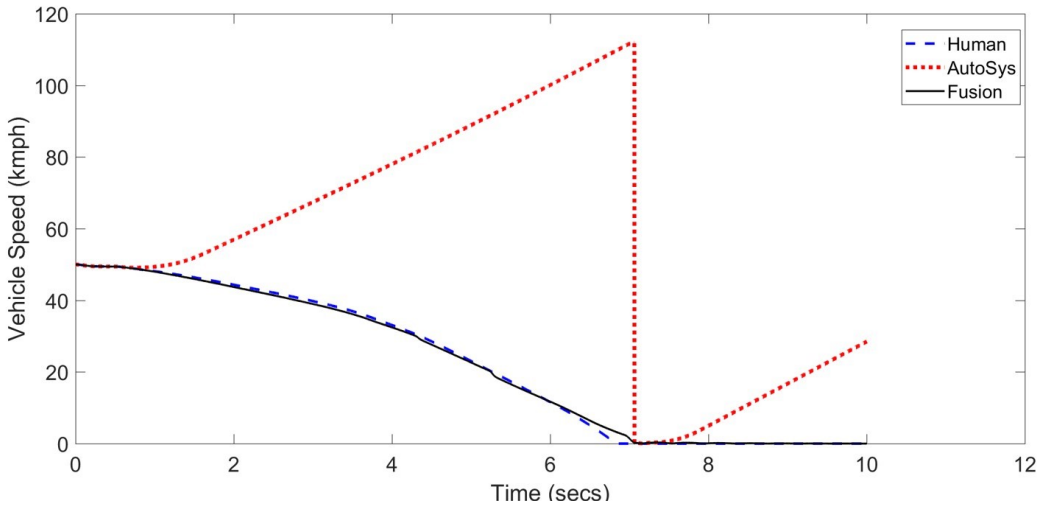

Figure 5.27 – Scenario Type B: Intended and Final Speed profiles

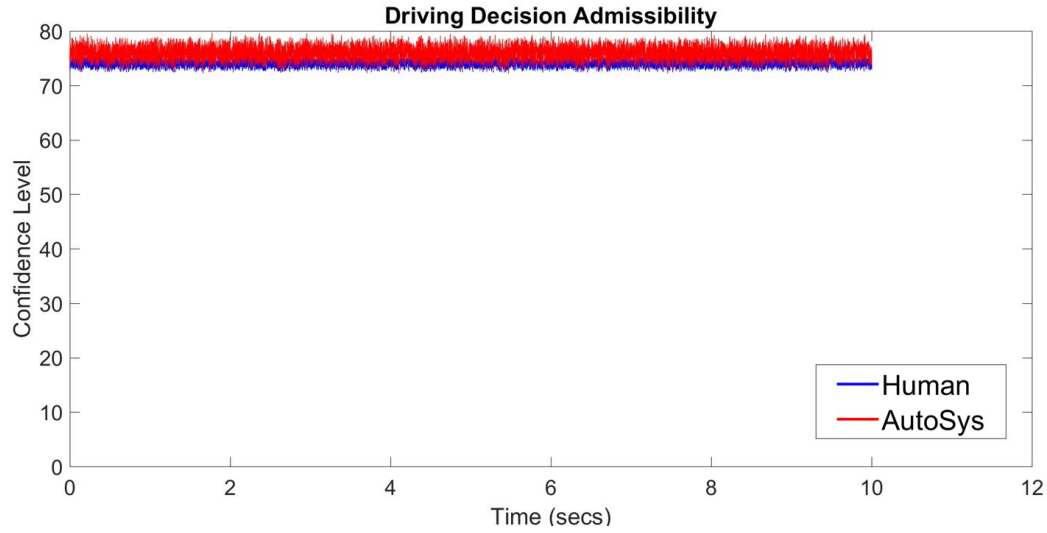

Figure 5.28 – Scenario Type B: Driving decision admissibility profiles

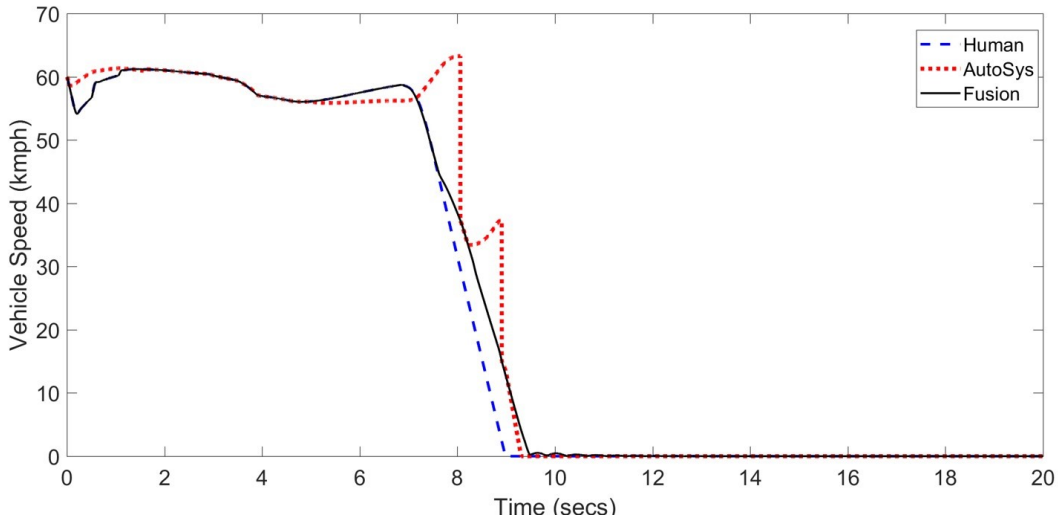

Figure 5.29 – Scenario Type C: Intended and Final Speed profiles

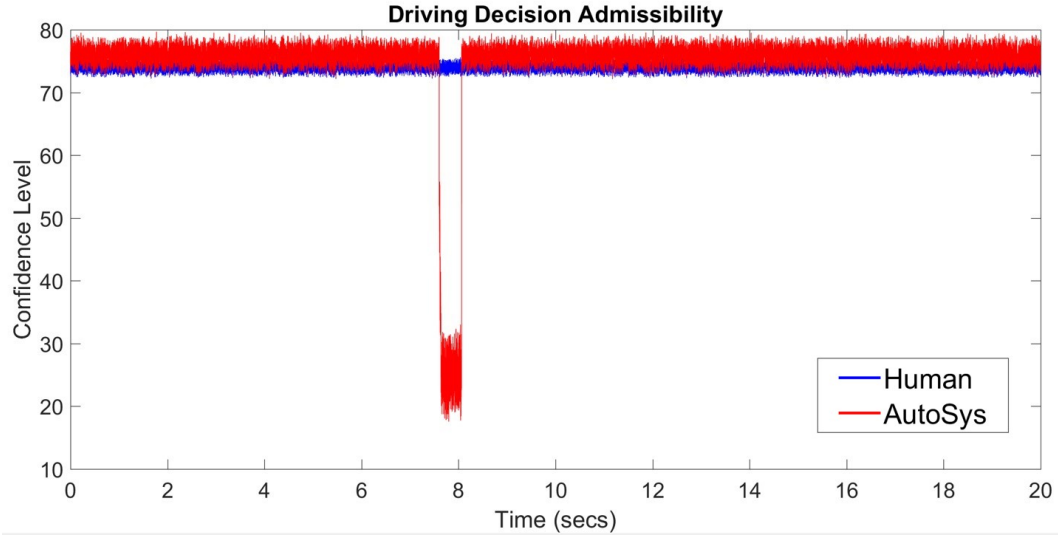

Figure 5.30 – Scenario Type C: Driving decision admissibility profiles

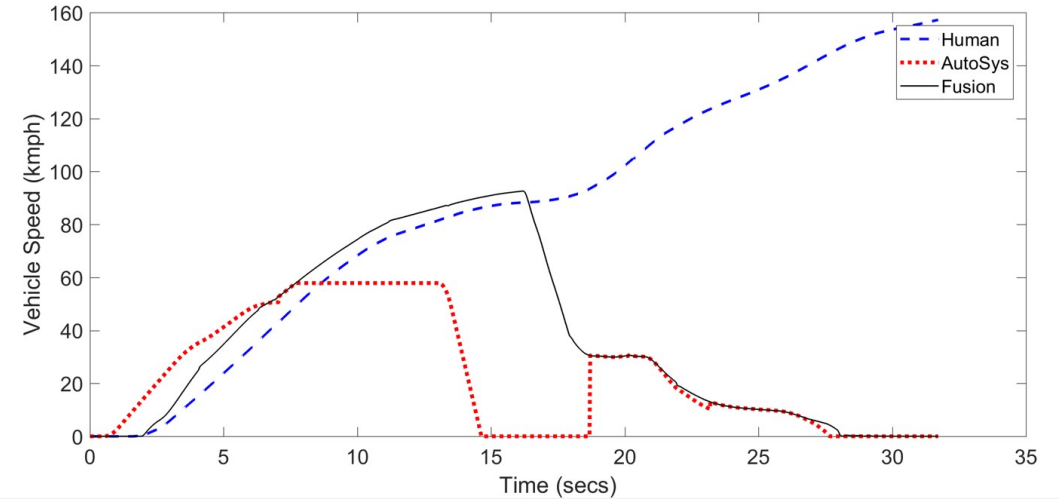

Figure 5.31 – Scenario Type D: Intended and Final Speed profiles

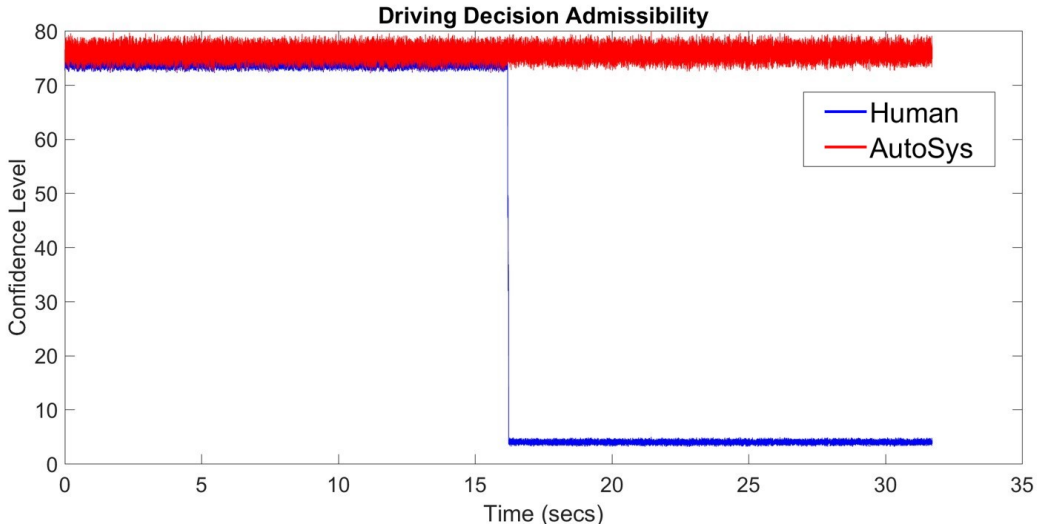

Figure 5.32 – Scenario Type D: Driving decision admissibility profiles

5.5 Conclusion

The presented strategy for decision making is based on non-cooperative game between human driver and autosys. This game minimizes the conflict between human driver and autosys through a bargaining solution. This solution acts as the final driving input for the vehicle. The parameters of this game are varied according to the individual driving decision admissibility and driving intentions. The predicted driving profiles (vehicle speed, steering wheel angle) are used to derive the driving intentions. Using the presented decision making strategy, the fusion system improves the driving safety and refines the driving performance of the human driver.

Conclusion and Future Works

This work presented a strategy for shared control authority between human and autonomous driving system using a separate fusion system. Beyond the existing contributions described in the related works, we proposed a solution to the shared driving problem using a decision making based approach. The problem was divided into different areas: shared control framework, driving decision admissibility, driving behavior prediction and fusion strategy etc. For each of these problems, separate methodologies were developed and validated using the softwares IPG CarMaker and SCANer Studio. The fusion system was developed as a high level controller for generating the final driving inputs in the form of intended vehicle speed and steering wheel angle. A separate low level controller can be used in the future for the tracking purpose. The decision based approach for the development of the strategy overcame the dependency on the vehicle and environment dynamical model. This is presented as an advantage over the control based approaches.

The shared control framework is developed with the target of conflict resolution. A case study is presented as an application to inverted pendulum for the purpose of demonstration. The driving input admissibility is computed using the Belief functions theory. The occupancy grid map derived from the LIDAR sensor data using an inverse sensor model acts as an input to the evidential model. The use of belief functions allow us to include the unknown aspect in the case of environment dynamics. The methodology is further enhanced for an early prediction of the collision risk and for the application to the driving scenarios with lateral collision risks. The validation is carried out in IPG CarMaker and SCANer studio with both human and autonomous driving system. Different sensors such as Camera, RADAR can be used instead of LIDAR to obtain the occupancy grid map. The methodology is independent of the prediction of trajectories of the ego and surrounding vehicles.

The driving behavior prediction methodology is based on the neural networks. The relevant data is filtered for the neural network. This data transformation reduces not only reduced the size of the neural network but also the amount of training/testing data. The accuracy of the model is inversely proportional to the

prediction horizon. The predicted driving input trajectories quantify the driving intention. Loss utility functions assigned to these predicted trajectories represent the driver resistance to the deviation from the individual driving intention. The nature of the loss utility function is assumed to be parabolic for the generalization. In the future, it can be replaced by a particular function obtained from the human factors research. The non-cooperative game between the human and autonomous driving system represent the conflict resolution as a bargaining problem. The non-cooperative game can also be defined with an objective different than conflict resolution.

The validation is carried out on a test rig integrated with Simulink and IPG CarMaker. A feedback is provided to the human driver by giving information such as intended vehicle speeds and steering wheel angles, driving decision admissibility etc. The amount of information is kept minimal to prevent any distraction. During the driving scenarios including lateral vehicle movement, the steering ratio is variable due to the fusion system. This variation is felt by the human driver at the steering wheel. Thus, a feel factor of steering resistance/assistance can be provided to the human driver without any haptic feedback. For the future works, steering wheel torque input can be used in the strategy instead of steering wheel angle. Considering the fusion system framework, a drive-by-wire vehicle along with an autonomous driving system will be required to carry experimental validation on an actual vehicle. The unavailability of such a vehicle leaves the experimental validation of shared driving control to be carried out in the future.

References

[Abbink et al., 2012] Abbink, D. A., Mulder, M., and Boer, E. R. (2012). Haptic shared control: smoothly shifting control authority? *Cognition, Technology & Work*, 14(1):19–28, doi: http://dx.doi.org/10.1007/s10111-011-0192-5.

[Ajoudani et al., 2018] Ajoudani, A., Zanchettin, A. M., Ivaldi, S., Albu-Schäffer, A., Kosuge, K., and Khatib, O. (2018). Progress and prospects of the human–robot collaboration. *Autonomous Robots*, 42(5):957–975, doi: http://dx.doi.org/10.1007/s10514-017-9677-2.

[Aldibaja et al., 2017] Aldibaja, M., Suganuma, N., and Yoneda, K. (2017). Robust intensity-based localization method for autonomous driving on snow–wet road surface. *IEEE Transactions on Industrial Informatics*, 13(5):2369–2378, doi: http://dx.doi.org/10.1109/TII.2017.2713836.

[Alonso-Mora et al., 2014] Alonso-Mora, J., Gohl, P., Watson, S., Siegwart, R., and Beardsley, P. (2014). Shared control of autonomous vehicles based on velocity space optimization. In *2014 IEEE International Conference on Robotics and Automation (ICRA)*, pages 1639–1645.

[Altché and de La Fortelle, 2017] Altché, F. and de La Fortelle, A. (2017). An lstm network for highway trajectory prediction. In *2017 IEEE 20th International Conference on Intelligent Transportation Systems (ITSC)*, pages 353–359.

[Alves de Lima and Corrêa Victorino, 2016] Alves de Lima, D. and Corrêa Victorino, A. (2016). A hybrid controller for vision-based navigation of autonomous vehicles in urban environments. *IEEE Transactions on Intelligent Transportation Systems*, 17(8):2310–2323, doi: http://dx.doi.org/10.1109/TITS.2016.2519329.

[Amirshirzad et al., 2019] Amirshirzad, N., Kumru, A., and Oztop, E. (2019). Human adaptation to human–robot shared control. *IEEE Transactions on Human-Machine Systems*, 49(2):126–136, doi: http://dx.doi.org/10.1109/THMS.2018.2884719.

[Anderson et al., 2013] Anderson, S. J., Karumanchi, S. B., Iagnemma, K., and Walker, J. M. (2013). The intelligent copilot: A constraint-based approach to shared-adaptive control of ground vehicles. *IEEE Intelligent Transportation Systems Magazine*, 5(2):45–54, doi: http://dx.doi.org/10.1109/MITS.2013.2247796.

[Andreetto et al., 2017] Andreetto, M., Divan, S., Fontanelli, D., and Palopoli, L. (2017). Path following with authority sharing between humans and passive robotic walkers equipped with low-cost actuators. *IEEE Robotics and Automation Letters*, 2(4):2271–2278, doi: http://dx.doi.org/10.1109/LRA.2017.2724772.

[Bagloee et al., 2016] Bagloee, S. A., Tavana, M., Asadi, M., and Oliver, T. (2016). Autonomous vehicles: challenges, opportunities, and future implications for transportation

policies. *Journal of Modern Transportation*, 24(4):284–303, doi: http://dx.doi.org/10.1007/s40534-016-0117-3.

[Banks et al., 2018] Banks, V. A., Eriksson, A., O'Donoghue, J., and Stanton, N. A. (2018). Is partially automated driving a bad idea? observations from an on-road study. *Applied Ergonomics*, 68:138 – 145, doi: http://dx.doi.org/https://doi.org/10.1016/j.apergo.2017.11.010.

[Banks and Stanton, 2016] Banks, V. A. and Stanton, N. A. (2016). Keep the driver in control: Automating automobiles of the future. *Applied Ergonomics*, 53:389 – 395, doi: http://dx.doi.org/https://doi.org/10.1016/j.apergo.2015.06.020. Transport in the 21st Century: The Application of Human Factors to Future User Needs.

[Belbachir, 2017] Belbachir, A. (2017). An embedded testbed architecture to evaluate autonomous car driving. *Intelligent Service Robotics*, 10(2):109–119, doi: http://dx.doi.org/10.1007/s11370-016-0213-6.

[Benloucif et al., 2019] Benloucif, M., Sentouh, C., Floris, J., Simon, P., and Popieul, J.-C. (2019). Online adaptation of the level of haptic authority in a lane keeping system considering the driver's state. *Transportation Research Part F: Traffic Psychology and Behaviour*, 61:107 – 119, doi: http://dx.doi.org/https://doi.org/10.1016/j.trf.2017.08.013. Special TRF issue: Driving simulation.

[Berthelot et al., 2011] Berthelot, A., Tamke, A., Dang, T., and Breuel, G. (2011). Handling uncertainties in criticality assessment. In *2011 IEEE Intelligent Vehicles Symposium (IV)*, pages 571–576.

[Berthelot et al., 2012] Berthelot, A., Tamke, A., Dang, T., and Breuel, G. (2012). A novel approach for the probabilistic computation of time-to-collision. In *2012 IEEE Intelligent Vehicles Symposium*, pages 1173–1178.

[Beynon et al., 2000] Beynon, M., Curry, B., and Morgan, P. (2000). The dempster–shafer theory of evidence: an alternative approach to multicriteria decision modelling. *Omega*, 28(1):37 – 50, doi: http://dx.doi.org/https://doi.org/10.1016/S0305-0483(99)00033-X.

[Borroni and Tanelli, 2018] Borroni, F. and Tanelli, M. (2018). A weighting approach to the shared-control of lateral vehicle dynamics. *IFAC-PapersOnLine*, 51(9):305 – 310, doi: http://dx.doi.org/https://doi.org/10.1016/j.ifacol.2018.07.050. 15th IFAC Symposium on Control in Transportation Systems CTS 2018.

[Brannstrom et al., 2010] Brannstrom, M., Coelingh, E., and Sjoberg, J. (2010). Model-based threat assessment for avoiding arbitrary vehicle collisions. *IEEE Transactions on Intelligent Transportation Systems*, 11(3):658–669, doi: http://dx.doi.org/10.1109/TITS.2010.2048314.

[Bresson et al., 2017] Bresson, G., Alsayed, Z., Yu, L., and Glaser, S. (2017). Simultaneous localization and mapping: A survey of current trends in autonomous driving. *IEEE Transactions on Intelligent Vehicles*, 2(3):194–220, doi: http://dx.doi.org/10.1109/TIV.2017.2749181.

[Broad et al., 2017] Broad, A., Schultz, J., Derry, M., Murphey, T., and Argall, B. (2017). Trust adaptation leads to lower control effort in shared control of crane automation. *IEEE Robotics and Automation Letters*, 2(1):239–246, doi: http://dx.doi.org/10.1109/LRA.2016.2593740.

[Broggi et al., 2008] Broggi, A., Zelinsky, A., Parent, M., and Thorpe, C. E. (2008). *Intelligent Vehicles*, pages 1175–1198. Springer Berlin Heidelberg, Berlin, Heidelberg.

[Brown, 2017] Brown, B. (2017). The social life of autonomous cars. *Computer*, 50(2):92–96, doi: http://dx.doi.org/10.1109/MC.2017.59.

[Campos and Cavalcante, 2003] Campos, F. and Cavalcante, S. (2003). An extended approach for dempster-shafer theory. In *Proceedings Fifth IEEE Workshop on Mobile Computing Systems and Applications*, pages 338–344.

[Chandrasekaran and Conrad, 2015] Chandrasekaran, B. and Conrad, J. M. (2015). Human-robot collaboration: A survey. In *SoutheastCon 2015*, pages 1–8.

[Chen and Barnes, 2014] Chen, J. Y. C. and Barnes, M. J. (2014). Human–agent teaming for multirobot control: A review of human factors issues. *IEEE Transactions on Human-Machine Systems*, 44(1):13–29, doi: http://dx.doi.org/10.1109/THMS.2013.2293535.

[Chen et al., 2019] Chen, W., Zhao, L., Tan, D., Wei, Z., Xu, K., and Jiang, Y. (2019). Human–machine shared control for lane departure assistance based on hybrid system theory. *Control Engineering Practice*, 84:399 – 407, doi: http://dx.doi.org/https://doi.org/10.1016/j.conengprac.2018.12.011.

[Das et al., 2015] Das, D., Rashed, M. G., Kobayashi, Y., and Kuno, Y. (2015). Supporting human–robot interaction based on the level of visual focus of attention. *IEEE Transactions on Human-Machine Systems*, 45(6):664–675, doi: http://dx.doi.org/10.1109/THMS.2015.2445856.

[Daziano et al., 2017] Daziano, R. A., Sarrias, M., and Leard, B. (2017). Are consumers willing to pay to let cars drive for them? analyzing response to autonomous vehicles. *Transportation Research Part C: Emerging Technologies*, 78:150 – 164, doi: http://dx.doi.org/https://doi.org/10.1016/j.trc.2017.03.003.

[De Nicolao et al., 2007] De Nicolao, G., Ferrara, A., and Giacomini, L. (2007). Onboard sensor-based collision risk assessment to improve pedestrians' safety. *IEEE Transactions on Vehicular Technology*, 56(5):2405–2413, doi: http://dx.doi.org/10.1109/TVT.2007.899209.

[de Winter et al., 2014] de Winter, J. C., Happee, R., Martens, M. H., and Stanton, N. A. (2014). Effects of adaptive cruise control and highly automated driving on workload and situation awareness: A review of the empirical evidence. *Transportation Research Part F: Traffic Psychology and Behaviour*, 27:196 – 217, doi: http://dx.doi.org/https://doi.org/10.1016/j.trf.2014.06.016. Vehicle Automation and Driver Behaviour.

[de Winter and Dodou, 2011] de Winter, J. C. F. and Dodou, D. (2011). Preparing drivers for dangerous situations: A critical reflection on continuous shared control. In *2011 IEEE International Conference on Systems, Man, and Cybernetics*, pages 1050–1056.

[Dröder et al., 2018] Dröder, K., Bobka, P., Germann, T., Gabriel, F., and Dietrich, F. (2018). A machine learning-enhanced digital twin approach for human-robot-collaboration. *Procedia CIRP*, 76:187 – 192, doi: http://dx.doi.org/https://doi.org/10.1016/j.procir.2018.02.010. 7th CIRP Conference on Assembly Technologies and Systems (CATS 2018).

[Eidehall and Petersson, 2008] Eidehall, A. and Petersson, L. (2008). Statistical threat assessment for general road scenes using monte carlo sampling. *IEEE Transactions on Intelligent Transportation Systems*, 9(1):137–147, doi: http://dx.doi.org/10.1109/TITS.2007.909241.

[Favarò et al., 2018] Favarò, F., Eurich, S., and Nader, N. (2018). Autonomous vehicles' disengagements: Trends, triggers, and regulatory limitations. *Accident Analysis and Prevention*, 110:136 – 148, doi: http://dx.doi.org/https://doi.org/10.1016/j.aap.2017.11.001.

[Flad et al., 2017] Flad, M., Fröhlich, L., and Hohmann, S. (2017). Cooperative shared control driver assistance systems based on motion primitives and differential games. *IEEE Transactions on Human-Machine Systems*, 47(5):711–722, doi: http://dx.doi.org/10.1109/THMS.2017.2700435.

[Fraedrich et al., 2019] Fraedrich, E., Heinrichs, D., Bahamonde-Birke, F. J., and Cyganski, R. (2019). Autonomous driving, the built environment and policy implications. *Transportation Research Part A: Policy and Practice*, 122:162 – 172, doi: http://dx.doi.org/https://doi.org/10.1016/j.tra.2018.02.018.

[Goodall, 2016] Goodall, N. J. (2016). Can you program ethics into a self-driving car? *IEEE Spectrum*, 53(6):28–58, doi: http://dx.doi.org/10.1109/MSPEC.2016.7473149.

[Guo et al., 2017] Guo, C., Sentouh, C., Popieul, J., and Haué, J. (2017). Mpc-based shared steering control for automated driving systems. In *2017 IEEE International Conference on Systems, Man, and Cybernetics (SMC)*, pages 129–134.

[Guo et al., 2018] Guo, Y., Liul, J., Song, L., Guo, H., Hu, Y., and a. H. Chen (2018). Hazard-evaluation-based driver-automation switched shared steering control for intelligent vehicles. In *2018 IEEE Intelligent Vehicles Symposium (IV)*, pages 244–249.

[Haboucha et al., 2017] Haboucha, C. J., Ishaq, R., and Shiftan, Y. (2017). User preferences regarding autonomous vehicles. *Transportation Research Part C: Emerging Technologies*, 78:37 – 49, doi: http://dx.doi.org/https://doi.org/10.1016/j.trc.2017.01.010.

[HECHT-NIELSEN, 1992] HECHT-NIELSEN, R. (1992). Iii.3 - theory of the backpropagation neural network**based on "nonindent" by robert hecht-nielsen, which appeared in proceedings of the international joint conference on neural networks 1, 593–611, june 1989. © 1989 ieee. In Wechsler, H., editor, *Neural Networks for Perception*, pages 65 – 93. Academic Press.

[Hillenbrand et al., 2006] Hillenbrand, J., Spieker, A. M., and Kroschel, K. (2006). A multilevel collision mitigation approach mdash;its situation assessment, decision making, and performance tradeoffs. *IEEE Transactions on Intelligent Transportation Systems*, 7(4):528–540, doi: http://dx.doi.org/10.1109/TITS.2006.883115.

[Houénou et al., 2014] Houénou, A., Bonnifait, P., and Cherfaoui, V. (2014). Risk assessment for collision avoidance systems. In *17th International IEEE Conference on Intelligent Transportation Systems (ITSC)*, pages 386–391.

[Hulse et al., 2018] Hulse, L. M., Xie, H., and Galea, E. R. (2018). Perceptions of autonomous vehicles: Relationships with road users, risk, gender and age. *Safety Science*, 102:1 – 13, doi: http://dx.doi.org/https://doi.org/10.1016/j.ssci.2017.10.001.

[Hussain and Zeadally, 2019] Hussain, R. and Zeadally, S. (2019). Autonomous cars: Research results, issues, and future challenges. *IEEE Communications Surveys Tutorials*, 21(2):1275–1313, doi: http://dx.doi.org/10.1109/COMST.2018.2869360.

[Itoh et al., 2016] Itoh, M., Flemisch, F., and Abbink, D. (2016). A hierarchical framework to analyze shared control conflicts between human and machine. *IFAC-PapersOnLine*, 49(19):96

– 101, doi: http://dx.doi.org/https://doi.org/10.1016/j.ifacol.2016.10.468. 13th IFAC Symposium on Analysis, Design, and Evaluation ofHuman-Machine Systems HMS 2016.

[Jensen et al., 2011] Jensen, M. J., Tolbert, A. M., Wagner, J. R., Switzer, F. S., and Finn, J. W. (2011). A customizable automotive steering system with a haptic feedback control strategy for obstacle avoidance notification. *IEEE Transactions on Vehicular Technology*, 60(9):4208–4216, doi: http://dx.doi.org/10.1109/TVT.2011.2172472.

[Jiménez et al., 2011] Jiménez, F., Naranjo, J. E., and Garcia, F. P. (2011). An improved method to calculate the time-to-collision of two vehicles. *International Journal of Intelligent Transportation Systems Research*, 11:34–42.

[Johns et al., 2016] Johns, M., Mok, B., Sirkin, D., Gowda, N., Smith, C., Talamonti, W., and Ju, W. (2016). Exploring shared control in automated driving. In *2016 11th ACM/IEEE International Conference on Human-Robot Interaction (HRI)*, pages 91–98.

[Kaempchen et al., 2009] Kaempchen, N., Schiele, B., and Dietmayer, K. (2009). Situation assessment of an autonomous emergency brake for arbitrary vehicle-to-vehicle collision scenarios. *IEEE Transactions on Intelligent Transportation Systems*, 10(4):678–687, doi: http://dx.doi.org/10.1109/TITS.2009.2026452.

[Kalra and Paddock, 2016] Kalra, N. and Paddock, S. M. (2016). Driving to safety: How many miles of driving would it take to demonstrate autonomous vehicle reliability? *Transportation Research Part A: Policy and Practice*, 94:182 – 193, doi: http://dx.doi.org/https://doi.org/10.1016/j.tra.2016.09.010.

[Khan et al., 2012] Khan, A. M., Bacchus, A., and Erwin, S. (2012). Policy challenges of increasing automation in driving. *IATSS Research*, 35(2):79 – 89, doi: http://dx.doi.org/https://doi.org/10.1016/j.iatssr.2012.02.002.

[Kim et al., 2017] Kim, B., Kang, C. M., Kim, J., Lee, S. H., Chung, C. C., and Choi, J. W. (2017). Probabilistic vehicle trajectory prediction over occupancy grid map via recurrent neural network. In *2017 IEEE 20th International Conference on Intelligent Transportation Systems (ITSC)*, pages 399–404.

[Kim et al., 2015] Kim, B., Son, Y., and Yi, K. (2015). Probabilistic threat assessment with environment description and rule-based multi-traffic prediction for integrated risk management system. In *2015 IEEE Intelligent Vehicles Symposium (IV)*, pages 642–647.

[Kim and Yang, 2017] Kim, H. J. and Yang, J. H. (2017). Takeover requests in simulated partially autonomous vehicles considering human factors. *IEEE Transactions on Human-Machine Systems*, 47(5):735–740, doi: http://dx.doi.org/10.1109/THMS.2017.2674998.

[Kim and Kum, 2018] Kim, J. and Kum, D. (2018). Collision risk assessment algorithm via lane-based probabilistic motion prediction of surrounding vehicles. *IEEE Transactions on Intelligent Transportation Systems*, 19(9):2965–2976, doi: http://dx.doi.org/10.1109/TITS.2017.2768318.

[Koopman and Wagner, 2017] Koopman, P. and Wagner, M. (2017). Autonomous vehicle safety: An interdisciplinary challenge. *IEEE Intelligent Transportation Systems Magazine*, 9(1):90–96, doi: http://dx.doi.org/10.1109/MITS.2016.2583491.

[Kuefler et al., 2017] Kuefler, A., Morton, J., Wheeler, T., and Kochenderfer, M. (2017). Imitating driver behavior with generative adversarial networks. In *2017 IEEE Intelligent Vehicles Symposium (IV)*, pages 204–211.

[Lefèvre et al., 2014] Lefèvre, S., Vasquez, D., and Laugier, C. (2014). A survey on motion prediction and risk assessment for intelligent vehicles. *ROBOMECH Journal*, 1(1):1, doi: http://dx.doi.org/10.1186/s40648-014-0001-z.

[Lefèvre et al., 2012] Lefèvre, S., Laugier, C., and Ibañez-Guzmán, J. (2012). Risk assessment at road intersections: Comparing intention and expectation. In *2012 IEEE Intelligent Vehicles Symposium*, pages 165–171.

[Levinson et al., 2011] Levinson, J., Askeland, J., Becker, J., Dolson, J., Held, D., Kammel, S., Kolter, J. Z., Langer, D., Pink, O., Pratt, V., Sokolsky, M., Stanek, G., Stavens, D., Teichman, A., Werling, M., and Thrun, S. (2011). Towards fully autonomous driving: Systems and algorithms. In *2011 IEEE Intelligent Vehicles Symposium (IV)*, pages 163–168.

[Li et al., 2018a] Li, L., Ota, K., and Dong, M. (2018a). Humanlike driving: Empirical decision-making system for autonomous vehicles. *IEEE Transactions on Vehicular Technology*, 67(8):6814–6823, doi: http://dx.doi.org/10.1109/TVT.2018.2822762.

[Li et al., 2018b] Li, L., Ota, K., and Dong, M. (2018b). Humanlike driving: Empirical decision-making system for autonomous vehicles. *IEEE Transactions on Vehicular Technology*, 67(8):6814–6823, doi: http://dx.doi.org/10.1109/TVT.2018.2822762.

[Li et al., 2018c] Li, M., Cao, H., Song, X., Huang, Y., Wang, J., and Huang, Z. (2018c). Shared control driver assistance system based on driving intention and situation assessment. *IEEE Transactions on Industrial Informatics*, 14(11):4982–4994, doi: http://dx.doi.org/10.1109/TII.2018.2865105.

[Li et al., 2018d] Li, M., Cao, H., Song, X., Huang, Y., Wang, J., and Huang, Z. (2018d). Shared control driver assistance system based on driving intention and situation assessment. *IEEE Transactions on Industrial Informatics*, 14(11):4982–4994, doi: http://dx.doi.org/10.1109/TII.2018.2865105.

[Li et al., 2019] Li, M., Song, X., Cao, H., Wang, J., Huang, Y., Hu, C., and Wang, H. (2019). Shared control with a novel dynamic authority allocation strategy based on game theory and driving safety field. *Mechanical Systems and Signal Processing*, 124:199 – 216, doi: http://dx.doi.org/https://doi.org/10.1016/j.ymssp.2019.01.040.

[Li et al., 2017] Li, R., Li, Y., Li, S. E., Burdet, E., and Cheng, B. (2017). Indirect shared control of highly automated vehicles for cooperative driving between driver and automation. *CoRR*, abs/1704.00866.

[Li et al., 2016a] Li, X., Sun, Z., Cao, D., He, Z., and Zhu, Q. (2016a). Real-time trajectory planning for autonomous urban driving: Framework, algorithms, and verifications. *IEEE/ASME Transactions on Mechatronics*, 21(2):740–753, doi: http://dx.doi.org/10.1109/TMECH.2015.2493980.

[Li et al., 2016b] Li, Y., Zhang, L., and Song, Y. (2016b). A vehicular collision warning algorithm based on the time-to-collision estimation under connected environment. In *2016 14th International Conference on Control, Automation, Robotics and Vision (ICARCV)*, pages 1–4.

[Liu et al., 2018] Liu, H., Fang, T., Zhou, T., Wang, Y., and Wang, L. (2018). Deep learning-based multimodal control interface for human-robot collaboration. *Procedia CIRP*, 72:3 – 8, doi: http://dx.doi.org/https://doi.org/10.1016/j.procir.2018.03.224. 51st CIRP Conference on Manufacturing Systems.

[Liu and Wang, 2018] Liu, H. and Wang, L. (2018). Gesture recognition for human-robot collaboration: A review. *International Journal of Industrial Ergonomics*, 68:355 – 367, doi: http://dx.doi.org/https://doi.org/10.1016/j.ergon.2017.02.004.

[Lu et al., 2016] Lu, Z., Happee, R., Cabrall, C. D., Kyriakidis, M., and de Winter, J. C. (2016). Human factors of transitions in automated driving: A general framework and literature survey. *Transportation Research Part F: Traffic Psychology and Behaviour*, 43:183 – 198, doi: http://dx.doi.org/https://doi.org/10.1016/j.trf.2016.10.007.

[Luettel et al., 2012] Luettel, T., Himmelsbach, M., and Wuensche, H. (2012). Autonomous ground vehicles—concepts and a path to the future. *Proceedings of the IEEE*, 100(Special Centennial Issue):1831–1839, doi: http://dx.doi.org/10.1109/JPROC.2012.2189803.

[Mahmud et al., 2017] Mahmud, S. S., Ferreira, L., Hoque, M. S., and Tavassoli, A. (2017). Application of proximal surrogate indicators for safety evaluation: A review of recent developments and research needs. *IATSS Research*, 41(4):153 – 163, doi: http://dx.doi.org/https://doi.org/10.1016/j.iatssr.2017.02.001.

[Mars et al., 2014] Mars, F., Deroo, M., and Hoc, J. (2014). Analysis of human-machine cooperation when driving with different degrees of haptic shared control. *IEEE Transactions on Haptics*, 7(3):324–333, doi: http://dx.doi.org/10.1109/TOH.2013.2295095.

[Meng et al., 2006] Meng, X., Lee, K. K., and Xu, Y. (2006). Human driving behavior recognition based on hidden markov models. In *2006 IEEE International Conference on Robotics and Biomimetics*, pages 274–279.

[Merat et al., 2014] Merat, N., Jamson, A. H., Lai, F. C., Daly, M., and Carsten, O. M. (2014). Transition to manual: Driver behaviour when resuming control from a highly automated vehicle. *Transportation Research Part F: Traffic Psychology and Behaviour*, 27:274 – 282, doi: http://dx.doi.org/https://doi.org/10.1016/j.trf.2014.09.005. Vehicle Automation and Driver Behaviour.

[Modares et al., 2016] Modares, H., Ranatunga, I., Lewis, F. L., and Popa, D. O. (2016). Optimized assistive human–robot interaction using reinforcement learning. *IEEE Transactions on Cybernetics*, 46(3):655–667, doi: http://dx.doi.org/10.1109/TCYB.2015.2412554.

[Mosbach et al., 2017] Mosbach, S., Flad, M., and Hohmann, S. (2017). Cooperative longitudinal driver assistance system based on shared control. In *2017 IEEE International Conference on Systems, Man, and Cybernetics (SMC)*, pages 1776–1781.

[Musić and Hirche, 2017] Musić, S. and Hirche, S. (2017). Control sharing in human-robot team interaction. *Annual Reviews in Control*, 44:342 – 354, doi: http://dx.doi.org/https://doi.org/10.1016/j.arcontrol.2017.09.017.

[Nadimi et al., 2016] Nadimi, N., Behbahani, H., and Shahbazi, H. (2016). Calibration and validation of a new time-based surrogate safety measure using fuzzy inference system. *Journal of Traffic and Transportation Engineering (English Edition)*, 3(1):51 – 58, doi: http://dx.doi.org/https://doi.org/10.1016/j.jtte.2015.09.004.

[Naujoks et al., 2016] Naujoks, F., Purucker, C., and Neukum, A. (2016). Secondary task engagement and vehicle automation – comparing the effects of different automation levels in an on-road experiment. *Transportation Research Part F: Traffic Psychology and Behaviour*, 38:67 – 82, doi: http://dx.doi.org/https://doi.org/10.1016/j.trf.2016.01.011.

[Nudehi et al., 2005] Nudehi, S. S., Mukherjee, R., and Ghodoussi, M. (2005). A shared-control approach to haptic interface design for minimally invasive telesurgical training. *IEEE Transactions on Control Systems Technology*, 13(4):588–592, doi: http://dx.doi.org/10.1109/TCST.2004.843131.

[Ohn-Bar and Trivedi, 2016] Ohn-Bar, E. and Trivedi, M. M. (2016). Looking at humans in the age of self-driving and highly automated vehicles. *IEEE Transactions on Intelligent Vehicles*, 1(1):90–104, doi: http://dx.doi.org/10.1109/TIV.2016.2571067.

[Polychronopoulos et al., 2007] Polychronopoulos, A., Tsogas, M., Amditis, A. J., and Andreone, L. (2007). Sensor fusion for predicting vehicles' path for collision avoidance systems. *IEEE Transactions on Intelligent Transportation Systems*, 8(3):549–562, doi: http://dx.doi.org/10.1109/TITS.2007.903439.

[Roesener et al., 2016] Roesener, C., Fahrenkrog, F., Uhlig, A., and Eckstein, L. (2016). A scenario-based assessment approach for automated driving by using time series classification of human-driving behaviour. In *2016 IEEE 19th International Conference on Intelligent Transportation Systems (ITSC)*, pages 1360–1365.

[Rusinowska, 2003] Rusinowska, A. (2003). *Axiomatic and Strategic Approaches to Bargaining Problems*, pages 124–146. Springer Berlin Heidelberg, Berlin, Heidelberg.

[Sadigh et al., 2019] Sadigh, D., Sastry, S. S., and Seshia, S. A. (2019). Verifying robustness of human-aware autonomous cars. *IFAC-PapersOnLine*, 51(34):131 – 138, doi: http://dx.doi.org/https://doi.org/10.1016/j.ifacol.2019.01.055. 2nd IFAC Conference on Cyber-Physical and Human Systems CPHS 2018.

[Saito et al., 2018] Saito, T., Wada, T., and Sonoda, K. (2018). Control authority transfer method for automated-to-manual driving via a shared authority mode. *IEEE Transactions on Intelligent Vehicles*, 3(2):198–207, doi: http://dx.doi.org/10.1109/TIV.2018.2804167.

[Scheggi et al., 2017] Scheggi, S., Aggravi, M., and Prattichizzo, D. (2017). Cooperative navigation for mixed human–robot teams using haptic feedback. *IEEE Transactions on Human-Machine Systems*, 47(4):462–473, doi: http://dx.doi.org/10.1109/THMS.2016.2608936.

[Scheggi et al., 2014] Scheggi, S., Morbidi, F., and Prattichizzo, D. (2014). Human-robot formation control via visual and vibrotactile haptic feedback. *IEEE Transactions on Haptics*, 7(4):499–511, doi: http://dx.doi.org/10.1109/TOH.2014.2332173.

[Schreier et al., 2016] Schreier, M., Willert, V., and Adamy, J. (2016). An integrated approach to maneuver-based trajectory prediction and criticality assessment in arbitrary road environments. *IEEE Transactions on Intelligent Transportation Systems*, 17(10):2751–2766, doi: http://dx.doi.org/10.1109/TITS.2016.2522507.

[Schubert and Wanielik, 2011] Schubert, R. and Wanielik, G. (2011). A unified bayesian approach for object and situation assessment. *IEEE Intelligent Transportation Systems Magazine*, 3(2):6–19, doi: http://dx.doi.org/10.1109/MITS.2011.941331.

[Shim et al., 2015] Shim, I., Choi, J., Shin, S., Oh, T., Lee, U., Ahn, B., Choi, D., Shim, D. H., and Kweon, I. (2015). An autonomous driving system for unknown environments using a unified map. *IEEE Transactions on Intelligent Transportation Systems*, 16(4):1999–2013, doi: http://dx.doi.org/10.1109/TITS.2015.2389237.

[Soualmi et al., 2014a] Soualmi, B., Sentouh, C., Popieul, J., and Debernard, S. (2014a). Automation-driver cooperative driving in presence of undetected obstacles. *Control Engineering Practice*, 24:106 – 119, doi: http://dx.doi.org/https://doi.org/10.1016/j.conengprac.2013.11.015.

[Soualmi et al., 2014b] Soualmi, B., Sentouh, C., Popieul, J., and Debernard, S. (2014b). Automation-driver cooperative driving in presence of undetected obstacles. *Control Engineering Practice*, 24:106 – 119, doi: http://dx.doi.org/https://doi.org/10.1016/j.conengprac.2013.11.015.

[Soualmi et al., 2011] Soualmi, B., Sentouh, C., Popieul, J. C., and Debernard, S. (2011). Fuzzy takagi-sugeno lq controller for a shared control of vehicle. In *2011 14th International IEEE Conference on Intelligent Transportation Systems (ITSC)*, pages 956–961.

[Takano et al., 2008] Takano, W., Matsushita, A., Iwao, K., and Nakamura, Y. (2008). Recognition of human driving behaviors based on stochastic symbolization of time series signal. In *2008 IEEE/RSJ International Conference on Intelligent Robots and Systems*, pages 167–172.

[Thomsen et al., 2019] Thomsen, B. T., Annaswamy, A. M., and Lavretsky, E. (2019). Shared control between adaptive autopilots and human operators for anomaly mitigation. *IFAC-PapersOnLine*, 51(34):353 – 358, doi: http://dx.doi.org/https://doi.org/10.1016/j.ifacol.2019.01.018. 2nd IFAC Conference on Cyber-Physical and Human Systems CPHS 2018.

[Tian et al., 2018] Tian, Y., Pei, K., Jana, S., and Ray, B. (2018). Deeptest: Automated testing of deep-neural-network-driven autonomous cars. In *2018 IEEE/ACM 40th International Conference on Software Engineering (ICSE)*, pages 303–314.

[Wada et al., 2016] Wada, T., Sonoda, K., Okasaka, T., and Saito, T. (2016). Authority transfer method from automated to manual driving via haptic shared control. In *2016 IEEE International Conference on Systems, Man, and Cybernetics (SMC)*, pages 002659–002664.

[Wada et al., 2016] Wada, T., Sonoda, K., and Tada, S. (2016). Simultaneous achievement of supporting human drivers and improving driving skills by shared and cooperative control. *IFAC-PapersOnLine*, 49(19):90 – 95, doi: http://dx.doi.org/https://doi.org/10.1016/j.ifacol.2016.10.467. 13th IFAC Symposium on Analysis, Design, and Evaluation ofHuman-Machine Systems HMS 2016.

[Wang et al., 2018] Wang, Z., Zheng, R., Kaizuka, T., and Nakano, K. (2018). Driver-automation shared control: Modeling driver behavior by taking account of reliance on haptic guidance steering. In *2018 IEEE Intelligent Vehicles Symposium (IV)*, pages 144–149.

[Wang et al., 2019] Wang, Z., Zheng, R., Kaizuka, T., and Nakano, K. (2019). Relationship between gaze behavior and steering performance for driver–automation shared control: A driving simulator study. *IEEE Transactions on Intelligent Vehicles*, 4(1):154–166, doi: http://dx.doi.org/10.1109/TIV.2018.2886654.

[Watson, 2001] Watson, J. (2001). Strategy: An introduction to game theory.

[Wei et al., 2013] Wei, J., Snider, J. M., Kim, J., Dolan, J. M., Rajkumar, R., and Litkouhi, B. (2013). Towards a viable autonomous driving research platform. In *2013 IEEE Intelligent Vehicles Symposium (IV)*, pages 763–770.

[Wen et al., 2011] Wen, D., Yan, G., Zheng, N., Shen, L., and Li, L. (2011). Toward cognitive vehicles. *IEEE Intelligent Systems*, 26(3):76–80, doi: http://dx.doi.org/10.1109/MIS.2011.54.

[Yao et al., 2013] Yao, W., Zhao, H., Bonnifait, P., and Zha, H. (2013). Lane change trajectory prediction by using recorded human driving data. In *2013 IEEE Intelligent Vehicles Symposium (IV)*, pages 430–436.

[Yu et al., 2015] Yu, C., Cherfaoui, V., and Bonnifait, P. (2015). Evidential occupancy grid mapping with stereo-vision. In *2015 IEEE Intelligent Vehicles Symposium (IV)*, pages 712–717.

[Zhao et al., 2017] Zhao, C., Gong, J., Lu, C., Xiong, G., and Mei, W. (2017). Speed and steering angle prediction for intelligent vehicles based on deep belief network. In *2017 IEEE 20th International Conference on Intelligent Transportation Systems (ITSC)*, pages 301–306.

[Zhu et al., 2017] Zhu, H., Yuen, K., Mihaylova, L., and Leung, H. (2017). Overview of environment perception for intelligent vehicles. *IEEE Transactions on Intelligent Transportation Systems*, 18(10):2584–2601, doi: http://dx.doi.org/10.1109/TITS.2017.2658662.

[Zhu et al., 2018a] Zhu, M., Wang, X., and Wang, Y. (2018a). Human-like autonomous car-following model with deep reinforcement learning. *Transportation Research Part C: Emerging Technologies*, 97:348 – 368, doi: http://dx.doi.org/https://doi.org/10.1016/j.trc.2018.10.024.

[Zhu et al., 2018b] Zhu, M., Wang, X., and Wang, Y. (2018b). Human-like autonomous car-following model with deep reinforcement learning. *Transportation Research Part C: Emerging Technologies*, 97:348 – 368, doi: http://dx.doi.org/https://doi.org/10.1016/j.trc.2018.10.024.